Uropathogenic *Escherichia coli* (UPEC) cause impairment of spermatogenesis by inducing programmed necrosis

Inaugural Dissertation

submitted to the Faculty of Medicine

in partial fulfillment of the requirements

for the PhD-Degree of the Faculty of Medicine

Justus Liebig University Giessen

by

Lu, Yongning

Guangxi, China

Giessen 2011

From Department of Anatomy and Cell Biology

Director: Prof. Dr. Wolfgang Kummer

Faculty of Medicine

Justus Liebig University Giessen, Germany

First Supervisor and Committee Member: Andreas Meinhardt

Second Supervisor and Committee Member: Trinad Chakraborty

Committee Members: Prof. Dr. Christiane Kirchhoff

Prof. Dr. Ernst Petzinger

Prof. Dr. Eugen Domann

Date of Doctoral Dissertation: 08-12-2011

CONTENTS

ABBREVIATIONS

ABP	Androgen binding protein
AIF	Apoptosis inducing factor
AMH	Anti-Müllerian hormone
Apaf-1	Apoptotic protease activation factor-1
BEB	Blood-epididymis barrier
bp	Base pair
BSA	Bovine serum albumin
BTB	Blood-testis barrier
°C	Degree Celsius
CED-3	Caenorhabditis elegans cell death gene-3
dNTP	Deoxynucleoside triphosphate
DAMP	Damage-associated molecular pattern
DAPI	4', 6'-diamino-2-phenylindole
DC	Dendritic cells
DISC	Death-inducing signaling complex
DMSO	Dimethyl sulfoxide
EDTA	Ethylene diamine tetraacetic acid
FADD	Fas receptor associated death domain
h	Hour
HlyA	α-hemolysin
HMGB1	High-mobility group protein B1
IAPs	Inhibitor of apoptosis proteins
ICAD	Inhibitor of caspase activated DNase
ICE	IL-1 β converting enzyme
IFN	Interferon
IL	Interleukin
kb	Kilo base pair
kD	Kilo Dalton
LC	Leydig cells
MOI	Multiplicity of infection
mg	Milligram
min	Minute
ml	Milliliter
MTT	3-(4, 5-Dimethylthiazol-2-yl)-2, 5-diphenyltetrazolium bromide
NPEC	Nonpathogenic *Escherichia coli*
OD	Optical density
PAGE	Polyacrylamide gel electrophoresis

PAI	Pathogenicity islands
PAMPs	Pathogen associated molecular patterns
PARP	Poly-ADP ribose polymerase
PBS	Phosphate buffered saline
PFA	Paraformaldehyde
PI	Propidium iodide
RAGE	Receptor for advanced glycation endproducts
RIP	Receptor interacting protein serine/threonine kinases
RNase	Ribonuclease
PS	Phosphatidylserine
PTC	Peritubular cells
SC	Sertoli cells
sec	Second
SDS	Sodiumdodecylsulphate
TGF	Transforming growth factor
TLR	Toll-like receptors
TM	Testicular macrophages
TNF	Tumor necrosis factor
TRADD	Tumor necrosis factor receptor type 1-associated DEATH domain
TUNEL	Terminal deoxynucleotidyl transferase dUTP nick end labeling
UPEC	Uropathogenic *Escherichia coli*
UTIs	Urinary tract infections
V	Volt
v/v	Volume per volume
w/v	Weight per volume
µ	Micro
µg	Microgram
µl	Microliter
µM	Micromolar

1. INTRODUCTION

1.1 The male reproductive system

The male reproductive system consists of a number of sex organs: the testicles, the excurrent duct system (comprising the epididymides and vasa deferentia), accessory glands (including the seminal vesicle and prostate gland), as well as the penis. The penis and scrotum which contains the testes and epididymides are located externally. The testes are positioned inside the scrotum and fulfill two major functions: generating male the gamete--sperm and secreting male sexual hormones such as testosterone. The sperm are transported from the rete testis via testicular efferent ducts to the epididymis which is cupping the backside of each testis. In human, multiple efferent ducts form the caput epididymis and eventually unite into one single tightly coiled epididymal tubule [1]. In rodents, several ductules merge into a single duct prior to entering the epididymis, which displays three grossly distinguishable regions: caput, corpus and cauda epididymides. The spermatozoa shed from the testis are still immature and without fertilization capability. Sperm maturation takes place in the epididymis and this process is associated with morphological, physiological and biochemical changes in male gametes [1,2]. Mature sperm expelled by contractions from the epididymis are transported through the vas deferens which is a muscular tube connecting the epididymis and seminal vesicle. Within seminal vesicles, fructose and the majority of ejaculatory fluid is produced to provide sperm with energy aiding their motility [1]. Additional components of semen are secreted from the prostate which is also required for the nourishment of sperm.

1.2 Structure and functions of the testis

The testes are enclosed in a fibrous white organ capsule of dense connective tissue (the tunica albuginea). The tunica albuginea penetrates testicular parenchyma and continues on the posterior side of the testis as the mediastinum [3]. The parenchyma occupies up to 90% of testicular mass and is divided into a number of lobules by the loose areolar connective tissue (septa testis), which is the extension of

tunica albuginea inside testis [4]. Each lobule comprises a tubular compartment and an interstitial compartment which corresponds to two primary functions of testis: androgen secretion and spermatogenesis.

1.2.1 Tubular compartment and spermatogenesis

Spermatogenesis is the process by which testicular stem cells develop into spermatozoa, including four successive phase: (1) mitosis of spermatogonia (2) meiosis of spermatocytes (3) spermiogenesis and (4) spermiation [1]. It is facilitated within seminiferous tubules that contain Sertoli cells (SC), developing germ cells in the stratified epithelium and peritubular cells (PTC) at the basal compartment. Type A spermatogonia have two subtypes--dark (Ad) or pale (Ap) which are positioned on the basement membrane of seminiferous tubules. Ad spermatogonia represent testicular stem cells without proliferation activity [5]. They rarely divide only when the overall population of spermatogonia is dramatically reduced [6]. In contrast, Ap spermatogonia are able to divide and proliferate by mitosis to produce type B spermatogonia. Type B spermatogonia are able to mitotically divide into primary spermatocytes, which are characterized by prominent round nuclei with a coarse chromatin pattern. Following a long stage of development, primary spermatocytes undergo their first meiotic division to become secondary spermatocytes. These cells proceed through the secondary stage quickly and undergo second meiosis for engendering spermatids. The spermatid is a haploid male gamete containing only half the genetic material inherited from the primary spermatocyte. When formed, early spermatids are round shape, and must go through further maturation to develop into elongated spermatids which eventually differentiate into sperm. This process known as spermiogenesis comprises nuclear condensation, acrosome formation, flagellum formation and cytoplasm reduction [1]. The final phase of the spermatogenic process results in the release of sperm from the germinal epithelium into the lumen, which is affected by hormonal alteration, temperature variation and toxins [1].

The process of spermatogenesis is accomplished in close contact with SC, which support and nourish all stages of developing sperm cells. These nurse cells locate on

the basement membrane of seminiferous tubules and extend to the lumen with cytoplasm, surrounding different types of germ cells, and they also act as phagocytes consuming the unneeded portions of germ cells (residual bodies) and unreleased sperm [7]. In addition to the supportive and nurturing function, SC also play an important role in maintaining the special immune environment within the testis [8]. The occluding junctional complexes, also known as tight junctions, connect two adjacent Sertoli cells and give rise to the blood-testis barrier (BTB). BTB separates the epithelium into two compartments: the basal compartment in which only spermatogonia and very early primary (leptotene and zygotene) spermatocytes are found, and the adluminal compartment which contains the neo-antigens of more advanced meiotic and haploid germs cells. The tight junctions are able to dynamically dissolve and reassemble for the apical progression of spermatogonia [9]. Thus, spermatogonia can pass through the barrier and differentiate into haploid cells exhibiting new surface antigenic properties at the adluminal compartment. By controlling the exchange of nutrients, hormones and other essential materials, SC protect the isolated spermatocytes, spermatids and spermatozoa from the potentially detrimental factors. Furthermore, SC can secrete numerous substances such as inhibin, activins, transforming growth factor (TGF), androgen binding protein (ABP) and anti-Müllerian hormone (AMH) which are essential for spermatogenesis regulation [10-12]. Moreover, the expression of Toll-like receptors (TLRs), and secretion of cytokines including interferon (IFN)-alpha, IFN-beta, IFN-gamma, interleukin (IL)-1, IL-6 and tumor necrosis factor (TNF)-α have been identified in SC [13,14], which is indicative of SC playing a role in the innate immune system in the testis [15]. It has been suggested that SC may be derived from mesonephros [16]. Therefore, SC cannot divide once fully differentiated in adulthood and the number of them remains constant even after damage to the seminiferous epithelium has occurred [17].

The seminiferous tubules are surrounded by a lamina propria which consists of a basal membrane, a collagen layer and PTC. The PTC have been found in all mammalian species, but the organization of cellular layers varies by species [18]. In humans and some mammals, the seminiferous tubules are covered by several layers of

PTC. This is in contrast to laboratory rodents such as rats and mice where there is only one cellular layer in the lamina propria of tubules [19]. Apart from providing structural integrity, PTC are able to contract and take part in the transport of sperm and testicular fluid towards the rete testis [20,21]. Furthermore, previous studies have demonstrated that PTC express androgen receptors and secrete numerous of substances including extracellular matrix components, growth factors and cytokines [22-24]. This suggests that PTC may contribute to the regulation of spermatogenesis and host immune responses in the testis [18].

1.2.2 Interstitial compartment

Between the seminiferous tubules lies the interstitium, which contains various cell types including Leydig cells (LC), testicular macrophages (TM), dendritic cells (DC) and fibroblasts [1]. In human, the interstitial compartment of the testis comprises about 12-15% of the total testicular volume, whereas it represents only about 2.6% in experimental animals [1]. LC are considered the most important cells in this compartment, as they produce and secrete testosterone into neighboring tissues and blood. Secreted testosterone is able to influence testis functions and also affects other tissue types [25]. Not only LC but also immune cells including TM, DC, T cells and natural killer cells are present within the interstitium. Together with SC and PTC, these interstitial cells contribute to the maintenance of a special immune milieu in the testis [26].

1.3 Testicular immunology

1.3.1 Immune privileged status of the testis

It has been demonstrated in different laboratory rodents that the transplantations of sperm from the testis to other parts of body could cause autoimmune response, although they are tolerated in the testis [27-29]. The fact that the post-meiotic and haploid male gametes firstly appear at puberty after the establishment of body immune tolerance may explain why the germ cells are regarded as foreign and able to cause immune reaction outside the testis [30]. Therefore, certain mechanisms must

exist in the testis for gametes protection and autoimmune attack prevention. So far, experiments have uncovered a few unique features about testicular immunology. Most importantly, the testis has been proved as an immunologically privileged organ, which possesses a reduced ability to mount the rejection and inflammatory response [30,31]. Although the BTB provides a shelter for developing germ cells, it is believed that the barrier alone cannot account for the whole immunologically privileged situation in the testis [32]. However, the mechanisms responsible for the immunoprotective property of the testis are just partially understood. Recently, some studies have suggested that in addition to the BTB, a number of biological processes likely contribute to maintaining the special immune microenvironment in the testis. For example, in response to the challenge of bacteria component, the activated TM produce relatively lower levels of proinflammatory cytokines compared to peritoneal macrophages [33]. Moreover, co-transplantation experiments confirmed that the mature SC exert immunoprotective functions during allogeneic and xenogeneic transplantation [34,35]. It appears that SC are able to inhibit the proliferation and modify the differentiation of T cells by producing a series of immunomodulatory factors and Fas ligand [36,37]. Furthermore, the suppression of autoreactive T lymphocytes can also be mediated by regulatory T cell populations as well as the lacking of antigen-independent co-stimulatory molecules in the testis [29]. Finally, there are some locally produced factors such as testosterone and TGF-ß in the interstitial fluid of the testis which potentially inhibit the immune activation and result in weaken innate and adaptive immune response [38-40]. Instead of single mechanism acting alone, accumulating evidences suggested that both testicular somatic and immune cells synergistically create a tolerogenic milieu in the testis. Even though the testis is considered an immunologically privileged site, the immunocompetent cells such as leukocytes in the testis are still able to mount pro-inflammatory responses to combat infection [26].

1.3.2 Immunocompetent cells of the testis

Testicular leukocytes are found in the testicular interstitium, which comprise different types of populations. The primary function of these leukocytes is to mediate

immune response together; additionally they also play a role in the homeostatic regulation in the testis.

In rodent testis, TM are the largest population of immune cells. They originate from the circulating monocytes which migrate to the testis and differentiate into resident macrophage [41]. The resident TM do not move back to circulation, on which the integrin can be uniquely recognized with the marker ED2 in the rat (specific for CD 163). The macrophage marker ED1 (specific for a lysosomal molecule CD68) can help to distinguish another subset of "newly arrived" macrophages, which is also present within the testis [42]. The immunosuppressive role of the resident TM is supported by previous studies, whereas the ED1 (+) macrophages demonstrate distinct phenotypes associated to the statues of the testis [43]. These newly arrived TM isolated from the normal rat testis showed even relatively poor responsiveness to LPS [44]. However, upon inflammatory stimuli the ED1 (+) TM, of which the majority may be infiltrating monocytes, are regarded as pro-inflammatory macrophage and responsible to sustain inflammatory responses for at least a limited period of time inside the testis [45]. In response to infectious insults, TM can get activated and be able to eliminate the invading micro-organism, but to a less extent than other types of macrophages like peritoneal macrophages [15,46]. Aside from the role of immunological regulator in the testis, TM also contribute to the maintenance of normal testicular functions and modulation of Leydig cell steroidogenesis [47-50]. These evidences indicate that immune-endocrine interactions play a role in regulating the functions of the testis under normal and pathological conditions.

DC is another kind of antigen-presenting cell present in the testis, although with a relative small population. Some studies have shown that dendritic cells are implicated in the development of experimental autoimmune orchitis (EAO) [51,52], as they likely contribute to inflammation within the testis [53]. T lymphocytes which form an essential part in the cell-mediated immune response are also present and constitute about 10~20% of immune cells in the testis of rodents and humans under normal condition [54]. Also the natural killer T cell, the special type of lymphocytes which bridges the adaptive immune system with the innate one, is found in the testes of

rodents and human [55]. In the rat testis, the numbers of both effector T cells and regulatory T cells increase dramatically whilst autoimmune orchitis occurs [56]. However, there is remarkable evidence showing the existing T cells inhibition mechanisms in the testis. Some regulatory factors in the testis such as TGF-ß, prostaglandin and activin all exhibit lymphocyte-inhibiting activity [55]. As the most abundant type of leukocyte in blood stream, neutrophils normally are not present in testis, but they can be recruited from circulation to the sites of injury in response to pathogen invasion, inflammatory stimulus or tissue damage. For example, upon intraperitoneal injection with LPS, testicular torsion or the treatment with human chorionic gonadotropin (hCG) which increase the permeability of blood vessel, neutrophils could enter the testis in rat [45,57,58]. Once be activated, neutrophils together with migrating monocytes-macrophage and lymphocytes may not be affected by the immunosuppressive environment in the testis, thus the inflammatory reaction brought by these cells should be tightly regulated since inflammation-induced damage can potentially disrupt the testicular functions and lead to infertility [59].

Aside from testicular immune cells, accumulating studies have suggested that testicular somatic cells including SC, LC as well as PTC are also immunocompetent cells in this organ. These somatic cells, particularly SC and LC, are able to produce several pro-inflammatory mediators, including IL-1, IL-6, MIF, IFN, and iNOS [60,61]. However, the crosstalk between testicular somatic cells and immune cells is largely unclear, further studies may help to gain a deeper insight into the exact role of testicular cells in maintaining testicular homeostasis.

1.3.3 Innate immunity of the testis

Toll-like receptors (TLRs) are a group of membrane spanning proteins which play a pivotal role in innate immunity. Recent studies have confirmed the expression of TLRs 1-11 in rat testicular macrophage, and TLRs 2-5 are found in rat SC, PTC and LC [15]. These TLRs expressed in mouse SC can be activated by their specific ligands and induce the increasing expression of pro-inflammatory cytokines in the testis [62,63]. Increasing data demonstrate that a series of cytokines play a key role in

the immunological homeostasis of the testis [64]. Some of them are also secreted within the testis under physiological conditions, such as IL-1α, IL-6 and TNF-α [65-68], acting as modulators in spermatogenesis, blood-testis barrier and steroidogenesis [69-76]. However, the upregulation of cytokine expression during infection and inflammation or trauma within the testis can contribute to fertility impairment and testicular dysfunction, either via directly inducing germ cell apoptosis or altering somatic cells functions and disturbing testicular microenvironment. Additionally, antimicrobial peptides such as defensins are also produced by various cell types in human and rodent testis. It is assumed that these peptides may play an important role in innate defence against invading pathogens in the testis [77].

1.4 Male infertility and genital tract infections/inflammation

Infertility can be defined as the inability to conceive after one year of regular sexual intercourse without the use of contraception [78]. Approximately 15% of couples cannot conceive within one year [79]. The underlying etiological factors can be the abnormalities or pathological situations affecting one or both members of an infertile couple. Various factors contributing to infertility from the male side are found in up to 50% unintended childlessness families [78]. Male infertility is usually associated with testicular dysfunction as a result of various abnormalities or disruptions. Recent studies on human testicular biopsies samples observed a pathology-associated increase in transcript levels corresponding to inflammatory activity and tissue remodeling in this organ [80,81]. These molecular changes included positive regulation of NF-κB cascade, MAPK pathways, as well as some other pathways implicated in inflammation, allergy and autoimmunity. At present, infections and inflammation of urogenital tracts, including the acute and chronic forms, are widely accepted as an important aetiological factor which accounts for about 10~15% of cases with male infertility [79]. The male reproductive tract can become a route of pathogen invasion via the urethra. Therefore, bacterial infections in male genital tract mainly originate from ascending urinary tract infections (UTIs) as well as sexually transmitted infections. Although male UTIs are not as frequent as in

females, once the infection occurs it may spread and affect different parts of the male reproductive tract incorporating the epididymis and testis [1]. UTIs exert detrimental influence on spermatozoa during development, maturation and transport. Compared to urethritis and prostatitis, infection or inflammation of the epididymis and testis are more likely to cause impairment of male reproductive function, as spermatozoa or germ cells may be directly exposed to pathogens and inflammatory products [59,82-84]. Critically, antibiotic treatment which efficiently eliminates bacterial infection within the epididymis or testis does not reverse anatomical or functional damage resulting from infection or inflammation [85]. To date the role of bacterial infection and inflammation within the testis and epididymis contributing to male infertility has yet to be elucidated.

1.4.1 Pathogens involved in orchitis

Previous studies have demonstrated a correlation between bacterial infection and male infertility. Orchitis is an inflammatory condition of the testes secondary to infections. It results in leukocytes infiltration outside the seminiferous tubules, which can be observed inside the tubules in more severe cases as well [59]. With the exception of specific viral infections, orchitis is usually in combination with acute epididymitis due to retrograde infection, known as epididymo-orchitis [86]. Among the sexually active men between 14~35 year of age, sexually transmitted pathogens including *Chlamydia trachomatis* and *Neisseria gonorrhoeae* are among the most common pathogens related to epididymo-orchitis [86-88]. *Escherichia coli* (*E. coli*) and other Enterobacteriaceae belonging to the genera *Klebsiella*, *Salmonella* and *Proteus* are the primary pathogens implicated in non-sexually transmitted epididymo-orchitis [59,89]. Uropathogenic *E. coli* (UPEC) account for the vast majority of urinary tract infections and thus are assumed to be the likely substrain responsible for the *E. coli* elicited epididymo-orchitis [90-92]. Apart from those bacteria mentioned above, mumps virus is the most common pathogen which can cause isolated orchitis in pre-pubertal males [93,94]. Others pathogens which are found in male reproductive tract and related with subfertility include Herpesvirus

(HSV), Human papilloma viruses (HPV), Coxsackie A virus, Mycobacterium tuberculosis as well as Human immunodeficiency viruses (HIV) [90,95,96].

1.4.2 Uropathogenic *E. Coli*

As a primary candidate in UTIs, *E. coli* are commonly isolated from semen or the prostatic fluid of infertile men and the patients with prostatitis or epididymitis [91,92,97]. Despite most of the *E. coli* strains are harmless, some are able to persist in the urinary tract and initiate infections. Since the specific pathotype of *E. coli* has yet to be determined for UTIs, "Uropathogenic *E. coli*" (UPEC) becomes a designation in common usage for all *E. coli* strains eliciting UTIs [98]. UPEC are responsible for approximately 70~90% of cases with community acquired urinary tract infections and most likely account for *E. coli* induced epididymo-orchitis [99]. Numbers of virulence factors expressed by UPEC enable the pathogen to adhere to the uro-epithelial cells and spread from low urinary tract up to bladder, kidneys, as well as genital tract in males, resulting in ascending infections. In general, two main types of virulence factors in UPEC were described, one is produced on the bacterial surface and the other one is synthesized inside the bacteria and subsequently exported to the site of infection [100]. The surface virulence factors include different types of pili (type I, P, S, and F1C) which facilitate the pathogen adhesion to mucosal and endothelial cells, the capsular material protecting bacteria from host immune attack, as well as the endotoxin Lipopolysaccharide (LPS) exhibiting endotoxic effects and evoking inflammatory response [101-103]. On the other hand, the exported virulence factors of UPEC mainly exert the cytotoxic and anti-host cells activities, including toxins (such as α-hemolysin [HlyA], cytotoxic necrotizing factor 1 [CNF1], cytolysin A, autotransporter toxin), iron acquisition systems and others [104-106].

The virulence factors are usually encoded by genetic elements termed pathogenicity islands (PAIs) [107,108]. Generated by horizontal gene transfer which contributes to the microbial evolution, PAIs comprise large DNA regions (10~200 kbp) with flexible sequences associating with tRNA genes [100]. UPEC strains usually possess several PAIs, which largely determine the virulence traits of bacteria

[100,109]. Individual deletion of any single PAI could not affect the survival curves in murine urosepsis model, whereas simultaneously loss of two PAIs significantly attenuated the virulence [110]. Thus far, the genome of a representative member of UPEC, strain CFT073 (O6:K2:H1), has been entirely sequenced and published [GenBank: AE014275. 1] [111], with a recent reannotation in 2009 [112]. These publications provide a comprehensive understanding on the genetic basis of uropathogenic potential of this pathogen.

Like other microbial pathogens, UPEC can also evolve various strategies to evade host defense response, including invasion/penetration inside host cells, elimination of key immunocompetent cells, and suppression of host immune defence [15]. For example, the pore-forming toxin HlyA, which is one of the most important virulence factors of UPEC, can not only lysis erythrocytes but also target other cells types including leukocytes and uro-endothelial cells [113]. Recent observation further confirmed that hemolytic activity is possessed in more than 50% of *E. coli* samples isolated from patients with epididymitis (Clinic of Urology, Giessen, personal communication). Intriguingly, recent studies suggested that HlyA also contributes to the UPEC induced immunosuppression in peritoneal macrophages and testicular somatic cells (Sudhanshu Bhushan, et al. data is not published). Better understanding of host response against pathogens in epididymo-orchitis can shed more light on the mechanisms of UTIs caused male infertility.

1.5 Host response in UTIs

Upon the UTIs the immune surveillance molecules present in urinary tract (such as TLRs) recognize the invading pathogens by special pathogen associated molecular patterns (PAMPs) [114]. In response to infections, host defence initially mobilizes innate and adaptive immune systems in various ways to clear infections, which is carried out by recruiting and activating immune cells, triggering various inflammatory pathways, secreting antimicrobial peptides, synthesizing specific antibodies in serum and urine and resisting bacterial invasion [115-117]. Once the infections persist and pathogens invasion occurs, a variety of cell death modes are actively triggered to

eliminate the infected cells and expose intracellular pathogens to the immune system [118]. These inherently regulated or intracellular program mediated cell death modes are termed “programmed cell death” [119]. By far three major programmed cell death mechanisms are characterized, named apoptosis, programmed necrosis, and pyroptosis [120]. The biochemical basis and features of these three types of cell death are described as follows.

1.6 Programmed cell death

1.6.1 Apoptosis

Apoptosis, a term stemming from a Greek word with the meaning of “dropping off” or “falling off” of petals or leaves from plants, was first reintroduced to describe a form of controlled cell deletion in 1972 by Kerr and his colleagues [121]. To date, apoptosis has been well-studied and characterized as a special kind of cell suicide phenomenon. Classically, a cell undergoing apoptosis shows a series of characteristic morphologic features in sequence: cell shrinkage and plasma membrane blebbing (without losing membrane integrity), chromatin condensation into compact patches (pyknosis), DNA fragmentation and nucleus breakage (karyorrhexis) and membrane-enclosed cell fragments formation (apoptotic bodies) [122,123].

1.6.1.1 Process of apoptosis

Apoptosis is not only viewed as an important physiological event during embryogenesis, nervous system development and homeostasis maintenance of adult organisms, but also implicated in a variety of stress induced injury. Certain stress stimuli (i.e. hypoxia, radiation, microbial infection, heat shock, intracellular calcium influx and nutrient or growth factors deprivation) can trigger the transduction of apoptotic signals, which subsequently interact with regulatory proteins and initiate different apoptosis pathways [124,125]. Generally apoptosis or apoptosis-like cell demise can be categorized into two distinct mechanisms according to the involvement of a family of cysteine-dependent aspartate-directed proteases (caspases): entitled caspase-dependent (classical apoptosis) and -independent pathway [124,126].

1.6.1.2 Caspase-dependent pathway

So far, at least 14 caspases have been identified in mammals of which 11 were confirmed in human [127-129]. Apart from the inflammatory caspases including caspase-1, -4, -5, -11~-13, the rest of the caspases members which belong to the Caenorhabditis elegans cell death gene-3 (CED-3) subfamily are apoptotic related proteases comprising two subgroups: initiator and executor caspases [127,130]. The former subgroup comprises caspase-2, -8, -9, and -10, and the latter one includes caspase-3, -6 and -7. These caspases trigger apoptotic machinery via two distinct ways: the intrinsic and extrinsic apoptotic signaling pathways (Figure 1). The mitochondrial regulation is the core process of intrinsic signaling pathways, in which Bcl-2 family members play a central role [131]. These proteins share at least one of the four homological regions named the Bcl-2 homology (BH) domains (BH1~4) and they are able to form hetero- or homodimers [132]. In response to a certain apoptotic stimuli such as chemotherapeutics or UV irradiation, a group of pro-apoptotic Bcl-2 family members (i.e. Bax, Bak, Bid and Bim) can either permeabilize or form pores on the mitochondrial membrane and thereby induce the release of mitochondrial apoptogenic factors like cytochrome c, SMAC/Diablo (Second Mitochondria-derived Activator of Caspases/Direct IAP Binding Protein with Low PI) and HtrA2/Omi [133]. Following the formation of mitochondrial outer membrane permeabilization pore (MAC), cytochrome c is leaking out and recruited by the central scaffold protein apoptotic protease activation factor-1 (Apaf-1) together with ATP and pro-caspase-9 in cytosol. Together they form the apoptosome followed by the activation of caspase-9 within this complex, which in turn proteolytically activates the executor caspases [134,135]. The spilled out SMAC/Diablo and HtrA2/Omi exert their pro-apoptotic function by deactivating IAPs (inhibitor of apoptosis proteins), which exerts suppression of caspases activity [136,137]. On the other hand, mitochondrial permeability is also regulated by anti-apoptotic Bcl-2 family members including Bcl-2, Bcl-w and Bcl-xL, which can reduce Bax activation by binding to Bid or directly inhibit the pore-forming function of Bax and Bak by heterodimerization [133].

Therefore the ratio of Bcl-2/Bax indicates the balance that decides a given cell will either execute or ignore an apoptotic stimulus [138]. Beside the mitochondrial regulation, apoptotic signals can be transducted via the extrinsic signaling pathway that is initiated by the binding of death receptor ligands (i.e. TNF-a, Fas ligand) to their respective transmembrane receptors [139,140]. The interaction between these ligands and death receptors leads to the formation of the death-inducing signaling complex (DISC) containing Fas-associated death domain protein (FADD), caspase-8 and -10 [141]. The initiator caspases are activated in DISC and they can either cleave downstream executor caspases or truncate and activate another Bcl-2 homology domain 3 (BH3)-only protein -- Bid, which in turn leads to the insertion of Bax onto the mitochondrial membrane, acting as a link between the intrinsic and extrinsic pathways [142].

Generally the caspase-dependent pathway is activated in two-step cascade. Firstly the initiator caspases are recruited in two distinct protein complexes (the apoptosome complex and DISC) which are respectively implicated in the intrinsic and extrinsic apoptotic signaling pathways. The initiator caspases get autoactivated in these complexes and thereby trigger the proteolytic maturation of executor caspases. Then the activated executor caspases amplify the lethal signal by cleaving their protein substrates (i.e. poly-ADP ribose polymerase [PARP], inhibitor of caspase activated DNase [ICAD], nuclear lamins) and initiate irreversible disassembly of cell into apoptotic bodies [143].

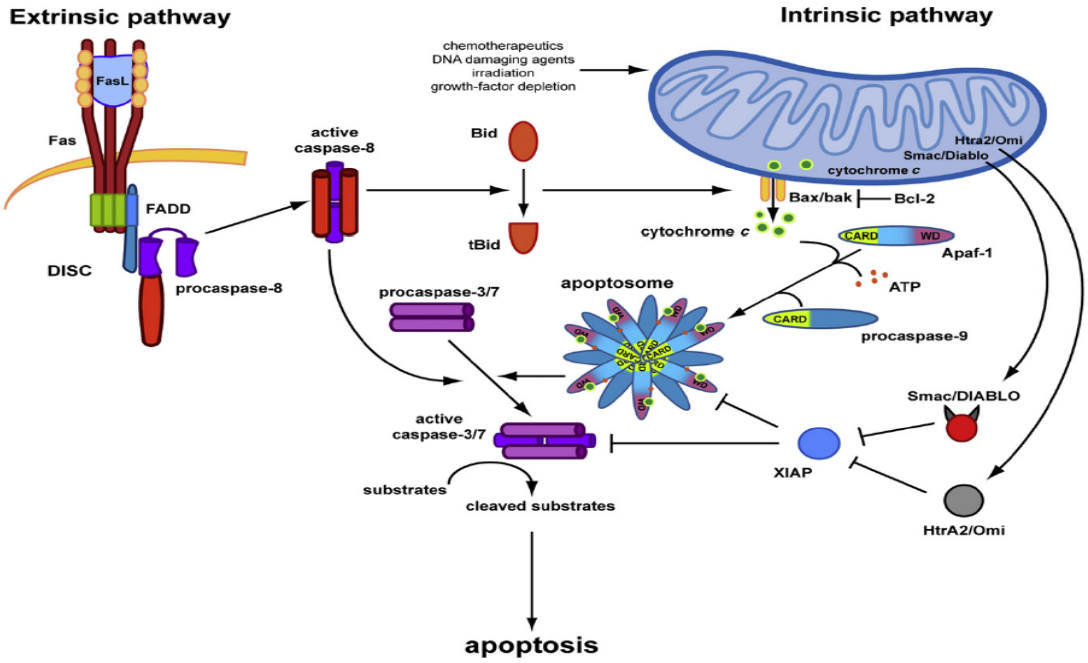

Figure 1 The intrinsic and extrinsic apoptotic signaling pathways (Lamkanfi, M. and V. M. Dixit, 2010).

1.6.1.3 Caspase-independent pathway

Apoptosis-like cell death can also be carried out by mechanisms other than the traditional caspases-mediated cleavage cascade. There are several death effectors that also can trigger cell death independently without participation of caspases [144]. Apoptosis inducing factor (AIF) is one of the best characterized proteins implicated in caspase-independent pathway, although the exact mechanism is still not fully understood. AIF is a flavoprotein which is secluded behind the outer membrane of mitochondria under normal circumstances [145]. This flavoprotein exerts vital function in mitochondrial respiration and displays NADH oxidoreductase and peroxide scavenging activities [146]. Apart from its vital role, AIF can also act as a cell death effector. Upon cell death signaling, AIF is released from the permeabilized mitochondria and translocates via cytosol to nucleus. Once AIF is move into the cytosol, it can facilitate further release of this protein from mitochondria and therefore it triggers a positive feedback amplification loop [147]. In nucleus AIF binds to DNA and induce peripheral chromatin condensation (chromatinolysis) and high molecular weight (~50 kbp) DNA fragmentation in a caspases-independent manner [122,145].

Notably, in particular conditions AIF can also trigger necrosis-like programmed cell death, which is characterized with cellular membranes rupture and pro-inflammatory consequence [148,149]. It has been shown that the AIF mediated apoptosis-like or necrosis-like cell demise is largely dependent upon the cell types and specific lethal stimuli [150].

1.6.1.4 Outcome of apoptosis

During the procedure of apoptosis, dying cells are marked by the exposure of some phagocytic molecules like phosphatidylserine (PS) on the extracellular surface [151]. The neighboring phagocytic cells such as macrophages recognize the phagocytic molecules labeled apoptotic cells and remove them by phagocytosis. The engulfment and ingestion of apoptotic cells debris actively prevents leakage of cytoplasmic content. A great body of evidence has shown that apoptosis does not elicit inflammatory response, it may even suppress the release of pro-inflammatory cytokines and inhibit maturation of dendritic cells in most of cases [152,153]. Therefore, for a long time it is believed that apoptosis is a noninflammatory form of cell death, which distinguishes itself from other cell death modes like necrosis. However, the apoptosis related immune unresponsiveness can be overridden by unclear mechanism, as accumulating studies demonstrated that apoptosis can also provoke inflammatory response by stimulating neutrophil chemoattractant release, inducing monocytes infiltration, activating antigen presentation by dendritic cells [154-156]. Nevertheless, it is increasingly recognized that apoptosis plays an essential role in immune regulation more than just elimination of unwanted cells [157].

1.6.2 Programmed necrosis

The term of “necrosis” originates from the Greek word “nekros” which means “death or the stage of dying” [158]. Necrosis is an important mode of cell death under pathological conditions, which distinguishes itself from apoptosis by many visible morphological and biochemical features as well as by the pathological consequence [159]. Necrotic cell death is usually triggered by a variety of extreme

non-physiological stress such as hypoxia, ischemia, microbial infection and toxins. Morphologically necrosis is characterized by electron-lucent cytoplasm, swelling of cellular organelles and loss of plasma membrane integrity followed with total cell lysis [158,160]. In contrast to apoptosis, the DNA of necrotic cells is randomly degraded during cell death, giving rise to a smear after agarose gel electrophoresis. Unlike the formation of membrane bounded apoptotic bodies observed during apoptosis, plasma membrane integrity is rapidly compromised in necrotic cells and results in spilling of intracellular contents into extracellular space [161]. A cytokine mediator high-mobility group protein B1 (HMGB1) is one of the "danger signals" sent by necrotic cells [162,163]. In physiological conditions, HMGB1 stabilizes nucleosome formation and may regulate transcription as an architectural chromatin-binding factor in nucleus [164]. Upon immune stimulus, HMGB1 can be secreted by the activated monocytes and macrophages [162,165], and also can be passively released from necrotic and damaged cells [166]. This chromatin protein has recently identified as a marker of necrosis as it retains in the nuclei of healthy or apoptotic cells but can be passively released into cytoplasm and extracellular space at a late stage of necrosis [167,168]. Therefore, necrosis inevitably affects neighboring cells, usually provoking significant inflammatory response and causing tissue injury [169].

Necrotic cell death is prevalent in a various acute pathologies such as infection, myocardial infarction and injury [158,170]. Currently, inhibition of necrosis is not yet accepted as a therapeutic strategy because necrosis has long been considered as an accidental and uncontrollable cell death mode without involvement of any cell signaling pathway [171]. However, increasing studies suggest that necrosis also can be a well-orchestrated form of cell demise under certain conditions [148,172]. Although the underlying mechanism of programmed necrosis has not been completely unraveled, some possible signal transduction cascades and key mediators involved in necrotic cell death are clearly described. For example, TNFa treatment combining with caspases inhibitor is able to induce programmed necrosis in some cell types since apoptotic signaling cascade is failed to initiate [173]. Although the involved necrotic

pathway is not yet completely confined, the receptor interacting protein serine/threonine kinases (RIP) 1 and RIP3 are proved to play a pivotal role in the death receptor initiated programmed necrosis (Figure 2) [174,175]. The RIP1/RIP3 signaling cascade is believed to trigger a series of downstream events that contribute to necrosis, such as calpain activation, lysosomal destabilization and mitochondrial dysfunction [176,177]. Mitochondrial dysfunction leads to excessive production of reactive oxygen species (ROS) and depletion of adenosine triphosphate (ATP). These key mediators are implicated in necrosis signaling cascade and determine the fate of cell death either by apoptosis or necrosis [178,179]. Furthermore, it is recently reported that AIF can also mediate alkylating DNA damage and consequently induce programmed necrosis [148]. These evidences suggest that programmed necrosis is the result of crosstalk between several cascades and cellular organelles [180]. Of note, the fact that the RIP1-specific inhibitors necrostatin-1, -3, -5 and RIP3 silencing are able to rescue cells from necrosis [171,173] sheds light on a better understanding of the regulation of this cell death mode and therefore facilitate the therapeutic intervention.

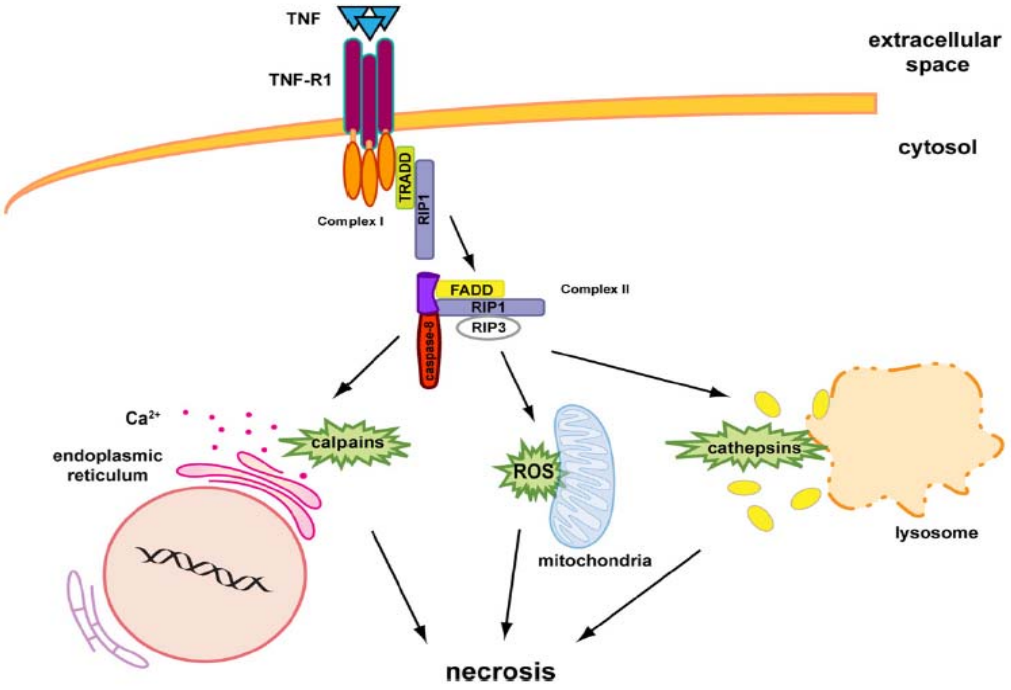

Figure 2 RIP1/RIP3 signaling induces necrosis (Lamkanfi, M. and V. M. Dixit, 2010).

1.6.3 Pyroptosis

Apart from apoptosis and necrosis, there is an increasing awareness of another kind of cell death mode responding to infection/inflammation named pyroptosis. Pyrotosis is caspase-1 dependent programmed cell death which partially retains morphological and biological features from both apoptosis and necrosis [181]. Similar to necrosis, pyroptosis is also a sort of pro-inflammatory cell death which is characterized by plasma-membrane rupture and intracellular contents release. The DNA degradation accompanying with nuclear condensation also occurs in pyroptotic cells [182,183]. Unlike the apoptotic caspases, the central regulator in pyroptosis--caspase-1 is recruited and autoactivated in the inflammasomes complexes in response to a range of microbial infections (i.e. Shigella flexneri, Salmonella typhimurium, Pseudomonas aeruginosa) [184-187] and non-infectious stimuli such as myocardial infarction and cerebral ischemia [187,188]. Caspase-1 was initially called IL-1 β converting enzyme (ICE) because it is essential for maturation and secretion of pro-inflammatory cytokines IL-1 β and IL-18. However, it is found that pyroptosis is independent of the IL-1β and IL-18 [186] and the molecular mechanism of caspase-1 inducing pyroptosis still remains unclear.

1.7 Aim of study

A growing body of evidence suggests that *E.coli* is one of the major pathogens implicated in bacterial epididymo-orchitis and potentially results in reduced fertility [90,189]. Currently, antibiotic treatment is the standardized therapy prescribed in acute bacterial epididymo-orchitis [85]. Unfortunately, successful elimination of invading pathogens with antibiotics administration doesn't necessarily mean fertility can be fully restored [29,59]. Furthermore, the impairment of spermatogenesis remained unrecoverable even after the invading pathogen was obliterated by the host immune system within the testis [190]. Consequently, the treatment of epididymo-orchitis and secondary infertility is hindered by the limited understanding of the detrimental impacts following infections in these organs. Previous studies have described the deleterious effects of *E. coli* on ejaculated sperm and spermatogenesis

[191,192]. However, to date underlying mechanisms of spermatogenic disturbance caused by *E.coli* infection has yet to be elucidated. Moreover, the influence of *E.coli* infection on testicular somatic cells such as SC and PTC which contribute to maintenance of spermatogenesis and testicular homeostasis is still poorly understood. Given the immunological privileged status within the testis, it is critical to gain a comprehensive understanding of the interaction between *E.coli* and testicular cells. Therefore, investigation of damaging effects on spermatogenesis and responses of testicular cells upon UPEC infection, may allow us to gain deep insight into underlying mechanisms of epididymo-orchitis associated infertility, thus potentially providing valuable therapeutic tools.

2 MATERIALS AND METHODS

2.1 Materials

2.1.1 Chemicals

Acetic acid	Merck, Darmstadt
Acrylamide 30% (w/v)	Roth, Karlsruhe
Agarose	Invitrogen, Karlsruhe
Bromophenol blue sodium salt	Sigma-Aldrich, Steinheim
Calcium chloride	Merck, Darmstadt
Dimethyl sulfoxide	Merck, Darmstadt
di-potassium hydrogen phosphate	Merck, Darmstadt
di-sodium hydrogen phosphate	Merck, Darmstadt
1,4-Dithiothreitol	Roche, Mannheim
Ethanol	Sigma-Aldrich, Steinheim
Ethidium bromide	Roth, Karlsruhe
Ethylene diaminetetraacetic acid disodium salt	Merck, Darmstadt
Formamide	Merck, Darmstadt
37% Formaldehyde solution	Merck, Darmstadt
Glycerol	Merck, Darmstadt
Glycine	Sigma-Aldrich, Steinheim
4-(2-hydroxyethyl)-1-piperazineethanesulfonic acid	Roth, Karlsruhe
Igepal CA-630 (NP-40)	Sigma-Aldrich, Steinheim
Ketamine	Inresa, Freiburg
Lipopolysaccharide	Sigma-Aldrich, Steinheim
Magnesium chloride	Merck, Darmstadt
Magnesium sulfate	Sigma-Aldrich, Steinheim
β-Mercaptoethanol	AppliChem, Darmstadt
Methanol	Sigma-Aldrich, Steinheim
MTT	Sigma-Aldrich, Steinheim

Non-fat dry milk	Bio-Rad, Munich
Orange G	Merck, Darmstadt
Paraformaldehyde	Merck, Darmstadt
Picric acid	Merck, Darmstadt
Phenylmethylsulfonyl fluoride	Sigma-Aldrich, Steinheim
Ponceau S	Roth, Karlsruhe
Potassium chloride	Merck, Darmstadt
Rotiphorese Gel 30	Roth, Karlsruhe
Proteinase cocktail inhibitor	Sigma-Aldrich, Steinheim
Sodium acetate	Roth, Karlsruhe
Sodium azide	Merck, Darmstadt
Sodium chloride	Sigma-Aldrich, Steinheim
Sodium dodecyl sulfate	Merck, Darmstadt
N, N, N', N'-Tetramethylethylenediamin	Roth, Karlsruhe
Tris (hydroxymethyl) aminomethane	Roth, Karlsruhe
Triton X-100	Sigma-Aldrich, Steinheim
Tween-20	Roth, Karlsruhe
Urea	Merck, Darmstadt
Xylazine	Bayer, Leverkusen

2.1.2 PCR reagents

DNase I	Invitrogen, Karlsruhe
EDTA	Invitrogen, Karlsruhe
dNTP	Promega, Mannheim
MMLV RT	Promega, Mannheim
Oligo dT	Promega, Mannheim
RNase A	Carl Roth, Karlsruhe
RNase inhibitor	Promega, Mannheim
Taq polymerase	Promega, Mannheim
SYBR green	Bio-Rad GmbH, Munich

2.1.3 Enzymes for Sertoli cell and peritubular cell isolation

Table 1 The list of enzymes used for Sertoli and peritubular cells isolation from rat testis.

Enzyme	Company	Catalogue No.
Collagenase A	Roche Diagnostics, Mannheim	103586
DNase I	Roche Diagnostics, Mannheim	104159
Hyaluronidase	Sigma-Aldrich, Steinheim	H3506-500MG
Trypsin	Roche Diagnostics, Mannheim	10109819001
Trypsin inhibitor	Roche Diagnostics, Mannheim	10109886001

2.1.4 Antibodies

Table 2 The information of primary antibodies used for Western blotting and immunofluorescence staining.

Primary Antibody	Manufacturer	Catalogue No.	Dilution (application)
Rabbit anti Caspase 1	Santa Cruz, California, USA	SC514	1:250 (WB*)
Rabbit anti Caspase 3	Abcam, Cambridge, UK	ab44976	1:500 (WB)
Rabbit anti Caspase 6	Cell Signaling Technology, Massachusetts, USA	9762	1:1000 (WB)
Rabbit anti Caspase 8	Cell Signaling Technology, Massachusetts, USA	D35G2	1:1000 (WB)
Mouse anti human β-actin	Sigma-Aldrich, Steinheim, Germany	A5441	1:5000 (WB)
Mouse anti rat ED1	Serotec, Martinsried, Germany	MCA341R	1:50 (IF**)
Mouse anti rat ED2	Serotec, Martinsried, Germany	MCA342R	1:50 (IF)
Goat anti human vimentin	Sigma-Aldrich, Steinheim, Germany	V4630	1:100 (IF)

Mouse anti human α-smooth muscle actin	Sigma-Aldrich, Steinheim, Germany	A2547	1:100 (IF)
Rabbit anti *E.coli*	Abcam, Cambridge, UK	ab68451	1:300 (IF)
Rabbit anti HMGB1	Abcam, Cambridge, UK	ab18256	1:500 (WB) 1:200 (IF)
Rabbit anti AIF	***	-	1:100 (IF)
Mouse anti IkBa	Cell Signaling Technology, Massachusetts, USA	4814	1:1000 (WB)
Mouse anti p65	Santa Cruz, California, USA	SC8008	1:250 (WB) 1:50 (IF)

* WB: Western blotting

** IF: immunofluorescence staining

*** A gift from Dr. J. Landry (Laval University, Québec, Canada)

Table 3 Secondary antibodies for Western blotting and immunofluorescence staining.

Secondary antibody	Manufacturer	Catalogue No.	Dilution
Donkey anti mouse IgG-Cy3	Dianova, Hamburg, Germany	715-165-151	1:1000
Donkey anti rabbit IgG-Cy3	Chemicon, Hampshire, UK	AP182C	1:1000
Donkey anti goat IgG-HRP	Santa Cruz, California, USA	SC-2020	1:1000
Goat anti rabbit IgG -HRP	ICN, Ohio, USA	55676	1:10,000
Sheep Anti mouse -HRP	Sigma-Aldrich, Steinheim, Germany	A5906	1:10,000

2.1.5 Cell culture reagents

Bovine serum albumin (endotoxin free)	Invitrogen, Karlsruhe
Dulbecco's Minimal Essential Medium	PAA Laboratories, Cölbe
Dulbecco´s PBS (1X) w/o Ca^{2+} & Mg^{2+}	PAA Laboratories, Cölbe
Fetal calf serum	PAA Laboratories, Cölbe
L-Glutamine 200 mM (100X)	PAA Laboratories, Cölbe
Penicillin/Streptomycin (100X)	PAA Laboratories, Cölbe
RPMI 1640 medium	PAA Laboratories, Cölbe
DMEM (high glucose) medium	PAA Laboratories, Cölbe
Trypsin/EDTA	PAA Laboratories, Cölbe

2.1.6 Equipments

Cell culture CO_2 incubator	Binder, Tullingen
Confocal laser scanning microscope TCS SP2	Leica, Wetzlar
Desktop centrifuge Biofuge Fresco	Heraeus, Hanau
Labofuge 400R	Heraeus, Hanau
Electronic balance SPB50	Ohaus, Giessen
Zeiss EM 109	Zeiss, Oberkochen
Flow cytometry	BD FACScan, San Jose, USA
Fluorescent microscope Axioplan 2 Imaging	Carl Zeiss, Göttingen
Gel Jet Imager 2000 documentation system	Intas, Göttingen
Heat block DB-2A	Techne, Cambridge, UK
Horizontal mini electrophoresis system	PEQLAB, Erlangen
Microwave oven	Samsung, Schwalbach
Microplate reader	Berthold, Bad Wildbad
Mini centrifuge Galaxy	VWR International
Mini-rocker shaker MR-1	PEQLAB, Erlangen
Mixer Mill MM 300	Retsch, Haan
MyiQ^{TM}2 Two-Color real-time PCR detection system	Bio-Rad, Munich
PCR thermo cycler	Biozyme, Oldendor

Potter S homogenizer	B. Braun, Melsungen
Power supply units	Consurs, Reiskirchen
Pre-cast gel system	Invitrogen, Karlsruhe
SDS gel electrophoresis chambers	Consurs, Reiskirchen
Semi-dry-electroblotter	PEQLAB, Erlangen
Vertical electrophoresis system	PEQLAB, Erlangen
Ultrasonic homogenizer Bandelin Sonopuls	Bandelin, Berlin
UV visible spectrophotometer Ultrospec 2100 Pro	Biochrom, Cambridge, UK

2.1.7 Miscellaneous

Bio-Rad Protein Assay	Bio-Rad, Munich
DNA Ladder (100 bp)	Promega, Mannheim
DAPI	Vector, Burlingame, USA
Enhanced chemiluminescence (ECL) reagents	Amersham, Freiburg
Hybond ECL nitrocellulose membrane	Amersham, Freiburg
Protein size markers	Invitrogen, Karlsruhe
Sterile plastic ware for cell culture	Sarstedt, Nümbrecht
X-ray Hyperfilm	Amersham, Freiburg

2.1.8 Primers

All primers were designed by using “Primer BLAST” which is available online at http://www.ncbi.nlm.nih.gov/tools/primer-blast/. Primer sequences and annealing temperatures for PCR analysis are summarized in Table 4. All primers were purchased from MWG-Biotech (Ebersberg, Germany) and diluted in 1 X Tris-EDTA (pH 8.0) buffer to achieve a final concentration of 100 pmol/µl and stored as stock solution at -20°C.

Table 4 Information on forward (FP) and reverse primers (RP) used in quantitative realtime PCR.

Gene	Primer Sequences	Annealing Temperature	Accession No./Reference	Amplicon Size (bp)
ß2M	FP:5´-CCGTGATCTTTCTGGTGCTT-3´ RP:5´-AAGTTGGGCTTCCCATTCTC-3´	60°C	NM_012512	109
bcl-2	FP:5´-GGGATGCCTTTGTGGAACTA-3´ RP:5´-CTCACTTGTGGCCCAGGTAT-3´	59.6°C	NM_016993	138
bid	FP:5´-CGACGAGGTGAAGACATCCT-3´ RP:5´-AGACGTCACGGAGCAGAGAT-3´	59.6°C	NM_022684	119
bax	FP:5´-TGTTTGCTGATGGCAACTTC-3´	59.6°C	NM_017059	104
	RP:5´-GATCAGCTCGGGCACTTTAG-3´			
bim	FP:5´-AGATACGGATCGCACAGGAG-3´	59.6°C	NM_171989	148
	RP:5´-ACCAGACGGAAGATGAATCG-3´			
bak	FP:5´-GGGAAGACCCTCACCTTCTC-3´	59.6°C	NM_053812	142
	RP:5´-ACATTGCAACCAGATCCACA-3´			
UPEC P pili	FP:5´-GACGGCTGTACTGCAGGGTGTG GCG-3´	62.0°C	[193]	328
	RP:5´-ATATCCTTTCTGCAGGGATGCA ATA-3´			

2.2 Methods

2.2.1 Animals

19 day old immature Wistar rats (Charles River Laboratories, Sulzfeld, Germany) were purchased for Sertoli cell and peritubular cell isolation, while UPEC induced epididymo-orchitis model was established with 250~275 g adult male Wistar rats (Harlan, Borchen, Germany). The animals were housed in standard conditions (12 h light/dark cycle, 20~22°C), with free access to water and food. All experiments involving animals were carried out in strict accordance with the recommendations in

the Guide for the Care and Use of Laboratory Animals of the German law of animal welfare. The protocol was approved by the Committee on the ethics of Animal Experiments of the Regierungspraesidium Giessen, Giessen, Germany (permit number GI 20/23 –No. 16/2009). All surgery was performed under Ketamine and Xylazine anesthesia, and all efforts were made to minimize suffering.

2.2.2 Bacterial strains and propagation

Although there is a well known correlation between *E. coli* infection and male infertility, the specific strain involved have yet to be identified [90]. Previously the pathogenic *E. coli* from serotype strain (O6) was frequently employed in high concentrations for investigation of the detrimental effects on spermatozoa and for establishment of epididymitis model in rat [82,194]. Considering clinical relevance and availability of the full genomic sequence, UPEC strain CFT073 (serotype O6:K2:H1) was employed for *in vivo* and *in vitro* characterization in my study. Non-pathogenic commensal *E. coli* (NPEC) strain 470 served as a negative control stain in *in vitro* studies. HlyA is the main virulence factor accounting for acute prostatitis, and may also contribute to UPEC induced sperm membrane disruption identified in a series of *in vitro* studies [82,83,195]. To further explore the potentially deleterious effects of HlyA on testicular cells, various *E. coli* strains possessing distinct HlyA expression patterns were employed. UPEC represents strain CFT073 without statement in the whole experiment.

UPEC strain CFT073 (NCBI: AE014075, NC_004431) was obtained from Ulrich Dobrindt (University of Muenster, Germany). Another pyelonephritic UPEC strain 536 prevalent in UTIs with acquisition of two α-hemolysin (*hlyA*) determinants was obtained from the same group. NPEC strain 470 was obtained from microbial collection of the Institute of Medical Microbiology (University of Giessen, Germany). The mutant with deletion of both *hlyA* determinants in the UPEC 536 strain (*hlyA* double mutant = UPEC 536 HDM) and fosmid carrying clone FOS 22 that spans base pairs 3400446 ~ 3433092 of the CFT073 genome enclosing only one *hlyA* allele were constructed as previously described (Sudhanshu B et al. unpublished data).

All bacterial strains were propagated over night on Columbia blood agar plates (Oxoid, Wesel, Germany). Fosmid carrying clones were propagated in Lysogeny broth (LB) agar medium supplemented with 20 µg/ml Cloramphenicol. Fresh cultures were inoculated in LB medium and grown to early exponential phase (OD600 = 0.5~1.0) at 37°C in a shaking incubator. The concentration of viable bacteria was calculated using standard growth curves. Bacteria (2×10^9 cfu) were centrifuged at 4,500×g for 8 min at room temperature and the pellet was washed once with PBS and resuspended in 10 ml saline or RPMI 1640 medium. For *in vivo* experiments, the bacterial suspension was diluted with sterile saline to achieve 4×10^6 cfu bacteria in 100 µl. For *in vitro* experiment, bacterial suspension was prepared with the concentration of 2×10^8 cfu/ml. The volume of bacterial suspension employed could be scaled up or down depending on the number of cells. For example, 100 µl bacterial suspension were added in one well of a 6-well cell culture plate with 1 million cells (Multiplicity of infection, MOI = 20).

2.2.3 UPEC induced epididymo-orchitis rat model

The adult male Wistar rats (250~275 g) were anaesthetized with 50 mg/ml Ketamine and 2% Xylazine (v:v=7:3). After general anesthesia, the scrotum incision was made to expose the testis, epididymis and vas deferens. 100 µl of UPEC CFT073-saline suspension (about 4×10^6 bacteria) for each side was injected to the vas deferens using 30-gauge needles. As a control group, the same volume of saline was injected into the sham operated rats. The vasa deferentia were ligated at the site of injection to prevent spreading of infection. An injection was considered to be successful when the vas deferens dilatation followed by the cauda epididymis became transparent, and without leakage of the fluid from the site of injection. After operation, animals were kept in standard condition until being sacrificed.

Rats were killed with an overdose of isoflurane in the morning of day 7. Both testicles and epididymides were removed aseptically, followed with the measurement of the weight and volume of these organs. The testis and epididymis from one side were fixed in Bouin's fluid (75 ml picric acid solution + 25 ml 37% formaldehyde

solution + 5 ml acetic acid), and the organs from the other side were preserved at -80°C. Before placement of each testicle into fixative, the tunica albuginea was shallowly punctured at each pole 3 times with a 24-gauge needle to facilitate the penetration of fixative.

For sperm concentration measurement, the cauda epididymis was homogenized in 5 ml of saline and sperm counting was performed using a Neubauer® camera. This data was collected and kindly provided by Dr. Marcelo Marconi who took part in the establishment of this epididymo-orchitis model in our group.

2.2.4 UPEC detection in the testis

2.2.4.1 Detection of UPEC P pili gene expression in the testis using PCR

DNA was isolated from the testes of saline injected control animals and UPEC infected rats with QIAamp® DNA Mini kit (Qiagen, Venlo, The Netherlands). Up to 25 mg of frozen testis from each sample was minced into small pieces and collected in 1.5 ml Eppendorf tube. 180 µl ATL buffer and 20 µl proteinase K were added into the tube for incubation at 56°C in shaking block until tissue was completely lysed. To eliminate possible contamination of RNA, the sample was incubated for 2 min at room temperature with 4 µl RNase A (100 mg/ml). 200 µl AL buffer was added to the sample, followed by pulse-vortexing for 15 min and incubation at 70°C for 10 min. 200 µl ethanol (96~100%) was added to the sample and mixed by vortexing for 15 sec. The mixture was transferred to the QIAamp Mini spin column in a 2 ml collection tube. The column was centrifuged at 6082×g for 1 min and placed in a new collection tube. Then 500 µl AW1 buffer was added into the column for washing and followed by centrifugation at 6082×g for 1 min. Placed into a new collection tube, the column was washed again with 500 µl AW2 buffer and centrifuged at full speed (16060×g) for 1 min. QIAamp Mini spin column was placed in a fresh 1.5 ml collection tube; 200 µl AE buffer was added into it and incubated at room temperature for 1 min. The DNA was eluted by centrifugation at 6082×g for 1 min. After the measurement of DNA concentration with spectrophotometer, a certain amount of DNA sample was

diluted with DNA/RNase free water to generate an aliquot with concentration of 200 ng/µl. Together with specific primers (shown in Table 4), 1 µl of such an aliquot from each sample was used for further PCR reaction to detect the expression of UPEC P pili gene. The reaction system is described as below. The PCR product was electrophoresed on 1.5% agarose gel. DNA sample isolated from the testis into which UPEC suspension was directly injected served as a positive control.

Component	**Volume**
DNA (200 ng/µl)	1.0 µl
Forward Primer (10 pmol/µl)	0.5 µl
Reverse Primer (10 pmol/µl)	0.5 µl
2X Bio-Rad SYBR green mix	12.5 µl
DNA/RNase-free water	10.5 µl

2.2.4.2 Streaking of testis homogenate on agar plate

One testis from saline injected control and UPEC infected rat was homogenized in 10 ml sterile PBS with the sterile glass potter. 100 µl of the testis homogenate from each sample was streaked on agar plate and incubated overnight at 37°C. Bacterial colonies were checked the next morning under translucent light.

2.2.4.3 Fluorescent and electron microscopy for UPEC detection inside the testis

(described in 2.2.13 and 2.2.7, respectively)

2.2.5 Histopathology and Hematoxylin & Eosin staining

After fixation in Bouin's fluid for 24 h, the testes and epididymides samples were transferred into 70% ethanol which was changed 3~4 times every day until the yellow color of Bouin's fluid completely disappeared. Tissues were hydrated serially in 80%, 90% and 100% ethanol and stored in isopropanol overnight at 60°C before embedding in paraffin. Paraffin sections were prepared at 8 µm thickness.

Paraffin sections were kept in incubator for 30 min at 60°C before deparaffinized in 2 changes of xylene. After deparaffinization, sections were re-hydrated serially in

absolute ethanol (2 times with 10 min each), 90% (10 min), 80% (10 min), 70% (30 min) and 50% (10 min) ethanol, and then rinsed briefly in distilled water. Slides were immersed into Harris hematoxylin solution for 10 min, subsequently washed in distilled water for a while and differentiated in 1% hydrochloric acid for 30 sec, then immersed in 0.2% ammonia water for 30 sec to 1 min. After washing in running tap water for 10 min, sections were counterstained in 0.2% eosin Y solution for 30 sec to 1 min. Sections were washed in distilled water and followed by serial dehydration through 50%, 70%, 80%, 90% ethanol and absolute alcohol. Slides were cleaned in 3 changes of xylene (10 min each), and then mounted with xylene based mounting medium (Merck, Darmstadt).

2.2.6 TUNEL assay

DNA fragmentation in the testis was semi-quantitatively examined with Terminal deoxynucleotidyl transferase dUTP nick end labeling (TUNEL) assay, which is able to enzymatically label the free 3'-OH termini of DNA strand breaks associated with apoptosis.

Sections of frozen and paraffin embedded testis were pretreated differently before TUNEL assay. Cryosections of the testes were fixed with 1% paraformaldehyde-PBS (pH 7.4) in a coplin jar for 10 min at room temperature, and post-fixed in precooled ethanol: acetic acid, 2:1 (v:v) for 5 min at -20°C to permeabilize cells. Sections were washed 2 times with PBS before proceeding. Paraffin embedded testis sections needed to be deparaffinized with xylene, and subsequently re-hydrated serially in 100%, 95% and 70% ethanol. To eliminate unspecific binding of nucleotides or enzyme conjugate, paraffin sections were treated with freshly prepared proteinase K (20 μg/ml) for 15 min digestion at room temperature, followed by 2 times washing with PBS. A positive control sample was prepared from the testis sample by treating with DNase I as follows. The testis section was pretreated with DN Buffer (30 mM Trizma base, pH 7.2, 4 mM $MgCl_2$, 0.1 mM DTT) at room temperature for 5 min, followed by incubation with DNase I in DN Buffer (specific activity is 10,000 U/ml -

1,000 U/ml) for 10 min at room temperature. Section was ready for TUNEL assay after 5 times rinsing with dH_2O.

Excess liquid was carefully removed from sections; equilibration buffer was immediately added directly on the specimen for at least 10 sec at room temperature. Sections were subsequently incubated with working strength TdT enzyme (77 µl Reaction Buffer + 33 µl TdT Enzyme) in a humidified chamber at 37°C for 1 h. Then slides were washed with working strength/wash buffer (1 ml Stop/Wash Buffer + 34 ml dH_2O) and PBS to terminate the reaction. For visualizing DNA damage, sections were incubated with anti-Digoxigenin-fluorescein conjugated antibody [Blocking Solution: Anti-Digoxigenin Conjugate, 53:47 (v:v)] in a humidified chamber for 30 min at room temperature in dark. After briefly washing with PBS, sections were mounted with Vectashield® mounting medium containing DAPI (Vector Laboratories Inc, CA, USA). TUNEL positive cells were finally examined with Fluorescent microscope Axioplan 2 Imaging system (Carl Zeiss, Göttingen, Germany) using 512~542 nm filter.

2.2.7 Electron microscopy

Animals were anesthetized with 50 mg/ml Ketamine and 2% Xylazine (v:v=7:3) followed by perfusion with 0.9% NaCl plus Heparin (25000 IE/5ml) via left ventricle. A solution containing 2% glutaraldehyde and 2% formaldehyde in 0.1 mol/l sodium cacodylate buffer (pH 7.3) was used for fixation. The identical fixative additionally contained 1% lanthanum nitrate for demonstration of blood-testis barrier and blood-epididymis barrier. Specimens of the testes and epididymides (1 mm^3) were fixed in fixative for 1 h, and post fixed in 1% osmium tetroxide for 3 h. Tissue blocks were embedded in Epon 812 following dehydration. Semithin sections (1 µm) were stained with toluidine blue, mounted in Eukitt (Riedel-de Haen, Seelze, Germany) and imaged in light microscope. Ultrathin sections (60 nm) were double stained with uranyl acetate and lead citrate for electron microscopy examination

2.2.8 Isolation of Sertoli and peritubular cells

Medium:

PBS-A

500 ml PBS Dulbecco's without Ca^{2+} and Mg^{2+}

5 ml 100X Penicillin & Streptomycin

750 mg D-Glucose (dissolved in 5ml of PBS and solution was passed through a 0.20 µm filter into 500 ml PBS bottle)

Trypsin-DNase-Solution in PBS

10 ml PBS-A

25 mg Trypsin

200 µg DNase I

Trypsin inhibiter-Solution A in PBS-A

5 ml PBS-A

50 mg Trypsin inhibiter

Trypsin inhibiter-Solution B in PBS-A

10 ml PBS-A

25 mg Trypsin inhibitor

Collagenase-Hyaluronidase-DNase-Solution in PBS-A

10 ml PBS-A

10 mg Collagenase

10 mg Hyaluronidase

200 µg DNase I

Hyaluronidase-DNase-Solution in PBS-A

10 ml PBS-A

10 mg Hyaluronidase

200 µg DNase I

All enzyme solvents above were sterilized by passing through a 0.20 µm filter (SARSTEDT, Nuembrecht, Germany).

Sertoli cell culture medium

500 ml RPMI-1640 medium with L-glutamine

5 ml 100X Penicillin & Streptomycin

Peritubular cell culture medium

500 ml RPMI-1640 medium with L-glutamine

5 ml 100X Penicillin & Streptomycin

50 ml Fetal Bovine Calf Serum

Sertoli and peritubular cells were isolated from 19-day old Wistar rats. Ten young rats were sacrificed by cervical dislocation and the twenty testes were collected via abdominal incision and stored in 20 ml PBS-A. After disinfection with 1% iodine-ethanol, all testes were washed 2~3 times with PBS-A. Each testis was decapsulated by grasping one end with forceps and making a small incision on the tunica albuginea of the other end with a scissor. Seminiferous tubules were pushed out and digested with 10 ml Trypsin-DNase-Solution at 32°C in shaking water bath (120 oscillations/min) for 5~10 min. When seminiferous tubules were properly separated, trypsin digestion was terminated by adding Trypsin inhibitor solution A (10 mg/ml) and B (2.5 mg/ml) in sequence. Seminiferous tubules were washed 8 times with PBS-A to get rid of contaminating interstitial cells, followed by incubation with Collagenase-Hyaluronidase-DNase-Solution at 32°C in shaking water bath (120 oscillations/min) for 10~15 min. Incubation was stopped when peritubular cells were free from tubules. Tubular fragments were settled down and the supernatant enriched with peritubular cells was transferred to a new 50 ml falcon tube. Peritubular cells were collected by centrifugation at 280×g for 10 min and resuspended with RPMI 1640 medium (supplemented with 10% FCS). Cells were divided and seeded into 5 cell culture flasks (75 cm^2) and cultured at 37°C with 5% CO_2. On the 3rd day after cell isolation, peritubular cells were split and seeded into 10 flasks. Cell splitting was repeated every two days. Two days before experiments, 5×10^5 cells / well were plated into 6-well plates and cultured with 10% FCS RPMI 1640 medium. Before experiments peritubular cells were starved overnight by culture in RPMI 1640 medium with 1% FCS.

For Sertoli cell isolation, remaining tubular fragments were digested with 10 ml of Hyaluronidase-DNase-Solution at 32°C in shaking water bath (120 oscillations/min) for 8~10 min. To control the timing of digestion, the digested tubular fragments were monitored under the microscope. The digestion of tubules should be stopped when tubular fragments become very short and mainly consisting of individual cells. The fragmented tubules were further washed for 5 times with PBS-A to get rid of contaminating germ cells and PTC. After the last wash, SC enriched fraction was dispersed by passing through an 18G needle 10 times using a 20ml syringe. Cells were spinned down by centrifugation at 300×g for 10 min. The supernatant was discarded and cell pellet was resuspended in 15 ml RPMI 1640 medium. The cell suspension was subsequently filtered with 70 µm nylon filter (BD Falcon, NY, USA) to remove the undigested tubular fragments. 3×10^6 cells / well were seeded in 6-well plates and incubated at 32°C with 5% CO_2. Cell numbers were adapted for culture in 12-well and 24-well plates. To remove contaminating germ cells the hypotonic shock treatment was applied on the 3rd day of culture. Briefly, SC were rinsed two times with PBS and incubated with 20 mM Tris-HCl (pH 7.5) for 1 min. Again cells were washed twice with PBS and cultured for three more days in RPMI 1640 medium. On the 6th day SC was ready for experiments.

Purity of PTC and SC preparations was estimated > 95% by immunofluorescence using antibodies directed against α-smooth muscle actin (for PTC) and vimentin (for SC).

2.2.9 cDNA synthesis and quantitative real-time PCR (qRT-PCR)

2.2.9.1 Isolation of RNA

Total RNA was extracted from the testes of control and infected rats as well as from SC and PTC samples with RNeasy mini kit (Qiagen, Venlo, The Netherlands). About 20~30 mg frozen tissue from each testis sample was homogenized in 600 µl RLT buffer using a TissueLyser. When UPEC infection experiments were finished, the Sertoli and peritubular cells grown in culture plates were collected into up to 600

µl RLT buffer by using cell scrapers after twice washing with PBS. Cells clumps were disrupted by passing 5~10 times through a 21-gauge needle fitted to a 1 ml syringe. The lysate was centrifuged at 16,060×g for 3 min; the supernatant was transferred to a new Eppendorf tube and mixed with 1 volume of 70% ethanol thoroughly. Up to 700 µl of the mixture each time was transferred to an RNeasy spin column placed in a 2 ml collection tube for centrifugation at 16,060×g for 15 sec. The flow-through was discarded after every centrifugation and 700 µl RW1 buffer was added to the spin column to wash column membrane by centrifuging at top speed for 15 sec. The collection tube was emptied completely and 500 µl RPE buffer was added to the column. The spin column was centrifuged for 15 sec at 16,060×g. The RPE buffer washing step was repeated followed by a centrifugation at full speed for 2 min. To eliminate any possible carryover RPE buffer, the column was placed in a new 2 ml collection tube and centrifuged at full speed for 1 min. The RNeasy spin column was placed in a new 1.5 ml collection tube, 30~40 µl RNase-free water was directly added to the column membrane. The RNA was eluted by centrifuging at 16,060×g for 1 min. RNA concentration of each sample was measured with a spectrophotometer.

2.2.9.2 DNA digestion

Prior to RT-PCR amplification, putative contamination of genomic DNA was eliminated by DNase I (Invitrogen, CA, USA) treatment. Two µg RNA from each sample was treated with 2 µl DNase I at room temperature for 15 min in the reaction mixture given below. The DNase I was inactivated by addition of 2 µl of 25 mM EDTA (pH 8.0) solution to each sample and subsequent heating at 65°C for 10 min.

DNase digestion reaction mix:

Component	**Volume**
2 µg RNA	X µl
DNase I (1 U/µl)	2 µl
10 X DNase I buffer	2.0 µl
RNase free water	to 20 µl

To make sure RNA samples were free of DNA contamination, each DNase I digested RNA sample was amplified by standard PCR to detect the expression of housekeeping gene (beta-2-microglobulin, ß2M). The absence of PCR product was verified on agarose gel.

2.2.9.3 Reverse transcription

Reverse transcription of each DNase I digested RNA sample was carried out sequentially by using Moloney Murine Leukemia Virus Reverse Transcriptase (M-MLV RT) and Oligo (dT) 15 Primer (Promega, Wisconsin, USA). For each sample, 2 µg of RNA was mixed with 2 µl of Oligo (dT) 15 Primer in a reaction volume of 22 µl, and then denatured at 70°C for 10 min.

Denaturation of RNA and primer annealing:

Component	**Volume**
2 µg of DNase I digested RNA	20 µl
Oligo dT_{15}	2 µl

After denaturation, samples were snap chilled on ice for 2 min. A RT mix was prepared as below and added to RNA & Oligo (dT) primer mixture.

RT mix:

Component	**Volume**
5 X M-MLV RT buffer	8 µl
dNTP Mix (A,C, G and T, each 10 mM)	2 µl
RNAsin (RNase inhibitor, 40 U/µl)	1 µl
RNase-free water	6 µl

The samples were preheated at 42°C for 2 min. 1 µl of reverse transcriptase (M-MLV RNase H-minus, 200 U/µl) was subsequently added to each sample in a total reaction volume of 40 µl. The reaction mix was incubated at 42°C for 75 min, followed with inactivation of reverse transcriptase by incubating samples at 72°C for 15 min. cDNA Samples were stored at -20°C.

2.2.9.4 Quantitative realtime PCR

The reagents of qRT-PCR differ from a normal PCR with addition of the double strands DNA (dsDNA) specific fluorescent reporter probes (such as SYBR green in this project). The reporter probes are able to bind to all dsDNA during polymerization and emit fluorescence. The increasing fluorescence signal that corresponds to the exponential increase of DNA product in each cycle can be detected and recorded in the real-time PCR thermocycler, which is used to determine the threshold cycle (Ct) value and facilitates quantifying gene expression.

For the detection of bcl-2, bid, bax, bim and bax expression, primers pairs were designed by "Primer BLAST" and synthesized by Eurofins MWG Operon. Gradient PCR was employed to determine the optimal annealing temperature for individual genes. The detailed information of these primers is shown in Table 4. The amplification efficiencies of these primers were estimated by the dilution method. All primers' efficiencies were between (100 ± 15)%. A typical 25 µl qRT-PCR reaction mix is described below.

Component	**Volume per reaction**
cDNA	1 µl
2X iQ SYBR green supermix	12.5 µl
Forward and reverse primer mix (10 pM/µl)	1 µl
DNase/RNase free water	10.5 µl
Total volume	**25 µl**

Realtime PCR amplification with iQ™ SYBR® Green Supermix was performed in triplicate by using the iCycler iQ® System (Bio-Rad, CA, USA) according to manufacturer's procedure. Cycling conditions were described as below: after an initial activation step at 95°C for 8 min, 45 cycles of denaturation (95°C for 20 sec), annealing (see Table 4), and extension (72°C for 30 sec) were performed.

The PCR products were examined using agarose gel electrophoresis for specific amplification. The relative quantification of PCR products was determined by the

comparative Ct method. The target genes expression is normalized to the non-regulated reference gene ß-2 microglobulin (ß2M).

2.2.9.5 Agarose gel electrophoresis

6 X gel loading buffer with Bromophenol blue

0.25% (w/v) Bromophenol blue

30% Glycerol in H_2O

50 X TAE electrophoresis buffer (1L, pH 8.0)

242 g of Tris base

57.1 ml of glacial acetic acid

100 ml of 0.5 M EDTA

1X TE buffer

10 mM Tris-HCl pH 8.0

1 mM EDTA

Ethidium bromide (0.5 µg/ml)

2.2.10 MTT assay for cell viability measurement

To determinate the cytotoxic effect of bacterial (UPEC CFT073, UPEC 536, NPEC 470, UPEC 536 HDM and FOS 22) infection, the viability of SC and PTC was measured with MTT [3-(4, 5-Dimethylthiazol-2-yl)-2, 5-diphenyltetrazolium bromide] assay. After 2 h bacterial treatment, cells were washed two times with pre-warmed MEM medium without phenol red. 0.5 mg/ml MTT working solution (in MEM medium) was added into wells being assayed (0.5 ml for each well of 24-well plate) for 1.5 h at 37°C. During this period, formazan crystals formed only within living cells, which indicating cell metabolic activity. Then 0.5 ml of DMSO was added to each well and mixed thoroughly to dissolve all the dark blue crystals at the bottom of each well. The absorbance is read by spectrophotometer, using 570 nm as test wavelength and 650 nm as the reference wavelength. The absorbance proportionally corresponding to cell viability and the result is expressed as a ratio of the treated cells compared to the untreated control: (A_{570} –A_{650}) of treated cell/ (A_{570} –A_{650}) of non-treated cells ×100%.).

2.2.11 Annexin V/PI staining

As an early event of apoptosis, the membrane phospholipid phosphatidylserine (PS) is translocated from the inner to the outer leaflet of apoptotic cell membrane, indicating the loss of plasma membrane. Annexin V is a phospholipid binding protein which has a high affinity for PS. Fluorochromes conjugated Annexin V retains such a binding affinity and can serve as a sensitive probe for quantitative analysis of apoptotic cells. Early apoptosis in SC and PTC after infection was evaluated by measuring the exposure of PS on the cell membranes by using FITC Annexin V apoptosis detection kit I (BD Biosciences, NJ, USA). After bacterial infection, cells were rinsed twice with PBS, and detached with Trypsin-EDTA. Cells were subsequently resuspended in 1 X working buffer at a concentration of 1×10^6 cells/ml. 100 µl of cells suspension was transferred to 5 ml culture tube and mixed with 2.5 µl of Annexin V and 2.5 µl propidium iodide (PI). The cells suspension was gently vortexed and incubated for 15 min in dark. After incubation, 400 µl of 1 X binding buffer was added to each tube to stop to the reaction. The population of Annexin V positive cells was evaluated by flow cytometry (BD FACScan, Becton Dickinson Immnunocytometry Systems, CA, USA) within 1 h. Samples were gated on the basis of forward versus side scatter for size, and the results are presented as the percentage of cells those were viable (Annexin V^- PI^-), early apoptotic (Annexin V^+ PI^-), late apoptotic or necrotic (Annexin V^+ PI^+) and damaged (Annexin V^- PI^+).

2.2.12 Immunoblotting

2.2.12.1 Buffers and solutions

10 X Tris buffered saline (TBS)

24.2 g Tris base

80 g NaCl

Dissolved in 1L water, pH to 7.4 with HCl

Washing buffer TBS/T

1 X TBS

0.1% (v/v) Tween-20

30% Acrylamide solution

Acrylamide/Bisacrylamide =37.5:1

RIPA buffer

25 mM Tris-HCl pH 7.6

150 mM NaCl

1% NP-40

1% Sodium deoxycholate

0.1% SDS

100 X Proteinase inhibitor cocktail (Sigma) *

* Added fresh just before cell lysis

Protein gel sample loading buffer

50 mM Tris-HCl; pH 6.8

2% SDS

10% Glycerol

1% β-Mercaptoethanol

12.5 mM EDTA

0.02 % (w/v) Bromophenol Blue

10 X Phosphate buffered saline (PBS)

4 g KCl

4 g KH_2PO_4

160 g NaC

23 g $Na_2HPO_4 * H_2O$

Dissolved in 1L H_2O, pH to 7.4 with HCl

Blocking buffer

0.1 ml Tween-20

5 g Non fat dry milk

100 ml 1 X TBS

10 X Electrophoresis buffer (pH 8.3)

30.3 g Tris base

144 g Glycine

10 g SDS

Dissolved in 1L water, set pH to 8.3 with HCl

Stripping buffer

6.25 ml 1 M Tris HCl

2 ml 10% SDS

700 µl β-mercaptoethanol*

Make volume up to 100 ml with water

* Added freshly just before stripping of membrane

Cathode buffer

25 mM Tris

40 mM 6-amino-hexanoic acid

20% (v/v) Methanol

10 X Anode buffer

300 mM Tris

20% (v/v) Methanol

1 X Anode buffer

30 mM Tris

20% (v/v) Methanol

Separating gel:

	7.5%*	10%*	12.5%*	15%*
Water	4.85 ml	4.01 ml	3.17 ml	2.35 ml
1.5 M Tris-HCl pH 8.8	2.5 ml	2.5 ml	2.5 ml	2.5 ml
10% (w/v) SDS	100 µl	100 µl	100 µl	100µl
Acrylamid	2.5 ml	3.34 ml	4.17 ml	5 ml
10% (w/v) APS**	50 µl	50 µl	50 µl	50 µl
TEMED	5 µl	5 µl	5 µl	5 µl
Total	10 ml	10 ml	10 ml	10 ml

Stacking gel:

	4%*
Water	3 ml
0.5 M Tris-HCl pH 6.8	1.25 ml
10% (w/v) SDS	50 µl
Acrylamide	0.65 ml
10% (w/v) APS**	25 µl
TEMED	5 µl
Total	5 ml

* Separating gels with different percentages were used according to the molecular weight of target proteins (based on 37.5:1 acrylamide/bisacrylamide ratio). 7.5% gel: 250~120 kDa; 10% gel: 120~40 kDa; 12.5% gel: 40~15 kDa; 15% gel: < 20 kDa.

** Ammoniumpersulfate (APS) was prepared fresh before each experiment.

2.2.12.2 Western blotting

After treatment with bacteria, cells were harvested by scraping them into RIPA lysis buffer (25 mM Tris-HCl pH 7.6, 150 mM NaCl, 1% NP-40, 1% Sodium deoxycholate and 0.1% SDS) supplemented with proteinase cocktail inhibitor. The concentration of protein in cell lysates was determined by the Bradford Method (Bio-Rad, Munich, Germany). Thirty µg protein of each sample was resolved on SDS-polyacrylamide gel and protein was electrophoretically transferred onto a 0.2 µm pore size nitrocellulose membrane (Hybond™ ECL™, GE Healthcare, UK) by using a PerfectBlue™ semidry electroblotter (PeqLab Biotechnologie, Germany). The nonspecific binding sites were blocked by incubating the membranes in 5% non-fat

milk in Tris-buffered saline (TBS) with 0.1% Tween (TBS-T) for 1 h at room temperature. The membranes were subsequently incubated with primary antibodies (Table 2) in blocking solution overnight at 4°C and then rinsed three times with TBS-T. Membranes were incubated with anti-mouse or anti-rabbit antibody conjugated with HRP (Table 3) for 1 h at room temperature and then rinsed three times with TBS-T for 10 min. Immunoreactive proteins were detected using an ECL Kit (Immobilon^{TM} Western Chemiluminescent HRP substrate, Millipore corporation, Billeria, MA, USA), according to the manufacturer's instructions.

2.2.13 Immunofluorescent staining

10 µm thick frozen tissue sections or cells grown on coverslips were fixed with precooled 4% PFA for 20 min. Then samples were permeabilized with 0.2% Trition-X 100 at room temperature. After 3 times washing with PBS, tissue sections or cells were incubated with blocking agent (5% BSA + 5% normal horse/sheep serum) for 1 h at room temperature, followed by incubation with primary antibodies (Table 2) at 4°C overnight. Samples were rinsed thoroughly and incubated with anti rabbit or anti mouse Cy-3 conjugated secondary antibody (Table 3) with 1:1000 dilution for 1 h at room temperature in dark. For confocal microscopy analysis, cell nuclei were counterstained with Cy5-conjugated To-Pro-3 (Invitrogen, Karlsruhe) for 15 min. Slides or cells were washed 3 times with PBS for 5 min each, and then mounted with Vectashield ® mounting medium containing DAPI. Samples were finally examined with Fluorescent microscope Axioplan 2 Imaging system or TCS SP2 confocal scanning microscope (Leica Microsystems, Wetzlar, Germany).

2.2.14 Calpain activation analysis

7-amino-4-chloromethylcoumarin, t-BOC-L-leucyl-L-methionine amide (CMAC, t-Boc-Leu-Met) is a cell-permeable fluorogenic calpains substrate, which can emit blue-fluorescence with excitation/emission at 351/430 nm after cleaved by activated calpains. SC and PTC cultured on cover slides were pre-incubated for 30 min with 50 mM and 100 µM of this calpain substrate in RPMI 1640 medium, and then cells were

treated with UPEC (MOI = 20) for 30 min. Calpain activation within cells was observed in a Zeiss fluorescence microscope with filter of 420~460 nm wavelength.

2.2.15 Reactive oxygen species (ROS) level measurement

H2DCF-DA (2', 7'-dichlorodihydrofluorescein diacetate) is a cell-permeable indicator for ROS, which is non-fluorescent until the acetate groups are removed by intracellular esterases and oxidation occurs within the cell.

To detect the ROS production in UPEC infected SC and PTC, cells were pretreated with 10 μg/ml H2DCF-DA for 30 min. The medium was replaced with fresh culture medium without antibiotic and cells were treated with UPEC CFT073 or NPEC 470 (MOI = 20) for different time points. After infection, cells were detached with Trypsin-EDTA and suspended in PBS at a concentration of 1×106 cells/ml. 500 μl cell suspension of each sample was prepared in culture tube for flow cytometry analysis.

2.2.16 Intracellular ATP determination

Intracellular ATP release from SC and PTC cells were determined by luciferin-luciferase assay using a bioluminescence analyzer. Bioluminescence determination of ATP was performed by using ATP assay mix and dilution buffer. ATP assay mix contains luciferase and luciferin. ATP assay mix dilution buffer contains $MgSO_4$, DTT, EDTA, bovine serum albumin and tricine buffer salts. The basic principle of this reaction can be explained by the below equation:

$$\text{ATP + Luciferin} \underset{Mg^{2+}}{\overset{\text{Firefly luciferase}}{\rightleftharpoons}} \text{Adenyl-luciferin + PPi} \quad \textbf{(1)}$$

$$\text{Adenyl-luciferin + } O_2 \longrightarrow \text{Oxyluciferin + AMP + } CO_2 \text{ + light} \quad \textbf{(2)}$$

Reaction (1) is reversible and reaction (2) is irreversible. The light emitted is proportional to ATP present in the sample.

SC and PTC grown to confluence in 12 well plates were treated with UPEC CFT073 (MOI = 20) for up to 4 h. Each hour cells were washed to remove excess of bacteria. After treatment cells were washed 3 times with PBS and subsequently lysed with 150 µl of boiling lysis buffer (100 mM Tris-HCl, pH 7.75, 4 mM EDTA) and boiled for an additional 2 min to inactivate ATPase. Lysates were then centrifuged at 3600×g to remove cell debris and the supernatants were kept on ice for measurement. ATP levels were assayed using an ATP Bioluminescent Assay kit (Sigma), where 100 µl of luciferase reagent mix (50 µl of ATP assay mix + 1.5 ml of ATP assay mix dilution buffer) was added to 100 µl of lysate by automated injection and the luminescence read immediately with 1 sec integration, using a microplate reader (Berthold, Bad Wildbad, Germany). Intracellular ATP level of the untreated cells lysate was set to 100% and those of infected samples were normalized with of the untreated control sample.

2.2.17 Isolation and analysis of genomic DNA degradation

Cell lysis buffer

50 mM Tris-HCl (pH 8.0)

400 mM NaCl

100 mM EDTA

0.5% SDS

0.5 mg/ml proteinase K*

* Added fresh before digestion

Proteinase k (20 mg/ml) stock solution

20 mg of proteinase K was dissolved in sterile 1 ml solution with 50 mM Tris (pH 8.0) and 1.5 mM calcium acetate to get a concentration of 20 mg/ml.

RNase A (10 mg/ml) stock solution

10 mg RNase A was dissolved in 0.9 ml of 0.01 M sodium acetate (pH 5.2). The solution was heated to 100°C for 15 min to inactivate potentially contaminated DNase. After cooling down to room temperature, pH was adjusted by adding 0.1 ml of 1 M Tris-CI (pH 7.4).

6 X DNA loading buffer with Orange G

1% (w/v) Orange G

40% sucrose

After bacterial treatment, cells were washed once with PBS and harvested by centrifugation at 856×g for 5 min. The cell pellet or minced testis tissue was resuspended in lysis buffer (50 mM Tris-HCl; 400 mM NaCl; 100 mM EDTA; 0.5% SDS; 0.5 mg/ml proteinase K, pH 8.0) and incubated overnight at 55°C in a shaking heating block (1000 rpm). 1/3 volume of 5 M NaCl was added to each sample and followed by vigorous shaking for 15 sec. The precipitated protein was spinned down by centrifugation at 16060×g for 5 min. The supernatant containing nuclear acid was transferred to new 1.5 ml Eppendorf tubes and mixed properly with 1 volume of 100% ethanol. The DNA was then precipitated by centrifugation at 16060×g for 5 min and the pellet was washed with 70% ethanol. After subsequent centrifugation for 5 min at highest speed, ethanol was removed and the tubes were placed with open lids in the heating block at 37°C for 10~15 min for air drying. The DNA samples were dissolved in 1 X TE buffer (10 mM Tris-HCl, 1 mM EDTA, pH8.0) and treated with 100 µl/ml DNase-free RNase A at 37°C for 1 h. Again DNA was precipitated and redissolved in TE buffer. Concentration of DNA samples was measured with spectrophotometer and equal amount of DNA samples were electrophoretically separated on 1.5% agarose gels and stained with ethidium bromide.

A positive apoptosis control for DNA laddering was generated by treating RAW 264.7 macrophage with 0.5 mM H2O2 for 24 h. Necrosis on RAW 264.7 macrophage was induced by repeated freeze – thaw cycles, which can cause random DNA degradation and results in “DNA smear” on agarose gel.

2.2.18 Hoechst 33342 staining

Hoechst 33342 is a fluorescent stain for labeling DNA and therefore commonly used to visualize nuclei structure. To observe the nuclei structure changes in infected SC and PTC, cells were seeded on coverslips in 24-well plates for bacteria experiments. After bacterial infection cells were washed two times with PBS and

incubated with Hoechst 33342 (1:500 in 1% BSA) at 37°C for 10 min. Then cells were again washed briefly with PBS and the cover slips were mounted on slides with glycerol. Nuclear structure was evaluated with Zeiss fluorescent microscope with the filter of 420~460 nm wavelength.

2.2.19 Caspase-3 enzyme activity assay

During cell death by apoptosis, activated caspase-3 recognizes the amino acid sequence Asp-Glu-Val-Asp (DEVD) within the DNA repairing enzyme PARP1 [poly(ADP-ribose) polymerase 1] and cleaves this DEVD sequence, resulting the inactivation of PARP1. The DEVD labeled with the chromophore p-nitroaniline (pNA) can still be specifically recognized and cleaved by caspase-3 and is widely used as a colorimetric substrate (DEVD- pNA) for this enzyme activity assay. After cleavage from DEVD- pNA, the light emission from pNA can be detected by spectrophotometer at 400 nm, the intensity of which is corresponding to the activity of caspase-3. To make sure whether UPEC infection caused caspase-3 activation or just degradation in PTC, the caspase-3 activity was measured with the Caspase-3/CPP32 Colorimetric Assay Kit (BioVision, CA, USA) based on the principle described above. Briefly, about 3 × 106 PTC of each sample were collected after UPEC treatment and resuspended in 50 µl of ice cold Cell Lysis Buffer. After 10 min incubation on ice, the samples were centrifuge at 10,000×g for 1 min. The supernatant was transferred into a fresh tube and the protein concentration was determined with Bradford assay. 100 µg of protein from each sample was diluted with Cell Lysis Buffer to 50 µl and mixed with 50 µl of 2X Reaction Buffer containing 10 mM DTT. 5 µl of 4 mM DEVD- pNA substrate was added into each sample and incubated at 37°C for 2 h. All samples were transferred into a 100-µl micro quartz cuvette and the absorbance was measured with a spectrophotometer at 400 nm. The caspase-3 activity was present as the optical density (OD_{400}).

3 RESULTS

3.1 Morphological changes in the epididymis and testis of UPEC infected rat

A UPEC induced *in vivo* epididymo-orchitis rat model was successfully established by injecting UPEC strain CFT073 bilaterally in vasa deferentia. Seven days after infection, swollen caudae epididymides, atrophic and inflamed testes with increased vascularization and vasocongestion were observed in UPEC injected rats (Figure 3A). Accordingly, the weight of bilateral testes was decreased about 30% in UPEC infected rats compared to the saline injected control animals (left: 1.02 ± 0.28 vs. 1.63 ± 0.09 g; right: 1.09 ± 0.36 vs. 1.61 ± 0.10 g, $p < 0.001$; Figure 3 B).

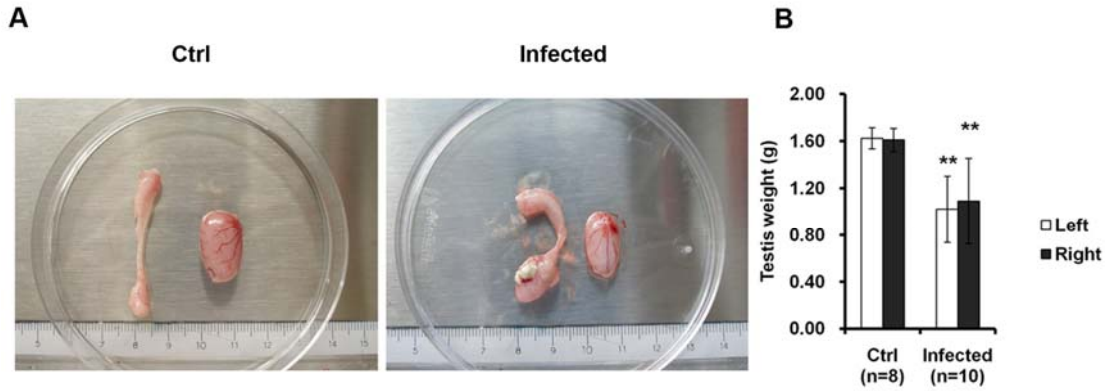

Figure 3 Morphological changes of the epididymis and testis in the rat epididymo-orchitis model. (A) A typical appearance of epididymides and testes from saline injected (left panel) and UPEC infected rats (right panel) are shown. **(B)** The testicular weight of control (n=8) and infected rats (n=10) are presented as mean ± standard deviation (SD). Student's t-test was employed for statistical analysis and the levels of significance is indicated as ** $p < 0.001$.

3.2 UPEC invasion inside the testis

To confirm that UPEC is able to reach the testis by ascending canalicular infection originating at the vas deferens, a number of techniques were applied to verify the presence of bacteria inside the testis, which include UPEC specific gene detection using PCR, streaking of testicular homogenate on agar plates to detect bacterial growth, fluorescent microscopy examination of infected tissues using an *E. coli* specific antibody and electron microscopical examination. The results of all named approaches demonstrated the presence of UPEC in testes on day 7 after bacterial injection (Figures 4~6). DNA isolated from testes was amplified by PCR to detect the gene expression of UPEC P pili. A specific band with the size of 328 bp on agarose gel was visible only in the samples of infected testes and the positive control (Figure 4A). Furthermore, streaking testicular homogenates on agar plates followed by overnight incubation revealed numerous yellowish-white translucent bacterial colonies exclusively in infected testes samples (Figure 4B).

Moreover, fluorescent and electron microscopy were employed to further explore the localization of UPEC inside testis (Figures 5 and 6). Intriguingly, the bacteria labeled with anti-*E. coli* antibody were mainly observed in testicular compartment but rarely found inside the lumen of the seminiferous tubules (Figure 5). In agreement, electron microscopy examination also confirmed the presence of *E. coli* inside the interstitial space of infected testis (Figure 6).

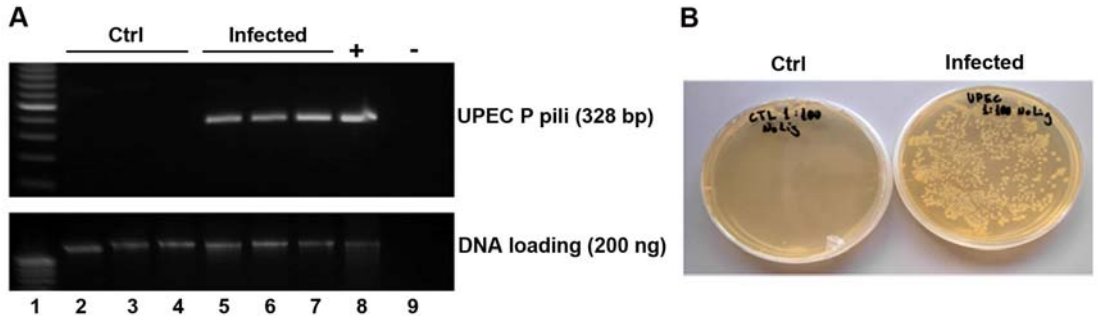

Figure 4 Presence of UPEC inside testes of infected rats on day 7 after bacterial injection in the vas deferens. (A) The genomic DNA was extracted from testicular tissue and 200 ng DNA from each sample were amplified with PCR using UPEC P pili primers. DNA isolated from one testis with direct UPEC injection served as a positive control. The PCR products were separated on 1.5% agarose gel and

stained with ethidium bromide. The same amount of DNA from each sample without PCR amplification was subjected to agarose gel electrophoresis and served as a loading control. Lane 1: 100 bp DNA marker (Promega, Mannheim); Lane 2~4: samples from saline injected animals; Lane 5~7: samples from UPEC infected rats; Lane 8: positive control; Lane 9: negative control. **(B)** Testes from saline injected (left panel) and UPEC infected rats (right panel) were homogenized in PBS, the homogenate were subsequently streaked on agar plates without antibiotics and kept at 37°C. After overnight incubation colonies were counted under translucent light.

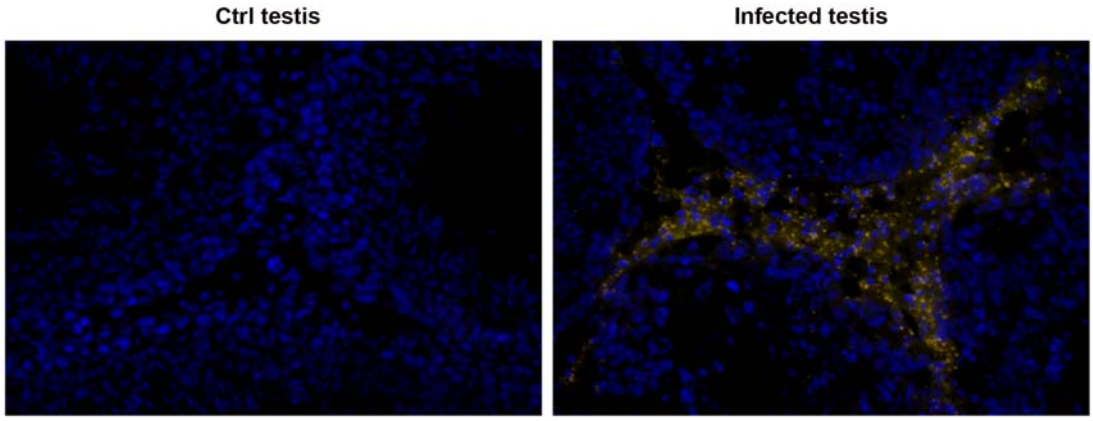

Figure 5 Fluorescent microscopy examination reveals the location of UPEC in infected testis. Cryosections of testes from control (left panel) and UPEC infected rats (right panel) were incubated with anti-*E. coli* antibody overnight and then stained with secondary anti-rabbit IgG antibody conjugated to Cy-3 (Orange). The nuclei were counterstained with DAPI (Blue). Images were captured using fluorescent microscope Axioplan 2 Imaging system at original magnification X200.

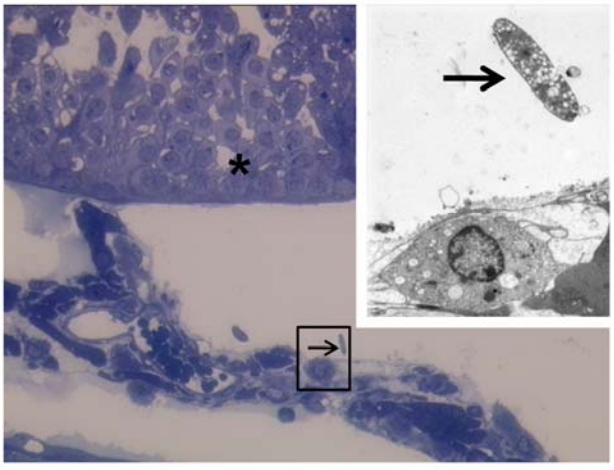

Figure 6 Presence of UPEC in the interstitium of infected testis. A semithin section of infected testis shows a part of seminiferous tubule (asterix) with the adjacent interstitial compartment. A bacterium is pointed with an arrow in the black frame; primary magnification X200. Inset: Electron microscopic examination on an ultrathin section shows the same bacterium in the identical area framed on the semithin section; primary magnification X3000.

3.3 The integrity of BTB and BEB in UPEC infected rats

The results above (Figure 5 and 6) suggest that UPEC are able to migrate through the seminiferous tubules and reach the interstitial space of testis within 7 days. To explore whether UPEC crossed the tubular epithelium by disrupting the junctional structures in the testis (BTB) and epididymis (BEB), ultrathin sections from infected testes (Figure 7A) and epididymides (Figure 7B) were examined with electron microscopy. Surprisingly, the integrity of both junctional complexes was not affected by UPEC invasion, as indicated by the lanthanum tracer application which did not pass beyond the tight junctions of BTB and BEB after perfusion. These results suggest that UPEC may employ other invasion strategies than permanently compromising the integrity of BTB and BEB, although the exact mechanism remains elusive.

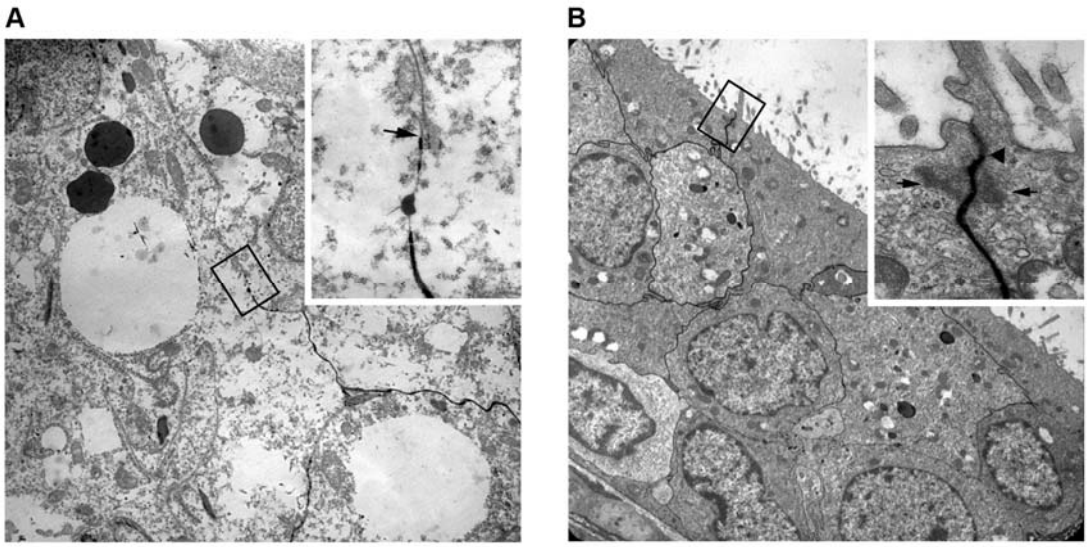

Figure 7 Electron microscopical examination of the blood-testis barrier (BTB) and blood-epididymis barrier (BEB). (A) Ultrathin tissue section from a UPEC infected testis shows the tracer penetration within the seminiferous epithelium at X3000 magnification. Inset is the identical area of the black frame at X20000 magnification showing that tracer penetration stopped at BTB tight junctions (arrow). **(B)** Ultrathin section from a UPEC infected epididymis demonstrates tracer penetration at epididymal epithelium at X3000 magnification. Inset indicates a BEB junctional complex consisting of a desmosome (arrow) and tight junctions (arrowhead) in the identical area represented in the black frame at X20000 magnification.

3.4 Histological changes in the testis following UPEC infection

To investigate the impairment caused by UPEC infection, Hematoxylin & Eosin (H&E) stained sections from testes and epididymides were evaluated using light microscopy. The sections of cauda (Figure 8A, left panel) and caput epididymis (Figure 8B, left panel) from saline injected rats show a normal appearance of the tubular epithelium and interstitium with lumens full of spermatozoa. In striking contrast, severe interstitial fibrosis, inflammatory cell infiltration and numerous immature germ cells present inside the lumen were observed in infected cauda epididymis close to the site of bacterial injection (Figure 8A, right panel). Immature germ cells sloughed from testis into the lumens of caput epididymis indicates a detrimental effect of UPEC on spermatogenesis (Figure 8B, right panel). Histopathological examination revealed that spermatogenesis was affected to different degrees in neighboring seminiferous epithelium in UPEC infected testis, while it was completely normal in saline injected control animals (Figure 9). In sections from infected testes, 42.5% of seminiferous tubules were not affected; in 19.0% of tubules spermatogenesis proceeded up to elongated spermatid without spermatozoa; in 10.1% of tubules germ cells developed until round spermatid; 20.9% of tubules present spermatogenesis ceased at the stage of spermatocyte; whilst in the remaining tubules (about 7.5%) there were only a few spermatogonia and SC present in germinal epithelium, without any other stages of germ cells (Figure 9, right panel).

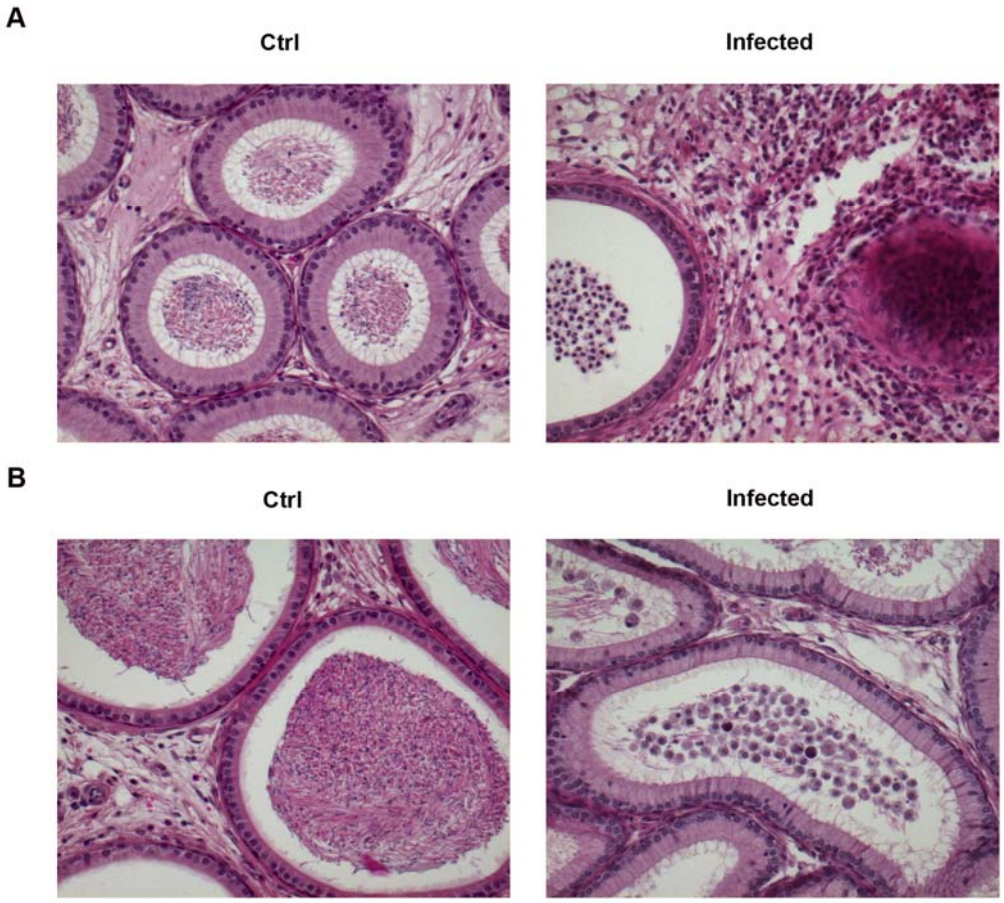

Figure 8 Histological changes in the cauda (A) and caput (B) epididymis. Tissue sections of paraffin embedded epididymides were stained with hematoxylin and eosin. Histopathological images were captured using Axioplan 2 Imaging system at magnification X200. Representative results from control (n = 5) and infected (n = 9) rats are shown.

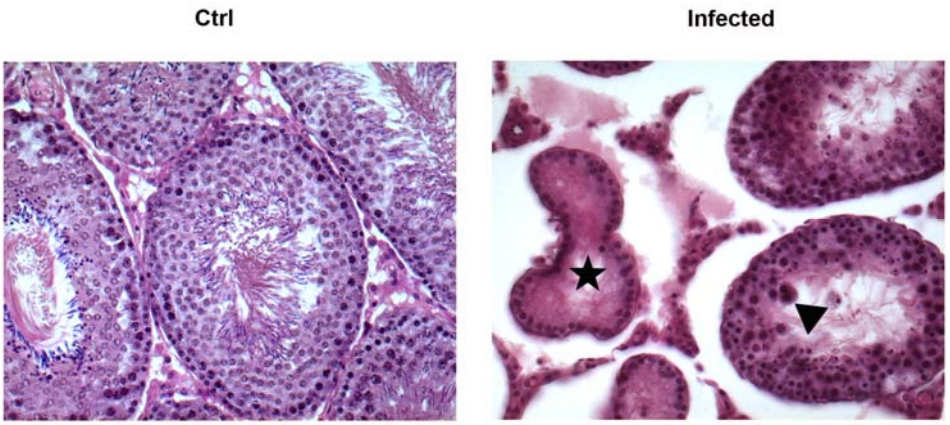

Figure 9 Histological changes in the testis on day 7 post injection. Tissue sections of paraffin embedded testes were stained with hematoxylin and eosin. Histopathological assessment was performed on control (n = 5) and UPEC infected (n

= 9) testes using light microscopy. The images were captured using Axioplan 2 Imaging system at magnification X200 and representative figures are shown. An affected seminiferous tubule with arrest of spermatogenesis at the stage of primary spermatocyte is labeled with a pentacle; a tubule with multinucleated germ cells is labeled with a triangle.

3.5 Sperm concentration on day 7 post infection

Consistent with the results of the histopathological analysis demonstrating germ cell loss in infected testes, the concentration of spermatozoa retrieved from the cauda epididymis was found to be significantly decreased on day 7 after infection (Figure 10) compared to control rats (100.2 ± 56.8 × 10^6 vs. 249.8 ± 111.6 × 10^6/g tissue, $p < 0.05$).

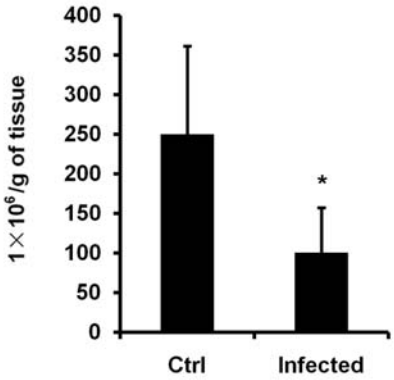

Figure 10 The concentration of sperm retrieved from the cauda epididymis. Sperm concentration was assessed in seven animals of each group and the results are presented as mean ± SD. Statistical analysis was performed with Student's t-test and statistical significance is denoted as * $p < 0.05$.

3.6 DNA damage in germ cells caused by UPEC infection

Since apoptosis is the dominating mechanism in regulating germ cell death under normal conditions, it was initially explored whether apoptosis was implicated in UPEC induced impairment of spermatogenesis and germ cell loss in epididymo-orchitis model. Therefore, TUNEL assay was carried out to detect DNA damage of testicular cells. The results (Figure 11) indicate that the number of TUNEL positive cells increased more than 20 folds in infected testes compared to controls (8.05 ± 2.99/tubule vs. 0.34 ± 0.07/tubule, $p = 0.001$). Moreover, the typical ring type chromatin aggregation under the nuclear membrane (early stage of apoptosis-like nuclei) [196] was also observed in some TUNEL positive cells (Figure 11, arrows). Of

note, there were a few TUNEL positive cells that lack the typical apoptotic ring-like nuclear structure, which might suggest that they were either at a different stage of apoptosis or undergoing necrosis. Strikingly, the majority of the TUNEL positive cells located within the seminiferous epithelium appeared to be germ cells.

A

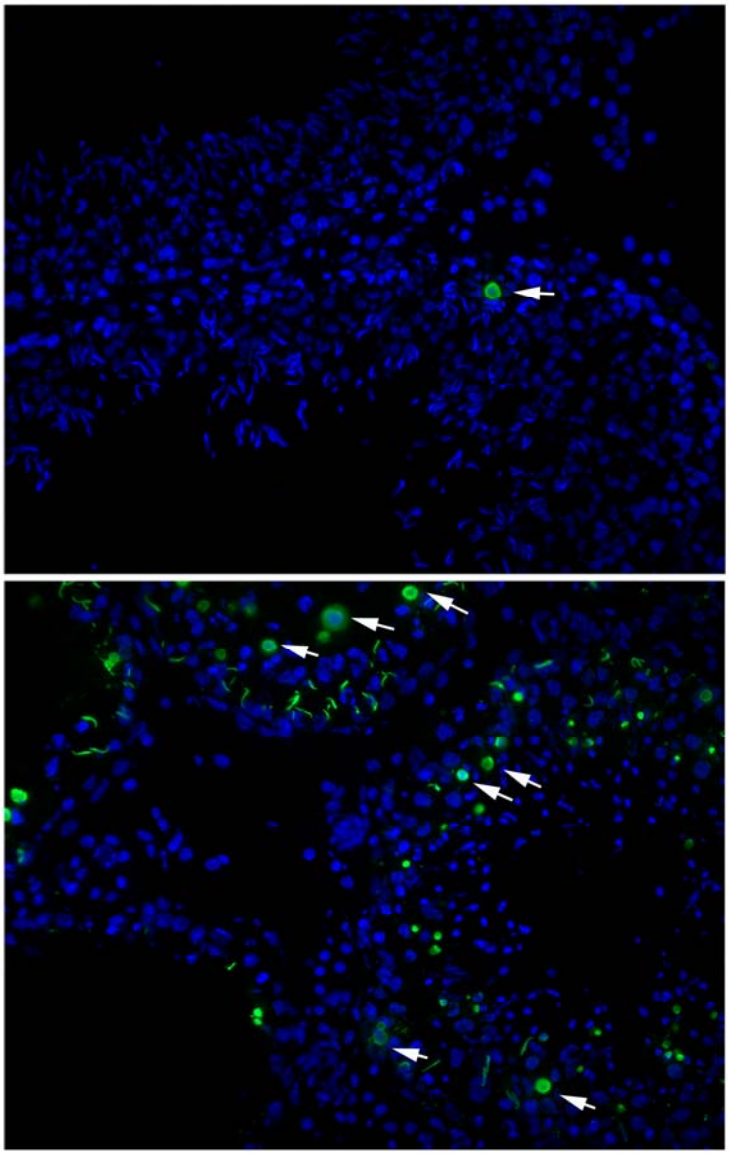

B

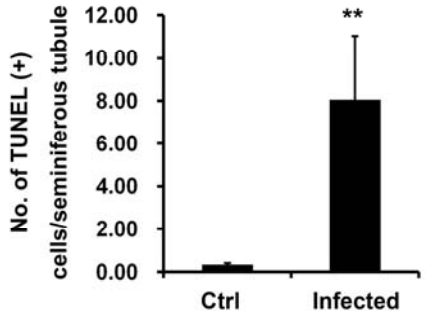

Figure 11 TUNEL assay on cryosections of testes. (A) DNA strand breakage in testicular cells from control (upper panel) and UPEC infected (lower panel) rats were labeled with digoxigenin-nucleiotide and subsequently stained with anti-digoxigenin-fluorescein conjugated antibody (Green). The nuclei were counterstained with DAPI (Blue). The results were evaluated using Axioplan 2 Imaging system and photographed at X200 magnification. The TUNEL (+) cells with ring-like nuclei are indicated with arrows. **(B)** The numbers of TUNEL (+) cells are presented as mean ± SD/seminiferous tubule. Student's t-test was used for statistic analysis and the level of significance is indicated as ** $p < 0.01$.

3.7 Expression pattern of apoptosis related genes in the testis

As the TUNEL assay indicates that UPEC can cause DNA damage in testicular cells, it was next sought to delineate the specific mechanisms implicated in UPEC infection induced cell death in testis. Firstly, the expression pattern of the *bcl-2* family genes was examined by quantitative realtime-PCR. The results (Figure 12) showed that *bcl-2*, an anti-apoptotic gene, was about two times upregulated in the testis on day 7 post infection (relative expression in Ctrl v. s. Infected testis: 0.0039 v. s. 0.0090, $p = 0.037$). However, except a slight upregulation of *bid* mRNA level was observed in infected testes (relative expression in Ctrl v. s. Infected testis: 0.0080 v. s. 0.0116, $p = 0.037$), no changes were found in *bax* (relative expression in Ctrl v. s. Infected testis: 0.0198 v. s. 0.0223, $p = 0.552$) and *bim* (relative expression in Ctrl v. s. Infected testis: 0.0309 v. s. 0.0252, $p = 0.078$) these two pro-apoptotic genes. The RNA level of another pro-apoptotic gene *bak* was even mildly down regulated (relative expression in Ctrl v. s. Infected testis: 0.0071 v. s. 0.0031, $p = 0.025$).

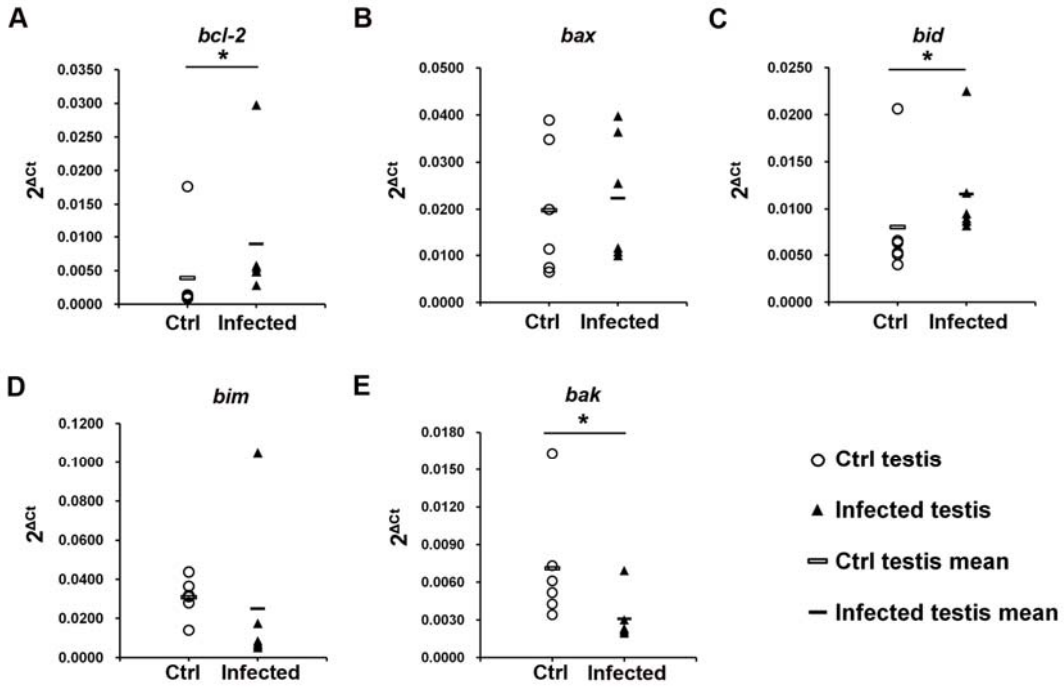

Figure 12 RNA expression pattern of the *bcl-2* family genes in the testis. The expression of the anti-apoptotic gene *bcl-2* **(A)**, pro-apoptotic genes *bax* **(B)**, *bid* **(C)**, *bim* **(D)** and *bak* **(E)** in the testis were determined with quantitative realtime PCR. Target genes expression levels were normalized with the endogenous control ß-2-microglobulin (ß2M). Data are present as $2^{\Delta Ct}$, $\Delta Ct = Ct_{target\ gene} - Ct_{ß2M}$. The Mann-Whitney U test was employed for statistical analysis (* $p < 0.05$). Each single symbol (circle and triangle) represents one individual testis sample.

3.8 Caspase activation in UPEC infected testis

Since caspase activation is a hallmark and essential step in apoptosis execution, the activation of these factors was next assayed in total testis by Western blotting. As a positive control, RAW 264.7 cells were treated with 50 µM sodium nitroprusside (SNP) for 8 h to induce apoptosis. Activation of the extrinsic pathway is usually indicated by the cleavage of caspase-8. Surprisingly, the precursor protein of caspase-8 remained at unchanged levels in all samples investigated, and no caspase-8 cleavage products were detected, indicating that an activation of this initiator enzyme did not occur (Figure 13A). Subsequent observation showed no activation of executor caspases (caspase-3 and -6) (Figure 13B). Furthermore activation of caspase-1 (a key enzyme in the pyrotosis pathway) was not observed in infected testis either (Figure 13C).

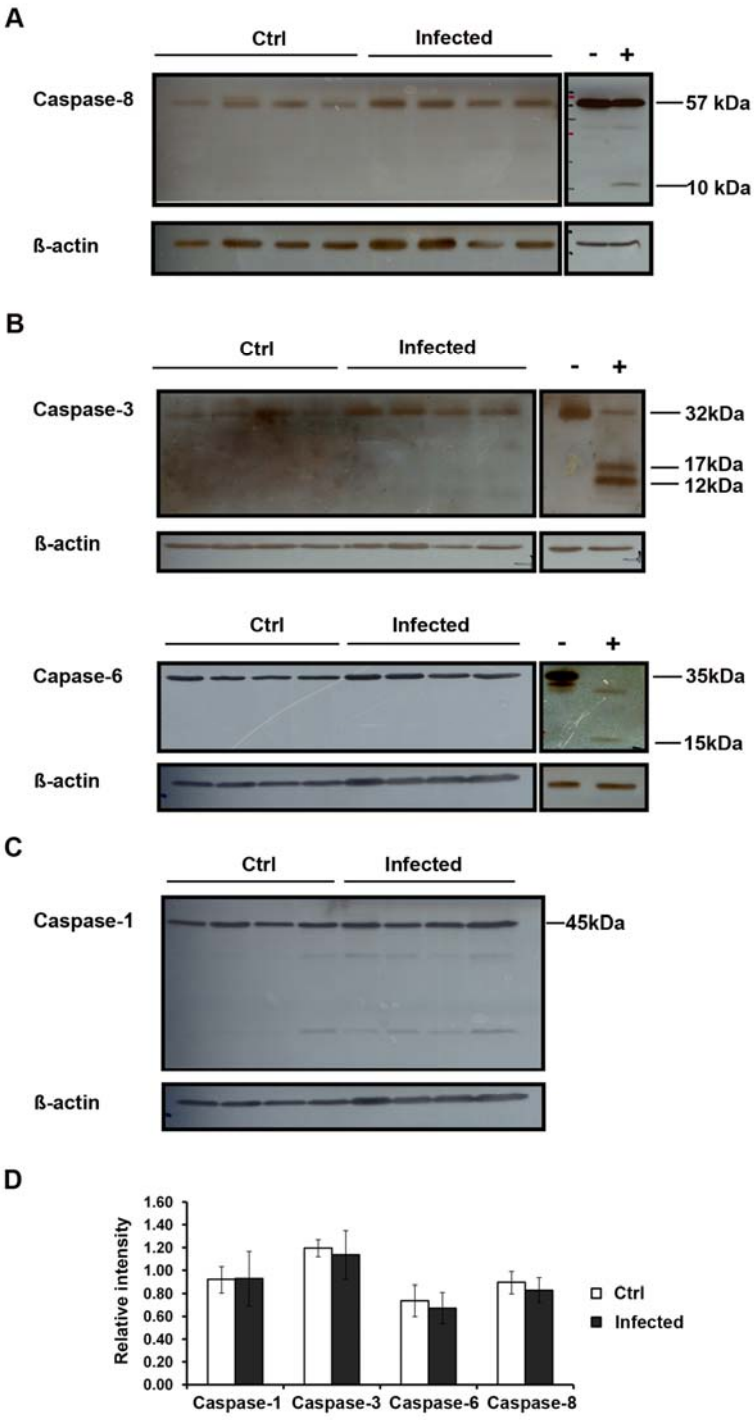

Figure 13 Detection of caspase activation in the testis. Total testis proteins (20µg) from four different animals in each group were separated on 15% SDS-PAGE polyacrylamide gels. The immunoblots were probed with anti-caspase-8 **(A)**, anti-caspase-3 **(B, upper panel)**, anti-caspase-6 **(B, lower panel)** and anti-caspase-1 **(C)** antibodies and then conjugated with a goat anti-rabbit-HRP secondary antibody for chemiluminescence detection. RAW 264.7 cells treated with sodium nitroprusside (SNP) served as a positive control. **(D)** The intensity of target bands on the films was measured with the ImageJ software (http://rsbweb.nih.gov/ij/). Semi-quantitative

results are presented as mean ± SD and Student's t-test was used for data analysis (Caspase-8, $p = 0.875$; Caspase-3, $p = 0.686$; Caspase-6, $p = 0.486$; Caspase-1, $p = 0.343$).

3.9 Electron microscopical examination of the seminiferous epithelium

With biochemical evidence supporting that apoptosis is not the predominant cell death mode in total testis upon UPEC challenge, electron microscopical examination was next employed to examine the morphological changes in testicular cells. Apart from a few apoptotic germ cells (not shown), typical necrotic changes (condensation of chromatin into small, irregular patches) in poorly defined nuclei were also evident in infected testes (Figure 14B, left panel). Of note, the vacuolization and accumulation of lipid droplets within the cytoplasm of SC was commonly observed, indicating damage elicited in these somatic cells (Figure 14B, right panel).

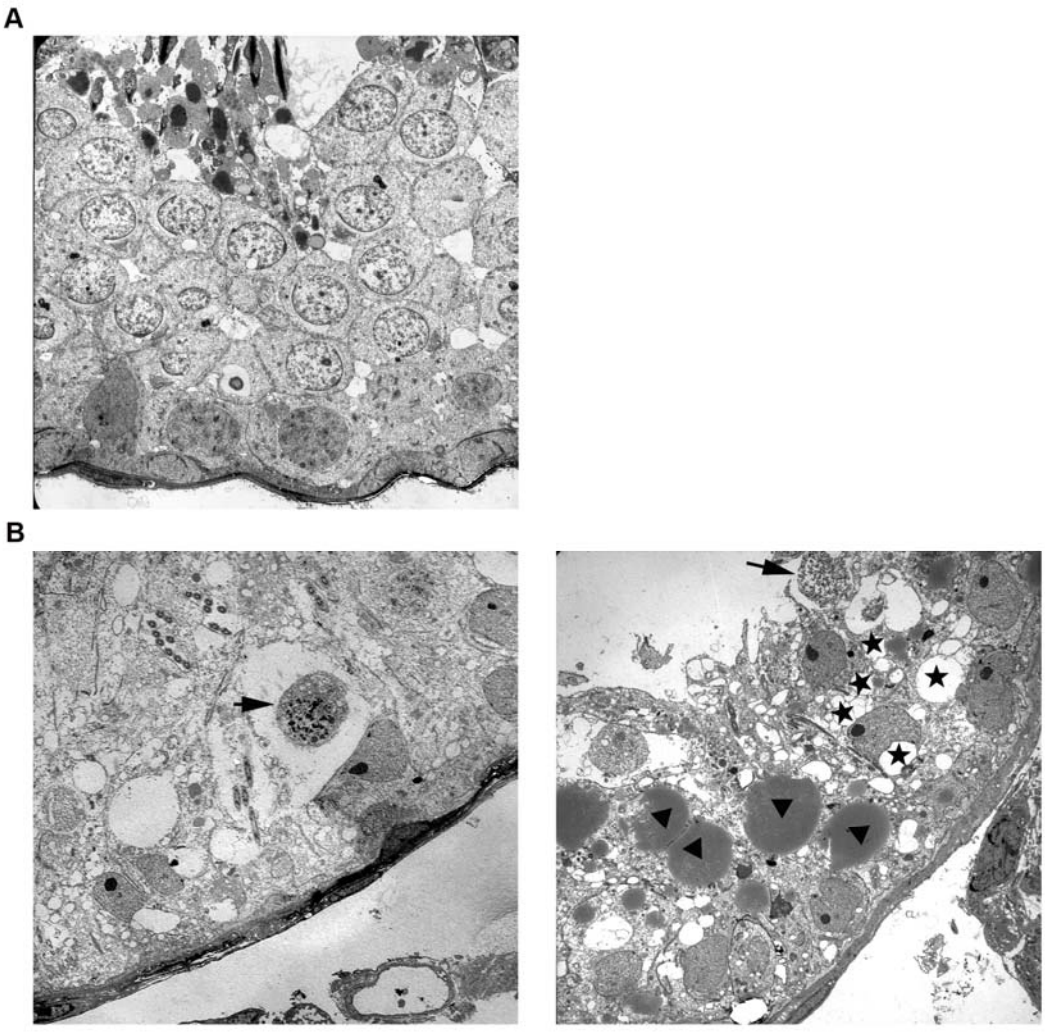

Figure 14 Electron microscopical examination on the germinal epithelium. (A) Ultrathin section from a control rat testis shows normal morphology of the seminiferous epithelium (X1100). **(B)** Representative electron microscopical pictures (X1100) of infected testes demonstrate germ cells with necrotic nuclei (arrows) as well as SC with cytoplasmic vacuolization (right panel, asterix) and large lipid droplets (right panel, arrowheads).

3.10 The viability of SC and PTC after *E. coli* infection

Based on the electron microscopical observation, the mechanisms of UPEC induced testicular somatic cells death were further investigated. The viability of isolated SC and PTC following UPEC treatment was measured using the MTT assay (Figure 15). After 2 h of treatment, the viability of both UPEC CFT073 treated cell types decreased below 30% (SC: 27.63 ± 7.84%, $p = 0.004$; PTC: 13.99 ± 4.95%, $p = 0.004$). Previous studies from our group suggests that the secreted pore-forming toxin α-hemolysin (HlyA) plays a main role in causing calcium influx and suppressing host immune responses against UPEC infection (Sudhanshu B et al. unpublished data). To verify the causative involvement of this virulence factor in the observed decrease of cell viability, *E. coli* strains with different HlyA expression patterns were used for comparison. The treatment with FOS 22, which is a non-pathogenic K12 *E. coli* mutant ectopically expressing HlyA, resulted in a comparable decrease of viability as the cells treated with UPEC CFT073 (SC: 22.47 ± 3.39%, $p = 0.001$; PTC: 11.11 ± 6.16%, $p = 0.002$). UPEC 536, which harbors two *hlyA* genes, demonstrated a higher cytotoxic activity indicated by a lower cell viability (SC: 7.90 ± 2.31%, $p = 0.000$; PTC: 7.55 ± 6.04%, $p = 0.001$). Of note, UPEC 536 double mutant HDM, which does not express HlyA due to deletion of both *hlyA* genes, did not cause any cell death (SC: 138.21 ± 19.15%, $p = 0.075$; PTC: 98.77 ± 0.43%, $p = 0.562$) similar to the results of non-pathogenic *E. coli* treatment (SC: 142.09 ± 18.02%, $p = 0.056$; PTC: 97.73 ± 2.14%, $p = 0.208$).

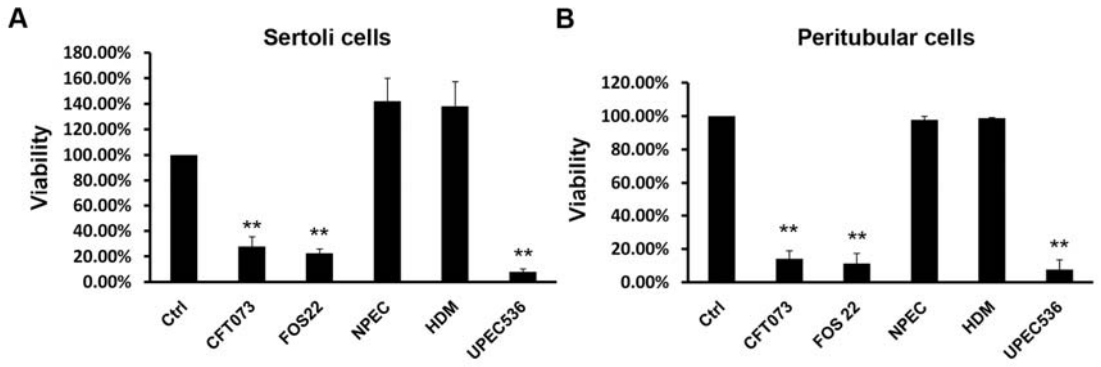

Figures 15 HlyA (+) *E. coli* strains cause a decrease of the viability in Sertoli (SC) and peritubular cells (PTC) in comparison to strains lacking HlyA (+). SC **(A)** and PTC **(B)** were treated with UPEC CFT073, FOS22, NPEC, Hemolysin Double Mutant (HDM) and UPEC 536 (multiplicity of infection, MOI = 20) for 2 h. Viability of cells was subsequently determined with the MTT assay. The data of infected samples were correlated to untreated control, which was normalized to 100%. Values are presented as mean ± SD of triplicate experiments. Student's t-test was used to analyzed the significance of difference between control and individual infected sample (** $p < 0.01$).

3.11 Annexin V/PI assay in SC and PTC

To identify the type of cell death mode, SC and PTC were infected with distinct *E.coli* strains for 90 min, and stained with FITC-Annexin V and propidium iodide (PI) for flow cytometry analysis. Compared to untreated control samples (early apoptotic SC: 8.23 ± 1.09%, PTC: 5.09 ± 1.62%; late apoptotic or necrotic SC: 0.8 ± 1.05%, PTC: 2.65 ± 2.35%), the results of FITC-Annexin V/PI staining demonstrated that the percentage of early apoptotic SC and PTC in UPEC CFT073 infected samples strongly increased to 51.26 ± 6.44% (Figure 16B) and 24.75 ± 2.04% (Figure 16D), respectively. Notably, the proportions of late apoptotic or necrotic SC (10.17 ± 9.12%, Figure 16B) and PTC (46.07 ± 7.82%, Figure 16D) also increased significantly. Similar patterns were found in samples treated with two other HlyA (+) *E. coli* strains, FOS 22 (early apoptotic SC: 42.80 ± 4.08%, PTC: 20.09 ± 8.09%; late apoptotic or necrotic SC: 16.21 ± 8.36%, PTC: 46.83 ± 9.70%) and UPEC 536 (early apoptotic SC: 37.08 ± 2.95%, PTC: 15.52 ± 4.99%; late apoptotic or necrotic SC: 6.48 ± 5.44%, PTC: 45.49 ± 9.78%). In agreement with the results of MTT assay, no increase of either Annexin V (+) or PI (+) cell numbers was observed in NPEC (early apoptotic

SC: 12.67 ± 5.70%, PTC: 5.17 ± 2.64%; late apoptotic or necrotic SC: 1.62 ± 1.30%, PTC: 5.03 ± 0.96%) and HDM treated samples (early apoptotic SC: 8.93 ± 1.42%, PTC: 4.72 ± 2.61%; late apoptotic or necrotic SC: 1.00 ± 0.9%, PTC: 3.17 ± 1.24%).

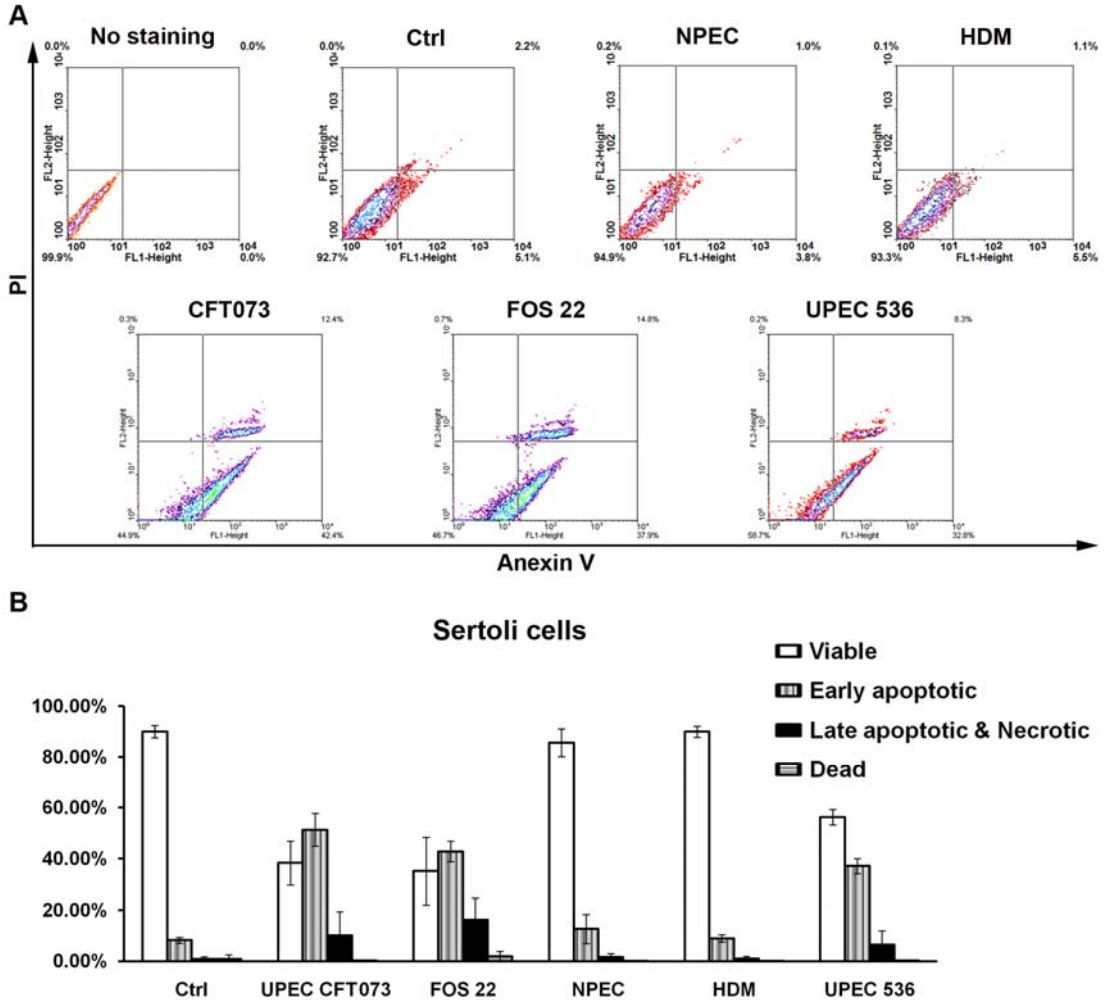

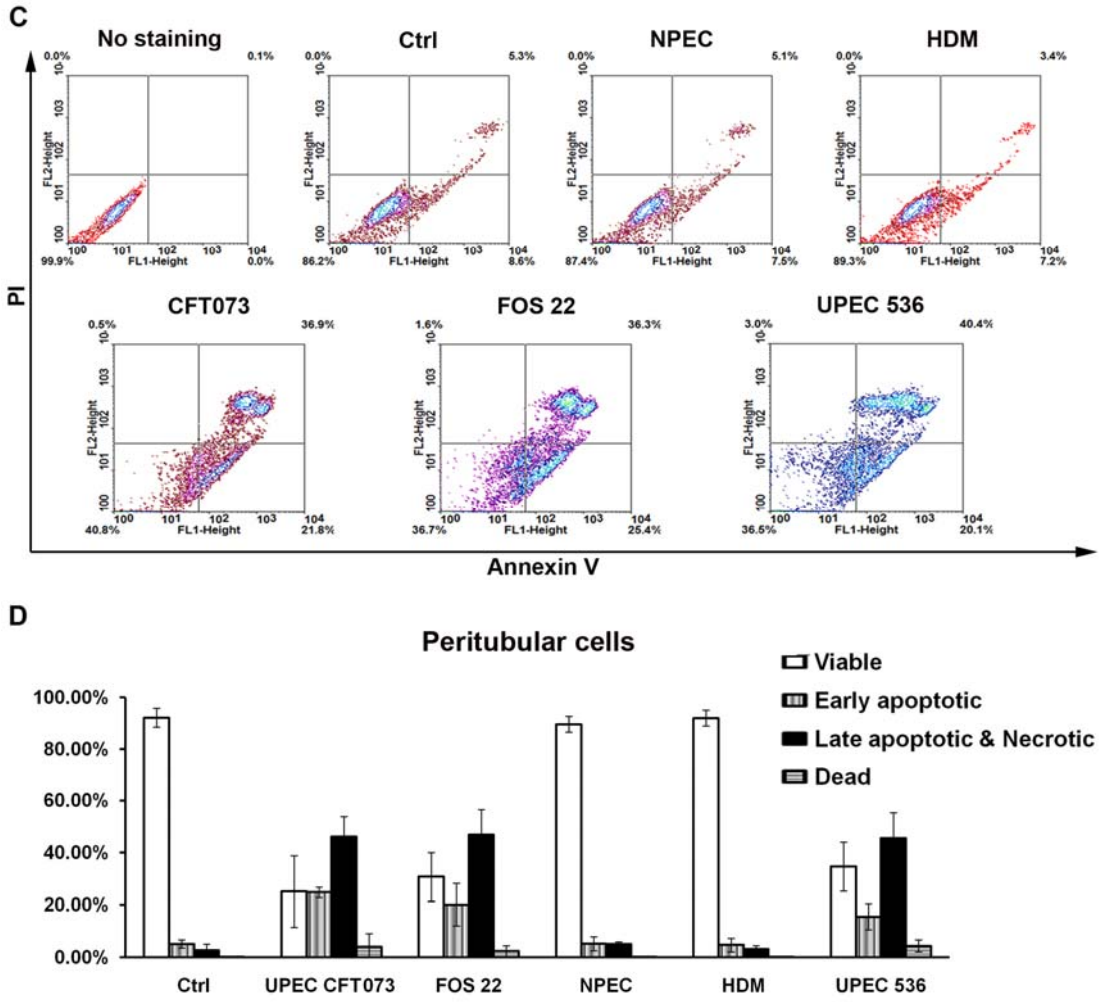

Figure 16 HlyA (+) *E. coli* strains induce apoptosis as well as necrosis in Sertoli (A and B) and peritubular cells (C and D). FITC-Annexin V/PI staining in SC and PT were analyzed using flow cytometry following *E.coli* (MOI = 20) infection for 90 min. Experiments were repeated three times and typical contour figures are demonstrated in panels **(A)** and **(C)**. The triplicate results are presented as mean ± SD and the corresponding summary is shown in panel **(B)** and **(D)**.

3.12 Expression of *bcl-2* gene family in SC and PTC

As demonstrated by Annexin V/PI assay, phosphoserine exposure (Annexin V positive only) was found in a considerable population of infected SC and PTC, which is widely accepted as a characteristic of early apoptosis. To further explore whether the intrinsic apoptotic pathway is implicated in UPEC CFT073 induced SC and PTC cell death, quantitative real-time PCR was employed to analyze the expression of apoptosis related genes. In UPEC infected SC (Figure 17A), a moderate upregulation of the anti-apoptotic gene *bcl-2* was evident (1.78 fold, p = 0.037); whereas no

changes were observed in the investigated pro-apoptotic genes, with the exception of *bim* was found to be mildly down regulated (0.34 fold, p = 0.037). In contrast, in UPEC infected PTC (Figure 17B) *bcl-2* was slightly down regulated (0.69 fold, p = 0.037) and the pro-apoptotic genes *bax* and *bim* were mildly up regulated (2.08 and 2.35 fold, p = 0.014 and 0.037, respectively).

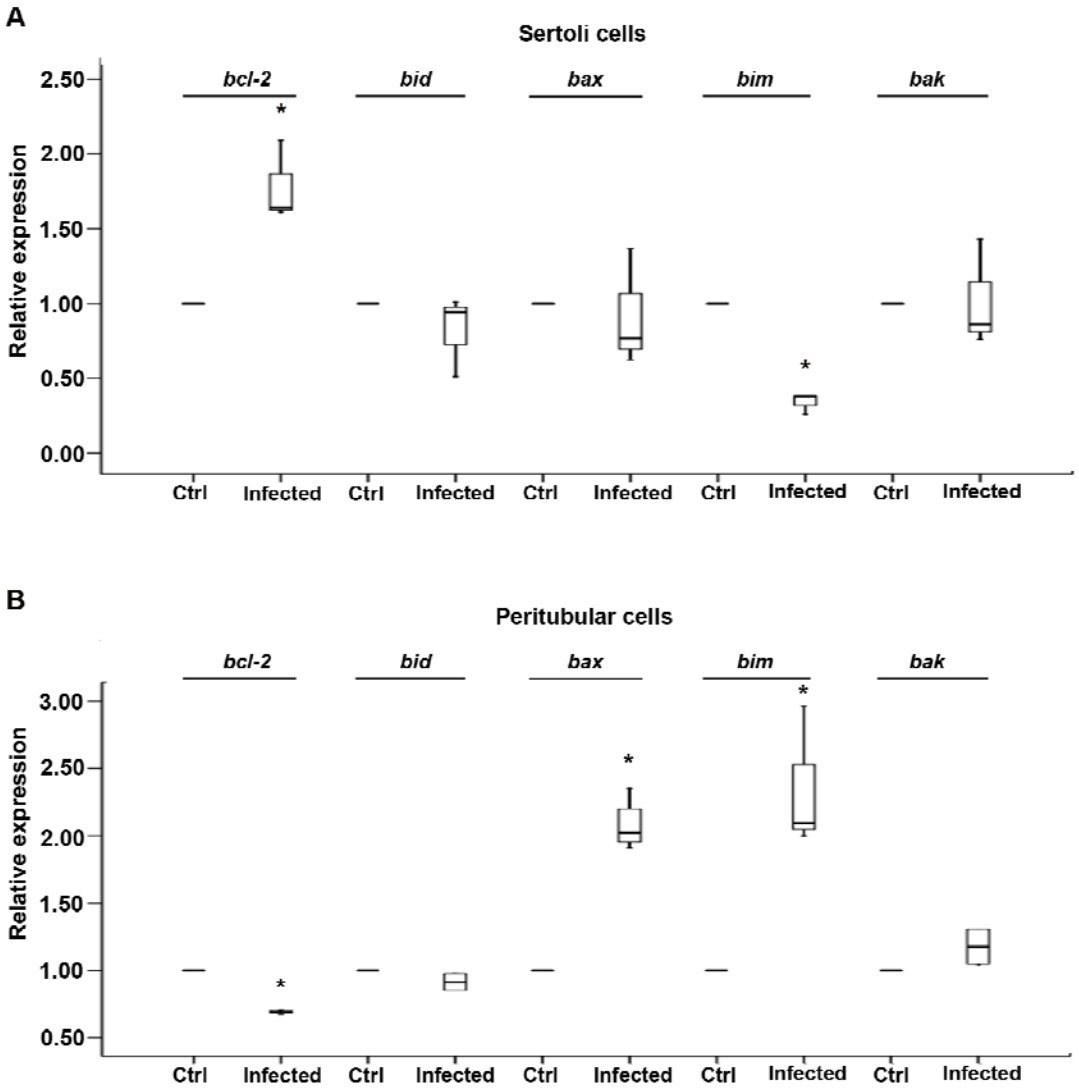

Figure 17 The expression of *bcl-2* gene family in isolated Sertoli (SC) and peritubular cells (PTC). RNA was isolated from SC **(A)** and PTC **(B)** following challenge with UPEC strain CFT073 (MOI = 20) for 3 and 4 h, respectively. The expression of *bcl-2* gene family was determined using quantitative realtime PCR. Target gene expression was normalized using ß-2-microglobulin (ß2M) as reference and data are presented as relative expression (RE): $RE = 2^{\Delta Ct\ UPEC-\Delta Ct\ Ctrl}$, $\Delta Ct = Ct_{target\ gene}-Ct_{ß2M}$. Mann-Whitney U test was used for the statistical analysis (* $p < 0.05$).

3.13 Caspase activation in SC and PTC

Caspase activation is the hallmark and commitment point of apoptosis [197]. To finally examine the putative involvement of apoptosis pathways in UPEC inducing SC and PTC death, caspase activation was determined by Western blotting (Figure 18). Similar to the observation from total testis, neither precursor degradation nor cleaved forms of caspase-8, -3 and -6 were found in infected SC at any time point investigated. Intriguingly, in infected PTC the full length protein levels of all three caspases were decrease in a time dependent manner, whereas the activated forms remained undetectable. To verify whether the degradation of full length precursors is indicative for caspase activation, enzymatic activity of the executor caspase-3 was measured in PTC. Of note, the caspase-3 activity remained at very low levels in PTC during the course of infection, which emphasizes that caspases were not activated. Furthermore, activated cleavage of caspase-1 was observed by Western blotting in neither SC nor PTC.

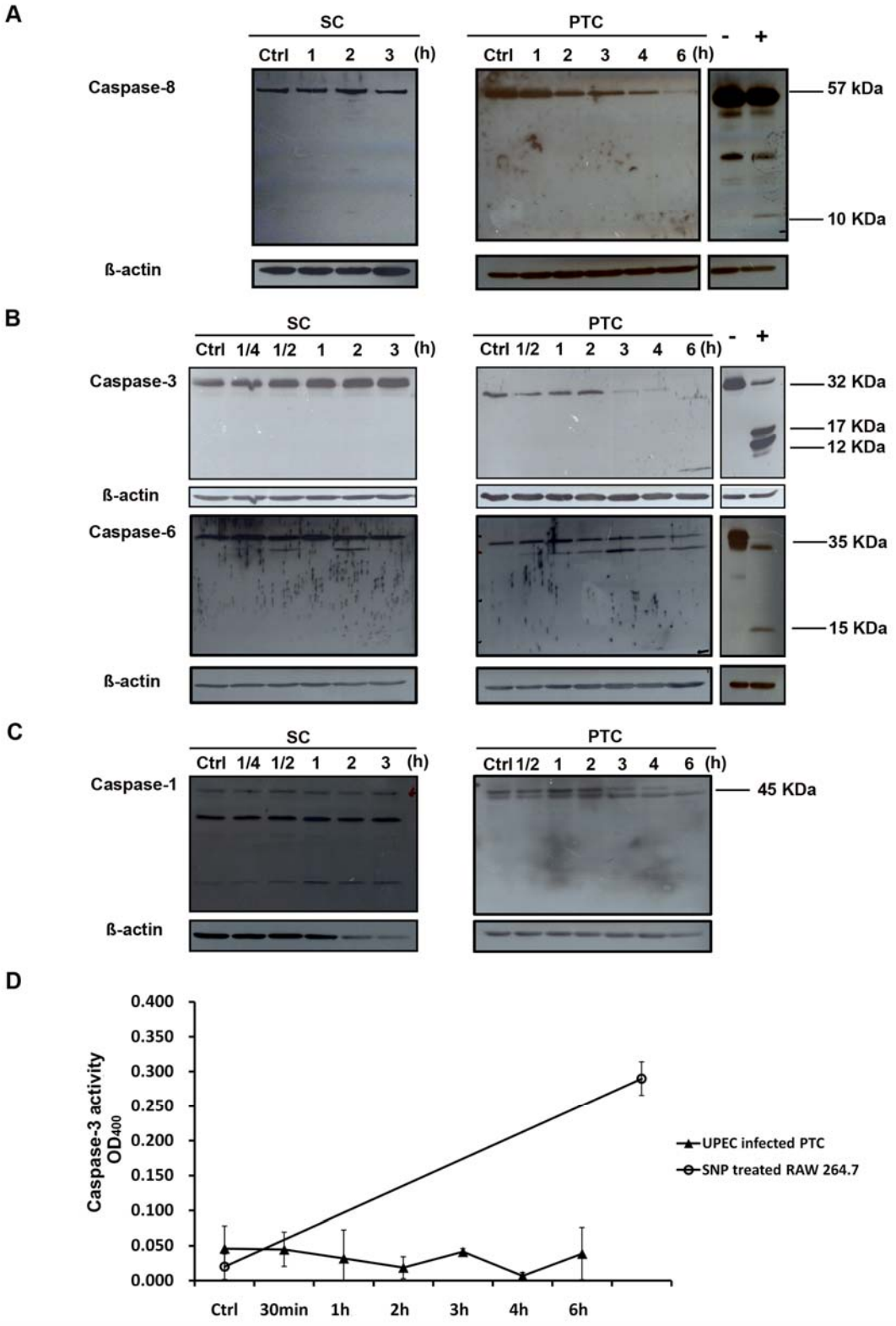

Figure 18 Detection of caspases activation in UPEC infected Sertoli (SC) and peritubular cells (PTC). SC and PTC were infected with UPEC CFT073 strain (MOI = 20) for various times as indicated. For Western blotting analysis, 20 µg of proteins were separated on 15% SDS-PAGE and immunoblots were probed with anti-caspase-8 **(A)**, -3 **(B, upper panel)**, -6 **(B, lower panel)** and -1 **(C)** antibodies.

ß-actin served as a loading control. RAW 264.7 cells treated with 50 µM sodium nitroprusside (SNP) for 8 h served as a positive control. Only in the positive control the cleaved forms of caspase-8, -3 and -6 could be specifically detected using Western blotting. **(D)** For caspase-3 enzymatic activity measurement 3×10^6 PTC in each sample were lysed and 100 µg of protein was assessed with Caspase-3/CPP32 Colorimetric Assay Kit. The optical density (OD) values were quantified using a spectrophotometer at a wavelength of 400 nm. Results are presented as mean ± SD. Each experiment was repeated three times.

3.14 DNA degradation in the testis following UPEC infection

A late event in cell death is genomic DNA degradation with characteristic patterns for diverse cell death modes. As an example, an orderly DNA fragmentation pattern is usually associated with caspase-dependent apoptosis. In apoptotic cells the activation of endonucleases results in oligonucleosomal DNA fragments (DNA ladder) with steps of about 180 base pair (bp), while DNA is cleaved into fragments of random size by nonspecific lysosomal nucleases in necrotic cells. To determine which cell death mode plays the predominant role in infected testis and more specifically in SC and PTC, genomic DNA was isolated for agarose gel electrophoresis following UPEC infection. Figure 19 shows that DNA laddering with approximately 180 bp fragmentation was visible only in RAW 264.7 cells treated with 5 µM H_2O_2 for 24 h (Figure 19A, lane 9; B, lane 6), which served as a positive control for apoptotic DNA laddering. In saline injected control rats, total testis DNA remained intact (Figure 19A, lane 2~4), whereas the DNA samples extracted from infected testes demonstrated a smear pattern (Figure 19A, lane 5~7) similar to the necrosis positive control (Figure 19A, lane 10; B, lane 7), indicating unspecific DNA degradation. In isolated SC and PTC, the intensity of high molecular DNA was decreased after UPEC infection but a regular pattern of DNA fragmentation was not observed (Figure 19B, lane 3 and 10). Of note, a smear pattern of DNA degradation as shown in necrotic positive control was not found in infected SC and PTC, despite cell death already occurred at that time points.

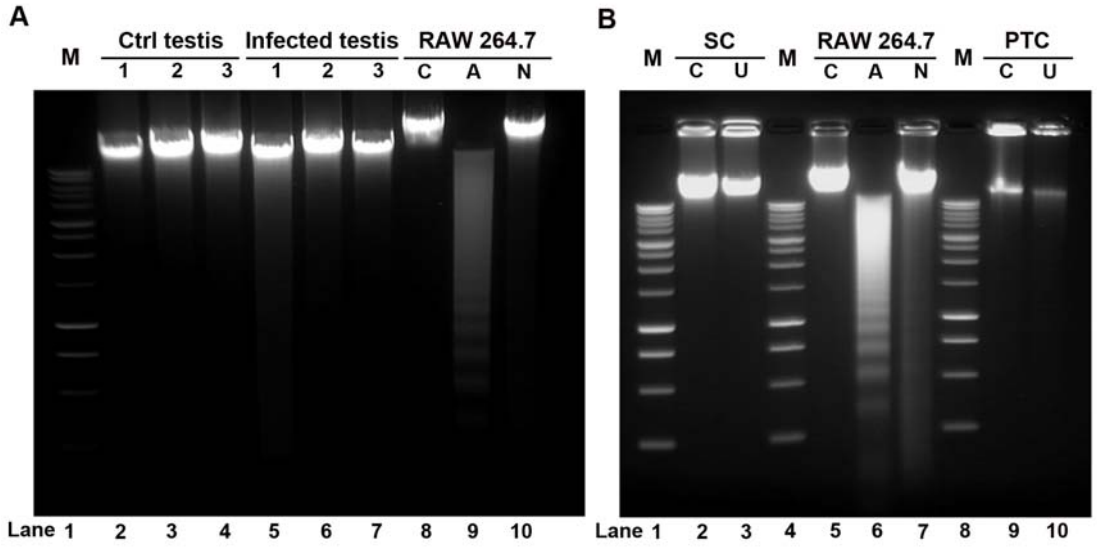

Figure 19 Pattern of oligonucleosomal DNA fragmentation. Genomic DNA was extracted from testes, isolated Sertoli (SC) and peritubular cells (PTC), respectively. For gel electrophoretic analysis, 5 µg of DNA from each sample were separated on 1.5% agarose gels and stained with ethidium bromide. **(A)** Lane 1: 1 kbp DNA ladder. Lane 2~4: DNA extracted from testes of control rats (n = 3). Lane 5~7: DNA samples extracted from testes of infected rats (n = 3). Lane 8: untreated RAW 264.7 cells. Lane 9: RAW 264.7 cells were treated with 0.5 mM H_2O_2 for 24 h as a positive control for apoptosis. Lane 10: RAW 264.7 cells were frozen and thawed repeatedly as a positive control for accidental necrosis. **(B)** SC and PTC were infected with UPEC strain CFT073 (MOI = 20) for 4 and 6 h, respectively. Lane 1, 4 and 8: 1 kbp DNA ladder. Lane 2: untreated SC; Lane 3: infected SC; Lane 5~7: untreated, apoptotic and necrotic RAW 264.7 cells; Lane 9: untreated PTC; Lane 10: infected PTC.

3.15 AIF nuclear translocation in UPEC infected SC

As the caspase-dependent pathway was found not to be activated in total testis and isolated SC and PTC upon UPEC infection (Figures 18 and 19), it was next investigated whether SC and PTC died by caspase-independent pathways. The intracellular localization of AIF, a well-characterized caspase-independent cell death effector, was examined in SC and PTC with confocal microscopy. In contrast to untreated and NPEC infected cells, AIF nuclear translocation was observed in UPEC treated SC at the indicated time points (Figure 20A). Moreover, similar results were evident in FOS 22 infected SC, which suggests that only the HlyA (+) *E. coli* strains

are able to induce AIF nuclear translocation in SC. However, AIF redistribution seems specific for SC as in infected PTC this protein was retained in the cytoplasm (Figure 20B).

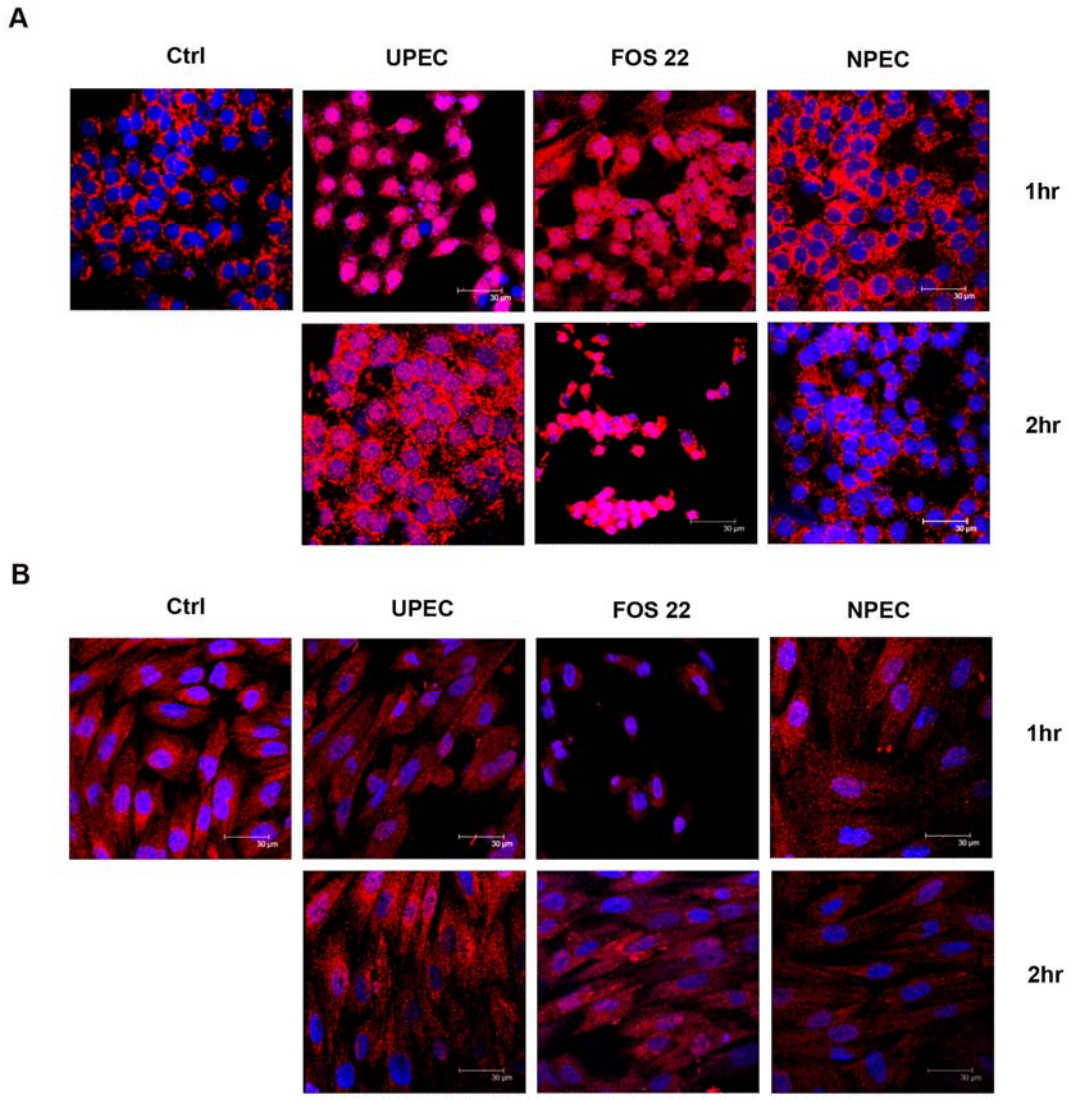

Figure 20 Localization of apoptosis inducing factor (AIF) in Sertoli (SC) and peritubular cells (PTC). SC **(A)** and PTC **(B)** were treated with UPEC CFT073, FOS22 and NPEC (MOI = 20) for the indicated time points, and subsequently probed with rabbit anti-AIF antibody. AIF was labeled with Cy-3 conjugated anti-rabbit IgG secondary antibody (red) and the nuclei were counterstained with Cy5-conjugated To-Pro-3 (blue). The samples were analyzed with confocal microscopy. Scale bar: 30 µm. Representative figures from triplicate experiments are shown.

3.16 Nuclear structure changes in UPEC infected SC and PTC

Once AIF translocates from mitochondria to the nucleus, it binds to DNA and triggers chromatinolysis and apoptosis-like chromatin condensation [198]. To analyze putative nuclear changes, nuclei stained with the cell-permeable DNA dye Hoechst 33342 were evaluated using fluorescence microscopy following UPEC treatment. Notably, partial chromatin condensation and transparent nuclei were observed in SC after 1 h of UPEC treatment. The changes of nuclear structure became more prominent with an advanced pattern of peripheral chromatin condensation in the majority of SC following infection for 2 h (Figure 21A). In contrast to SC, progressing changes in nuclei with shrinking size and homogeneous chromatin condensation were evident in infected PTC in the first two hours (Figure 21B), which were indicative of necrosis [149,199]. Of note, SC and PTC display a similar pattern of nuclear pyknosis after 4 h of UPEC infection.

3.17 Calpain activation in UPEC infected PTC

Previous studies from our group have proven that the UPEC pore-forming virulence factor HlyA is able to induce a rapid calcium influx in testicular and peritoneal macrophages (Sudhanshu Bhushan, et al. unpublished data). Calpain, a family of calcium dependent proteinases, can be activated by increased intracellular calcium and act as a key mediator implicated in AIF redistribution and programmed cell death [200]. Based on our observations, we speculated if calpain activation may play a role in UPEC induced SC and PTC death. Therefore, SC and PTC were pretreated with fluorogenic calpain substrate (CMAC, t-Boc-Leu-Met) followed with UPEC CFT073 infection up to 1 h. A strongly increased emission of blue fluorescence indicating calpain activation was observed only in PTC after 30 min of UPEC treatment (Figure 22). Surprisingly, there was no detectable fluorescence emitted from SC within 1 h of UPEC treatment (data not shown).

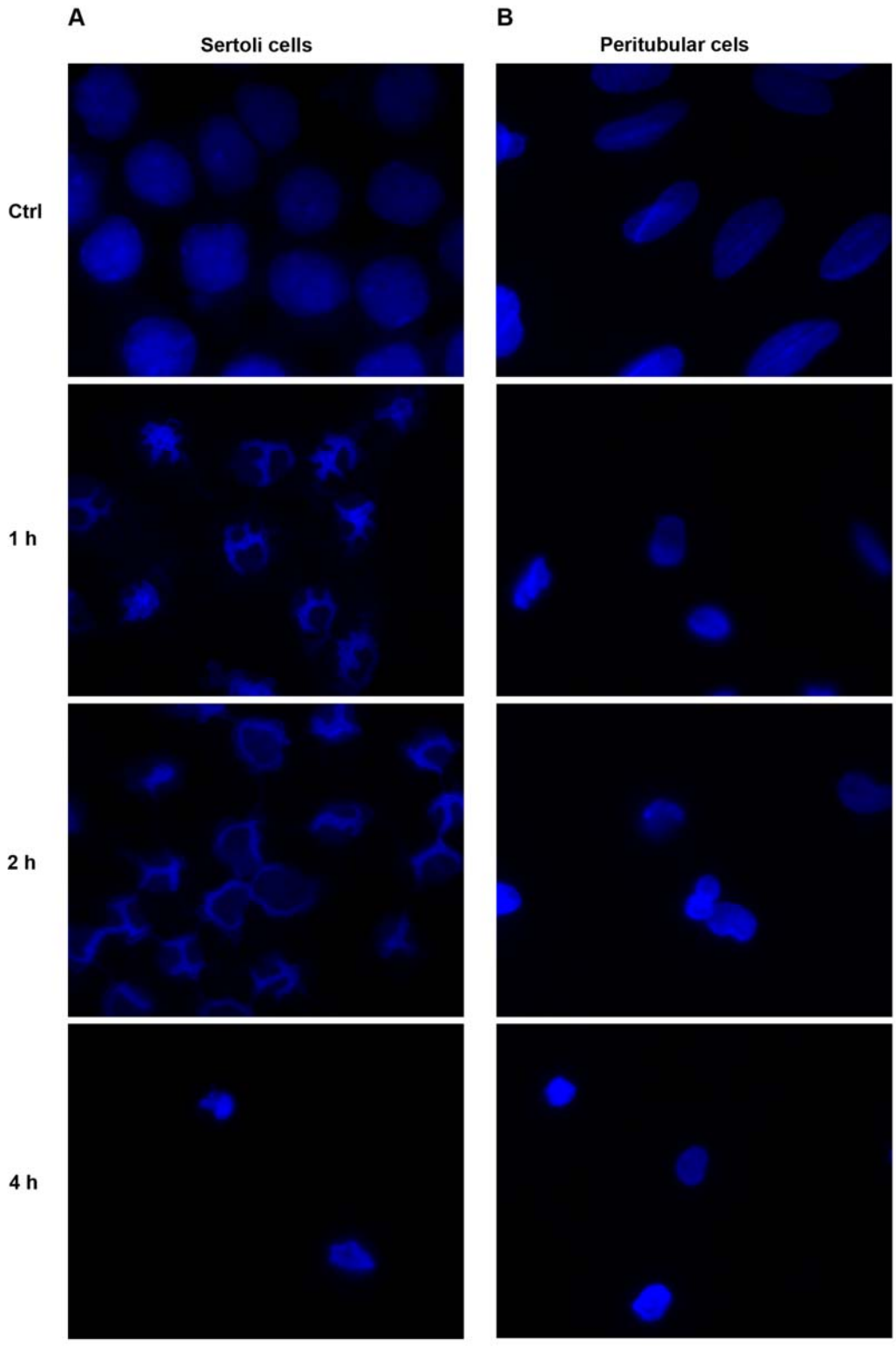

Figure 21 Influence of UPEC infection on nuclear structure in Sertoli (SC) and peritubular cells (PTC). SC **(A)** and PTC **(B)** were treated with UPEC CFT073 (MOI = 20) for the indicated time points. Nuclei of these cells stained with Hoechst 33342 were evaluated using fluorescence microscopy. Images were taken with the Axioplan 2 Imaging system at X1000 magnification. Results are representative of at least 80% cells/field observed in three independent experiments.

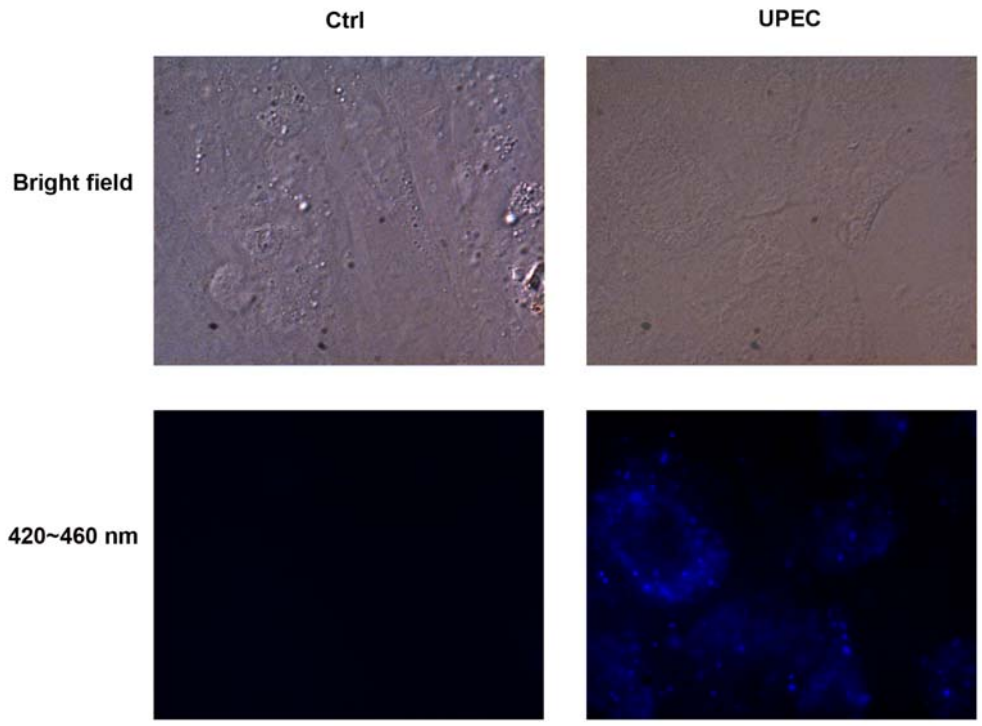

Figure 22 Calpain activation in UPEC infected PTC. PTC pretreated with fluorogenic calpain substrate (CMAC, t-Boc-Leu-Met) were subsequently infected with UPEC CFT073 (MOI = 20) for 30 min. Images were taken with the Axioplan 2 Imaging system at X1000 magnification. Representative pictures were selected from three independent experiments with similar findings.

3.18 Excessive ROS production in UPEC infected PTC

Overproduction of intracellular reactive oxygen species (ROS) as a major consequence of mitochondrial dysfunction is established to be strongly implicated in detrimental responses of host cells or tissues during microbial infection [201]. The MTT assay suggests that mitochondrial function is disrupted in SC and PTC during UPEC infection. Hence production of ROS in infected SC and PTC was examined using the oxidation sensitive fluorogenic probe 2', 7'dichlorofluorescindiacetate (H_2DCFDA). Intriguingly, UPEC treatment did not trigger any increase of ROS in SC within one hour (Figure 23A and C). In contrast to this observation in SC, a surge of ROS production was seen in PTC after 30 min of UPEC stimulation which gradually returned back to basal level in about 90 min (Figure 23B and D). However, NPEC treatment did not cause significant changes of ROS production in SC or PTC.

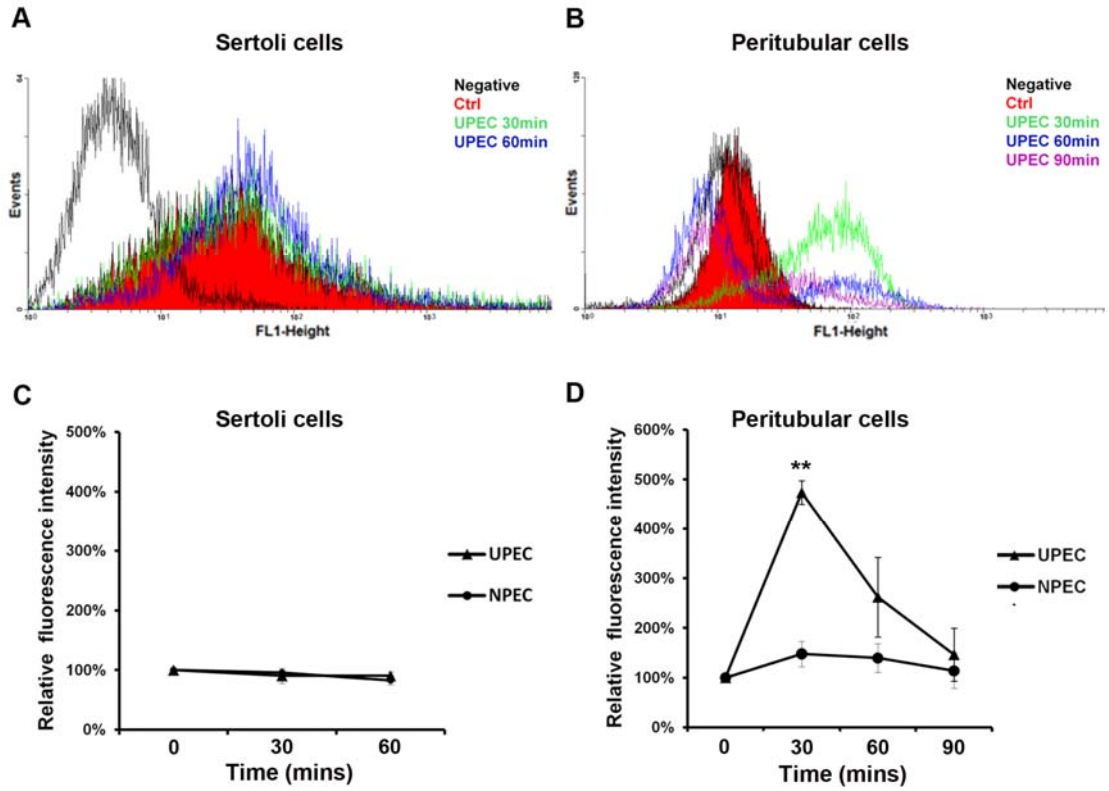

Figure 23 Intracellular reactive oxygen species (ROS) production in Sertoli (SC) and peritubular cells (PTC). SC and PTC were pretreated with H_2DCFDA for 30 min and ROS levels were assessed with flow cytometry following *E.coli* treatment. The fluorescence intensity of infected samples was referred to the basal level of untreated control, which was normalized as 100%. The representative histograms from untreated and UPEC infected samples are shown in panel **(A)** and **(B)**. The data points represent mean ± SD of three independent experiments and shown in panel **(C)** and **(D)**. Student's t-test was used for statistical analysis. (**) indicates $p<0.01$ compared to the untreated control.

3.19 ATP depletion in UPEC infected SC and PTC

The intracellular ATP level is an important switch to determine cell fate between apoptosis and necrosis [202]. Apoptosis is an active process requiring ATP for execution, e.g., for caspase activation, chromatin condensation and nuclear fragmentation [178]. Therefore, ATP levels in apoptotic cells are maintained at normal level until the very end of the cascade [203]. In contrast, necrosis can be continued even ATP storage is deleted. To determine whether UPEC can cause energy failure in infected SC and PTC, ATP levels were analyzed by the luciferin-luciferase assay following bacterial treatment. In SC, the intracellular ATP level started to decline after 1 h of UPEC treatment and rapidly decreased to lower than 10% within 2 h (Figure

24A). Similarly, the ATP level in infected PTC declined in a time dependent manner and gradually decreased to below 20% of normal levels within 4 h of UPEC treatment (Figure 24B).

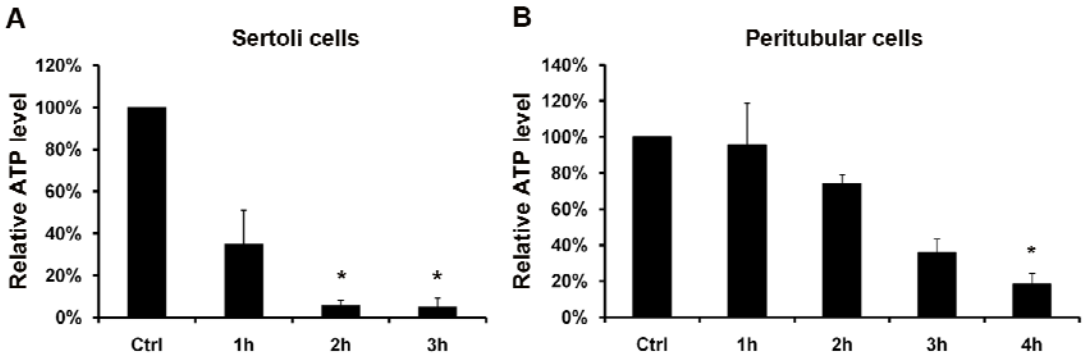

Figure 24 UPEC infection caused intracellular ATP depletion in Sertoli (A) and peritubular cells (B). ATP levels were quantified by the luciferin-luciferase assay following UPEC treatment for the indicated time points. The results were normalized to untreated control samples and are presented as relative percentages. The bars represent the mean ± SD of duplicate experiments. Student's t-test was employed for statistical analysis. (*) represents $p < 0.05$ compared to the untreated samples.

3.20 HMGB1 release in testicular cells after UPEC infection

Previous studies confirmed that high-mobility group box 1 (HMGB1), a nuclear factor and a secreted protein, can be a maker of necrosis as it is passively released into the cytoplasm of necrotic or damaged cell whilst it retains in the nucleus of healthy and apoptotic cell [166]. As indicated by the results above, necrosis likely occurred in SC and PTC after UPEC infection. To further determine the predominant cell death mode in UPEC treated SC and PTC, the subcellular localization of HMGB1 was investigated using immunofluorescent microscopy. Although the protein level of HMGB1 in total testis was not affected by UPEC infection (Figure 25A and B), different patterns of HMGB1 subcellular localization were observed between infected and control testes. In agreement with previous observations [204], mainly testicular somatic cells were probed with Cy3 conjugated anti-HMGB1 antibody. In control testes, HMGB1 was exclusively found in the nuclei of somatic cells, i.e., SC (arrows), PTC (arrow heads), and some other interstitial cells (Figure 25C, left column). In

contrast, a predominant cytoplasmic distribution of HMGB1 was observed in somatic cells of infected testes (Figure 25C, right column).

In agreement with the *in vivo* results, HMGB1 translocation from the nuclei to cytoplasm was verified *in vitro* using isolated SC and PTC which were treated with UPEC CFT073 and FOS 22 (Figure 26 A and B). In contrast, HMGB1 retained in the nuclei of NPEC infected and untreated SC. Consistent with the *in vivo* observation, a small proportion of HMGB1 was also detected in the cytoplasm of untreated PTC (Figure 26B).

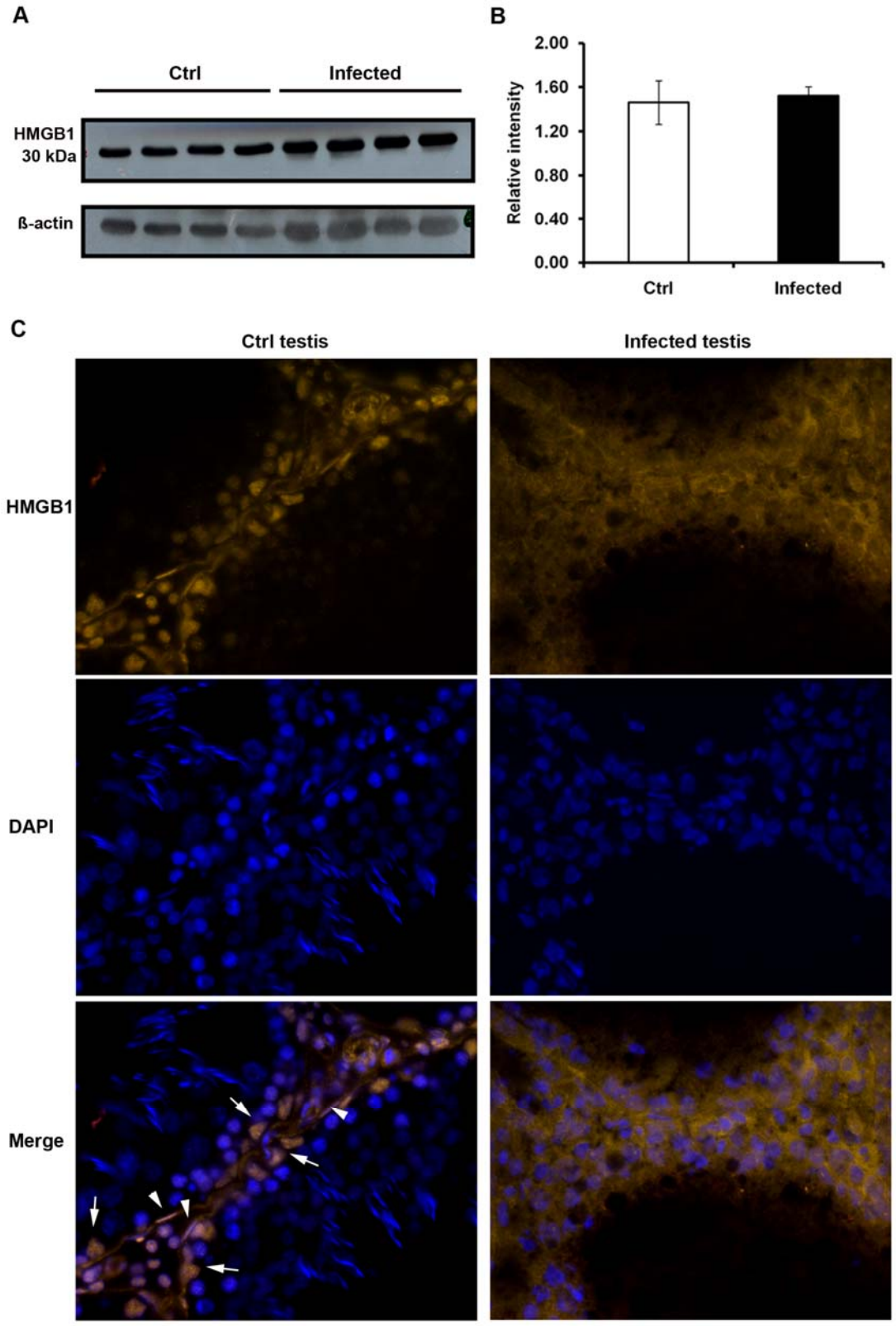

Figure 25 HMGB1 expression and localization in the testis. (A) For Western blotting analysis, 20 µg of protein extracted from total testis of control (n = 4) and infected (n = 4) rats was separated on a 12.5% SDS-PAGE. HMGB1 was detected by immunoblot using anti-HMGB1 polyclonal antibody and goat anti-rabbit HRP conjugated secondary antibody. ß-actin served as a loading control. **(B)** The intensity

of target bands was measured with the ImageJ software. The data are presented as the relative intensity = intensity of HMGB1/intensity of ß-actin. **(C)** Testis cryosections were probed with Cy-3 conjugated rabbit anti-HMGB1 and nuclei were counterstained with DAPI. Images were photographed using the Axioplan 2 Imaging system at X400 magnification. In control samples (left column), some Sertoli and peritubular cells were indicated by arrows and arrow heads, respectively.

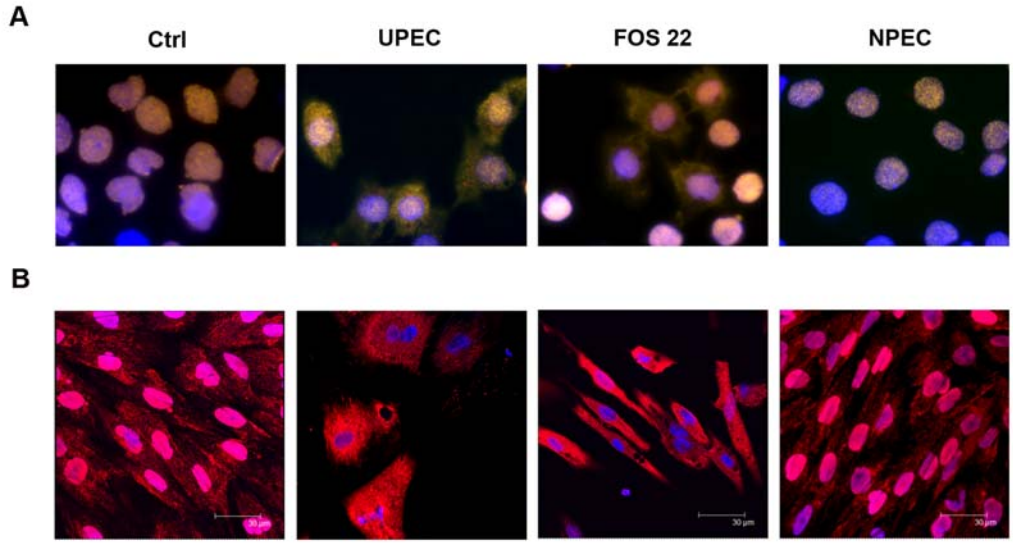

Figure 26 The subcellular HMGB1 localization in isolated Sertoli (A) and peritubular cells (B). HMGB1 was probed with rabbit anti-HMGB1 antibody and Cy-3 conjugated secondary antibody following challenge of the indicated *E. coli* strains for 2 h. The subcellular location of HMGB1 was determined with normal fluorescence microscopy (A, X1000 magnification) and confocal microscopy (B, scale bar: 30µM). Representative results of triplicate experiments are shown.

3.21 NF-κB signaling pathway in the testis upon UPEC infection

The NF-κB (nuclear factor kappa-light-chain-enhancer of activated B cells) signaling pathway plays a pivotal role in innate immune response upon infection. Activation of the NF-κB pathway is also associated with the secretion of the proinflammatory protein HMGB1 from the nucleus of activated macrophage [165]. Therefore, it was next to investigate if the NF-κB pathway is implicated in host response against UPEC infection and the observed HMGB1 release in testicular cells. The activation of NF-κB is essentially initiated by the degradation of its inhibitor IkBα (nuclear factor of kappa light polypeptide gene enhancer in B-cells inhibitor, alpha). Seven days after UPEC infection, the level of IkBα protein expression was found to be comparable between UPEC infected and control testes (Figure 27A and B). In agreement, the p65 subunit of NF-κB retained in the cytoplasm in all samples

(Figure 27C). Similar observations were found in rats after one day and three days of infection (data not shown), indicating that the NF-κB pathway is not involved in UPEC infection of the testis.

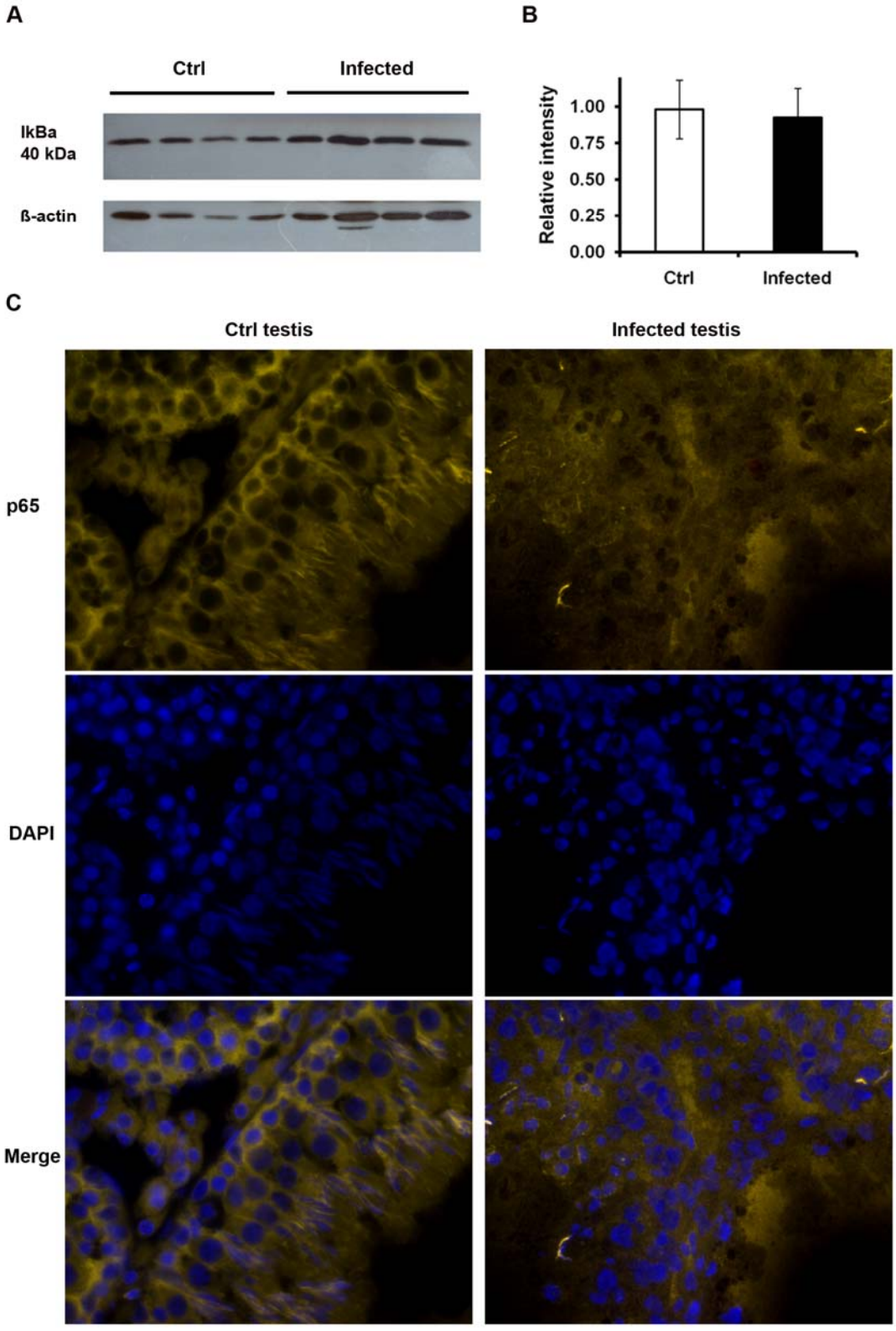

Figure 27 NF-κB pathway in UPEC infected testis. (A) Total testis proteins were separated on 10% SDS-PAGE. Immunoblots were labeled with mouse anti-IkBα antibody. ß-actin served as a loading control. **(B)** The intensity of target bands was measured with the ImageJ software. The results are presented as the relative intensity = intensity of p65/intensity of ß-actin. **(C)** Testis cryosections were probed with Cy-3 conjugated mouse anti-p65 and the nuclei were counterstained with DAPI. Images were captured using Axioplan 2 Imaging system at X400 magnification. Representative results from at least two independent experiments are shown.

4 DISCUSSION

4.1 The establishment of a UPEC induced epididymo-orchitis model

Infection and inflammation of the male urogenital tract is widely acknowledged as an important aetiological factor of infertility [79]. Anatomically, the testis, the excurrent duct system and accessory glands are all connected to the urethra, providing a potential gateway for the retrograde microbial infections [1]. Acute epididymitis secondary to retrograde UTIs spreading via the vas deferens can potentially affect the testis and manifest as epididymo-orchitis [1]. Microbial infections of the epididymis and testis may lead to direct exposure of gametes and germinal epithelium to invading pathogens and inflammatory products, thus ultimately resulting in reduced fertility [205]. *E. coli* is the most frequently isolated pathogen from semen samples of infertile men as well as patients with prostatitis and epididymitis [91,92,97]. Although the particular *E. coli* strain accounting for reduced fertility has yet to be identified, it is speculated that UPEC, a primary causative pathogen of UTIs, is most likely responsible for *E. coli* induced epididymo-orchitis [98,206]. This is supported by the recent observation that more than 50% of *E. coli* samples obtained from patients with epididymitis have hemolytic activity as is characterized for UPEC (Clinic of Urology, Giessen, personal communication). Therefore, in this study, the UPEC strain CFT073 was employed as it was assumed to be clinical relevant and its full genome has been sequenced. Studies conducted in the past outlined the deleterious effects of pathogenic *E. coli* on human spermatozoa [83,207]. These i*n vitro* investigations observed that high concentrations of pathogenic *E. coli* can cause a decrease of motility and mediate morphological alterations in sperm. A latest study further revealed sperm immobilization factor isolated from *E. coli* can induce receptor-dependent immobilization of sperm [208]. However, thus far the interactions between pathogenic *E. coli* and host cells in the testis have yet to be elucidated. Therefore, the aim of my PhD project was to investigate the impairment of spermatogenesis in UPEC induced epididymo-orchitis, as well as to characterize the responses of the testicular cells in the seminiferous epithelium upon infection.

The investigation of the pathogenesis of bacteria induced epididymo-orchitis has been facilitated by the development of *in vivo* animal models. Previously, *E. coli* induced epididymo-orchitis models have been generated by directly injecting bacteria into the testis or vas deferens [190,192]. It has been shown that unilateral bacterial injection into vas deferens is able to elicit an inflammatory response and cause damage to both the ipsilateral and contralateral epididymides as well as the testes [192]. In this study, UPEC were bilaterally injected into the vasa deferentia of the rat to induce epididymo-orchitis. The effect of UPEC infection on the testis was investigated on day 7 post infection to allow UPEC to reach the testis. In addition, preliminary studies performed in our group did not find significant changes in the testis at earlier time points (on days 1 and 3, data not shown). Importantly, inflamed epididymides and testes were observed on day 7 post infection, as indicated by gross morphological changes of these organs (Figure 3A). Furthermore, reduced testicular size and weight was evident in infected rats compared to control animals (Figure 3B), which is indicative of degenerative changes within the testis.

In addition to the inflamed appearance observed in the epididymides and testes of infected rats (Figure 3A), the presence of UPEC within the testes was also confirmed by PCR and bacterial colony formation (Figure 4). Critically, for the first time my investigation revealed UPEC localized within the testis of an epididymo-orchitis model. A recent study reported that *E.coli* injected into the interstitial space of the testis were eradicated by host immune responses within four days [190]. In contrast, bacteria injected into the seminiferous tubules still could be detected until 56 days post infection. These findings suggest that the level of immune response in the interstitium of the testis is much more robust than in the seminiferous epithelium. Intriguingly, in this study *E. coli* were predominantly found in the interstitial compartment of the testis on day 7 following UPEC infection (Figures 5 and 6), although bacteria face stronger immune response than in the lumen of seminiferous tubules. However, the mechanism of UPEC invasion through the germinal epithelium to interstitium of the testis remains unclear.

Importantly, the concentration of UPEC employed in my study was much lower

than previously used in other *in vitro* investigations where human spermatozoa were infected [83,207]. Previous clinical reports have suggested that bacterial concentrations in semen of confirmed cases of bacterial prostatitis ranged from 10^3 cfu/ml to more than 10^6 cfu/ml [189]. More recently a study employed similar amounts of *E. coli* (10^6 cfu) for microinjection into the seminiferous tubules to investigate spermatogenic disturbance in mouse [190]. These prior investigations have provided both clinical and experimental rationales for the concentration of bacteria used in my *in vivo* study.

Overall my findings showed the successful establishment of an *in vivo* model mounting inflammatory responses in the testis and epididymis. Furthermore, the localization of UPEC inside the testis suggests infection can potentially cause structural damage to the testis which ultimately disturbs spermatogenesis.

4.2 UPEC invasion does not compromise the integrity of the BTB and BEB

It is well acknowledged that the tight junction between adjacent SC (known as BTB) provides an anatomical separation between the adluminal compartment and the rest region of the testis [1]. Previous study has demonstrated that UPEC CFT073 can disrupt the tight junctions of murine renal inner medullary collecting duct cells thus facilitating bacterial dissemination into the renal interstitium [209]. Given my findings of bacterial localization within the interstitium of the testis, the impact of UPEC infection on the BTB was next investigated. The integrity of another tight junction in the epithelium of the epididymis (BEB) was also assessed. Intriguingly, electron microscopical examination revealed UPEC did not compromise the integrity of the BTB or BEB (Figure 7), albeit it was observed that bacteria were able to cross through the germinal epithelium. There are several likely explanations for these observations. Firstly, as UPEC can transiently invade and survive within epithelial cells of the urinary tract, these pathogens may probably internalize within SC and PTC, thus permitting invasion into the interstitium by directly passing through the cells in the seminiferous epithelium [210]. This assumption is further supported by a recent study demonstrating that TLR-4, which is also expressed in SC and PTC,

facilitates the passage of UPEC across renal collecting duct cell layers without altering the tight junctions [209]. On the other hand, it has been shown that the integrity of the BTB can be reversibly disrupted by TNF-α secreted from SC and germ cells [73]. In correlation, a significant upregulation of TNF-α at mRNA level was observed in UPEC infected testis in my *in vivo* model (Yongning L et al. unpublished data). This leads to another possibility that instead of permanently compromising the tight junctions, UPEC might temporarily affect the BTB by manipulating the expression of TNF-α or other mediators, which in turn facilitates bacterial invasion into the interstitium of the testis.

In addition, it was previously reported that *E. coli* injected inside the seminiferous tubules could disrupt the inter-SC tight junctions at later stage [190]. However, the morphological and functional alternations of the compromised tight junctions were not described. As no functional disruption of the BTB was observed in my investigation, future studies would need to include a greater range of time points to gain a comprehensive evaluation. Dynamically monitoring the integrity alternation of the BTB during infection, and investigations on UPEC invasion in SC and PTC, may provide a deeper insight to the mechanism by which UPEC disseminate inside the testis.

4.3 UPEC infection causes impairment of spermatogenesis

Given UPEC were able to invade through the genital ducts and caused a decrease in testicular weight, histopathological evaluation of the epididymis and testis was performed using H&E stained tissue sections. In the cauda epididymides of UPEC infected rats, immune cell infiltration was evident in the interstitium (Figure 8A, right panel). This indicated an inflammatory response was elicited in the epididymis proximal to the site of UPEC injection. Notably, numerous immature germ cells were also found to be sloughed inside the lumen of the epididymis (Figure 8A and B, right panel). This suggests a disturbance of spermatogenesis within the testis. Indeed, the loss of germ cells and degeneration of the seminiferous epithelium was evident in different regions of the infected testes (Figure 9). Importantly, varying degrees of

spermatogenic impairment were observed in neighboring seminiferous tubules, for example, from partial depletion of spermatozoa to only a few spermatogonia remained. Similar regional differences within the same testis in respect to spermatogenic lesions are also commonly found in experimental autoimmune orchitis animal models and non-obstructive azoospermia patients [1,211]. This suggests that the detrimental effect, which was caused by UPEC infection in my study, does not apply evenly throughout the whole testis. Furthermore, a significant decrease of sperm concentration was observed following 7 days of infection in comparison to control rats (Figure 10). These results demonstrate a pro-inflammatory response evoked by UPEC and the damaging effect induced by ascending infection in the epididymis and testis, which may result in reduced fertility. Future investigations on the functional and structural abnormalities of sperm in this *in vivo* model may provide a greater insight into the impact of UPEC infection on fertility.

Previous studies have described impairment of spermatogenesis in other *E. coli* induced orchitis models [190,192]. Nagaosa and colleagues have demonstrated a disturbance of spermatogenesis as early as day 1 by directly microinjecting *E. coli* into the seminiferous tubules in a mouse model [190]. Critically the majority of seminiferous tubules were found to be affected within 2 days. In contrast, severe impairment of spermatogenesis was found in my *in vivo* model by day 7 but not on days 1 and 3 post infection. These distinct observations may be due to different sites of bacterial injection. In comparison to direct injection into the seminiferous tubules, the disturbance of spermatogenesis may occur later if bacteria are injected into the vas deferens, as infection requires time to spread to the testis. In addition to germ cell loss and seminiferous epithelium lesions, Demir and colleagues also found mild interstitial fibrosis in the testis of their *E. coli* induced epididymo-orchitis model, which was not observed in my investigation [192]. This may be explained by the fact that in the previous study analysis of histological changes in the testis was conducted at a later time point (14 days), which may reflect the pathological lesions in an advanced stage. Of note, seminiferous epithelium could not recover from the disturbance caused by infection, even after the invading bacteria were eliminated either by host immune

responses or antibiotic treatment [190,192]. These findings suggest that the damaging effects caused by UPEC infection may not be limited to germ cells, but may also affect other somatic cells or even the whole testicular milieu. However, the underlying mechanism has yet to be elucidated.

4.4 UPEC do not activate classical apoptosis pathways in the testis

To obtain a comprehensive understanding of molecular mechanisms implicated in UPEC caused spermatogenic impairment, it was next to characterize possible cell death pathways involved in infected testis, specifically in investigated somatic cells (SC and PTC). Apoptosis has been found to be an important mechanism controlling germ cell populations in physiological conditions [212]. Moreover, apoptosis is also involved in urothelial cell death following UPEC infections [212,213]. Therefore, it was of great importance to investigate whether UPEC can induce apoptosis in the testis. TUNEL assay was initially employed to provide a quantitative examination of an apoptotic index in the testis. The result demonstrated a dramatic increase of TUNEL (+) testicular cells in infected rats in comparison to control animals (Figure 11). This finding indicates that UPEC infection can induce DNA breakage in affected testicular cells, the majority of which are located in the seminiferous epithelium and appeared to be germ cells based on their position. However, previous studies have suggested that in some cases the breakage of DNA strand detected by TUNEL (+) staining are probably associated with necrotic cells as well [196,214]. To distinguish apoptosis from necrosis, several techniques were employed to further identify both biochemical and morphological characteristics of infected testis. Klumpp and colleagues reported that a UPEC isolate NU14 was able to induce caspase-dependent apoptosis in urothelial cells by activating both extrinsic and intrinsic apoptotic cascades [213]. In this study, the apoptosis pathways were evaluated by detecting the expression pattern of the *bcl-2* gene family (Figure 12) and activation of caspase (Figure 13). However, all these findings indicate that UPEC infection does not activate the caspase-dependent pathway in the testis. This discrepancy may be explained by the finding of the TUNEL assay which illustrates that the amount of

cells with apoptotic nuclear feature was just a relative small proportion of total testicular cell population.

Furthermore, *in vitro* investigation demonstrated a lethal effect of UPEC infection on SC and PTC, as illustrated by the significant decrease of cell viability (Figure 15) and disruption of plasma membrane (Figure 16). However, as shown by qRT-PCR (Figures 17) and Western blotting (Figure 18), there was no evidence to suggest the activation of caspase-dependent pathways in infected SC and PTC. This was further supported by the lack of oligonucleosomal DNA fragmentation in infected total testis and investigated somatic cells, which is a hallmark of classical caspases-dependent apoptosis (Figure 19). These findings provide additional evidence to exclude the involvement of classical apoptosis as a predominant death mode in UPEC infected testis.

Apart from biochemical characterization, morphological evaluation can provide further indication of alternative modes of cell death. In previous investigations using epididymo-orchitis models, degeneration of the seminiferous epithelial cells was usually underscored based on H&E staining [190,192,194]. However, H&E staining based morphological assessment alone cannot provide sufficient information about the cellular alternations in various types of affected testicular cells. Therefore, electron microscopical examination was additionally employed in this study to evaluate the ultrastructural abnormalities of germ cells and somatic cells in UPEC infected testes. Interestingly, beside necrotic germ cells, electron microscopy revealed degeneration of SC in infected testis as indicated by severe cytoplasmic vacuolization and extensive lipid droplets accumulation (Figure 14B). Instead of apoptotic features, the cytoplasmic changes were observed in affected SC prior to DNA breakage. Similar ultrastructural abnormalities have been observed in several pathological conditions associated with impaired spermatogenesis [215,216]. It has been reported that the vacuolization in the cytoplasm of SC is due to swelling and coalescence of intracellular membrane bound organelles, particularly endoplasmic reticulum and vesicles [217,218]. Furthermore, the presence of extensive large lipid droplets in SC may be related to increased phagocytic activity following germ cell damage upon

UPEC infection, but may also indicate disturbance of lipid metabolism [216]. Importantly, these findings in damaged SC have not been described in any other *in vivo* epididymo-orchitis model to date. Considering the crucial role of SC in spermatogenesis maintenance, observation of the degenerative changes may provide a better understanding of the mechanism contributing to irreversible impairment of spermatogenesis in bacterial orchitis. However, future functional studies (such as inhibin B measurement) should be conducted to further evaluate the impact of UPEC infection on SC.

Taken together, these results suggest that the majority of testicular cells respond differently from other cell types such as urothelial cells following UPEC infection, as the classical apoptotic pathways are not activated. Given these findings, alternative mechanisms other than caspase-dependent pathway must be involved in the cell death of SC and PTC.

4.5 AIF mediates programmed cell death in UPEC infected SC

Caspase-dependent apoptosis has long been synonymous with programmed cell death (PCD), referring to a highly regulated form of cell suicide [219]. To date it is widely believed that even in absence of caspase activation, PCD can be achieved by different mechanisms [220,221]. For example, it was reported that in presence of pan-caspase inhibitor, the soluble O6-toxins of UPEC induced apoptosis in renal tubular cells in a caspase-independent manner [222]. Amongst all caspase-independent executioners in PCD, AIF is one of the best characterized thus far. In my study, AIF was found to relocate into the nuclei of SC following UPEC CFT073 or FOS 22 treatment (Figure 20A). In contrast, localization of AIF was found no change in PTC following infection (Figure 20B). This suggests that AIF is specifically involved in UPEC triggered SC death. Furthermore, it has been described that AIF mediated PCD shares some biochemical characteristics with classical caspase-dependent apoptosis such as phosphatidylserine externalization [148]. Impressively, the exposure of phosphatidylserine was also observed in the majority of SC following 90 min of infection using HlyA (+) strains (Figure 16A and B). It has

been established that exposure of phosphatidylserine can facilitate recognition and phagocytosis of dying cells, thus attenuating host immune responses elicited by cell death [223]. In addition, previous reports showed the release of AIF from the mitochondria could be triggered by calpain activation in a calcium-dependent fashion, or via PARP-1 and cathepsins activation independent of calcium [224]. However, in my investigations the putative activation of calpain was not observed in SC following UPEC infection. Therefore, further studies surrounding the activation of PARP-1 and cathepsin may help to gain deeper insight into the mechanism of AIF redistribution in UPEC infected SC. Additionally, previous findings have demonstrated that AIF is able to trigger peripheral chromatin condensation and subsequential apoptosis- or necrosis-like PCD depending on cell type and stimuli [148]. In agreement with previous reports, in my study a typical peripheral chromatin aggregation was evident only in SC at early stages of UPEC infection (approximately in 1~2 h), as assessed using Hoechst 33342 staining (Figure 21). Taken together, these results corroborate the specific involvement of AIF in UPEC induce SC death. Further studies on upstream signals triggering AIF release and the underlying mechanism involved in AIF induced DNA degradation may help to outline the AIF-dependent cascade implicated in UPEC induced SC death.

4.6 UPEC induce programmed necrosis in PTC

In contrast to SC, UPEC infected PTC underwent a distinct mode of cell death without the participation of AIF. Based on observation with Annexin V/PI staining, rapid loss of membrane integrity was evident in nearly half of UPEC infected PTC (Figure 16C and D). This indicates necrosis may be a dominant mode of cell death in this specific cell type. Necrosis has often been described as an accidental and uncontrolled consequence of extreme physico-chemical stress. However, accumulating evidence emphasizes that certain forms of necrosis are tightly regulated and occur under certain conditions [225]. In accordance with previous investigations on programmed necrosis, a sequence of intracellular events implicated in UPEC induced PTC death was delineated in my study, with observations of calpain

activation, excessive ROS production, ATP depletion and nuclear pyknosis [169,176].

The activation of calpain occurred very early in infected PTC following UPEC treatment (Figure 22). This is usually considered a consequence of Ca^{2+} influx and in turn contributes to a secondary intracellular Ca^{2+} spikes by abolishing the Na^{+}/Ca^{2+} exchanger [226]. Although intracellular Ca^{2+} level has not been determined in my study, observed calpain activation is widely accepted as a key procedure inducing cell death by multiple mechanisms, including the facilitation of death effectors (e.g. AIF and Cytochrome C) release from mitochondria [227], cleaving of cytoskeleton components [226], and the induction of cathepsin release from lysosomes [160]. Therefore, activation of calpain appears to have contributed to UPEC induced PTC death.

Furthermore, a rapid and transient burst of ROS level was also observed in UPEC infected PTC (Figure 23C and D). Increased oxidative stress usually occurs during microbial infection. Some clinical and experimental *in vivo* investigations have revealed that excessive ROS can be generated by spermatozoa and semen neutrophils in epididymitis [228,229]. Interestingly, Kaya and colleagues reported that an oxidative stress status also occurred in the testis of UPEC induced epididymitis in rat without neutrophil accumulation [230]. As indicated by excessive ROS generation, the balance between free radicals and scavengers must be disturbed and mitochondria may be affected in PTC following UPEC infection. The excessive production of ROS, acting as another cell death mediator, in turn leads to permeabilization of mitochondrial membranes [231], DNA damage [232], lipid oxidation [233] and subsequential cellular membrane disruption [159]. Interestingly, excessive ROS generation was not observed in infected SC (Figure 23A and B). A likely reason is the cytosolic ROS may be neutralized by AIF, which was released from the mitochondria of UPEC infected SC and could also act as peroxide scavenger.

Importantly, evidence in favor of SC and PTC undergoing necrosis is the observed decline of intracellular ATP level during UPEC treatment (Figure 24). It is widely accepted that ATP depletion is an initiator of necrosis, as the apoptotic machinery is hindered by energy failure in contrast to necrotic cell death which is

ATP-independent [202]. Earlier studies in different models were conducted to determine the threshold of ATP level before internal machinery switches the modality of cell death from apoptosis to necrosis. Although the results varied between cell types and lethal insults, it is widely accepted that once ATP declines below 15~25% of normal level, necrotic cell death is irretrievable [234,235]. In my study, ATP levels decreased below such thresholds in SC after 2 h and in PTC after 4 h of UPEC infection (Figure 24). Notably, in the initial stages of infection (1~2 h), the majority of SC demonstrated AIF nuclear translocation (Figure 20) and peripheral chromatin condensation (Figure 21), whilst did not display plasma membrane rupture (Figure 16). As the UPEC infection continued, similar nuclear condensation as infected PTC (Figure 21) and ATP depletion (Figure 24) was observed in SC. Based on nuclear features and the integrity of plasma membrane, AIF mediated cell death can be categorized into apoptosis- and necrosis-like PCD [126,148]. It is assumed that the declining ATP levels contributed to the switch of AIF mediated apoptosis-like to necrosis-like PCD in UPEC infected SC.

All these modulators investigated in this study are well known players in cell death irrespective of the stimuli. Taken alone neither calpain nor ROS is specific for necrosis, but different mediators participate simultaneously in an organized self-destruction cascade may define programmed necrosis [169]. Distinct cell death cascades were found to be implicated in UPEC infected SC and PTC. Indeed, even facing to a given death stimulus, the involved modulators and cascades can be cell type specific.

4.7 HlyA is a candidate virulence factor for induction of SC and PTC death

Given the lethal effect on SC and PTC, it is of great importance to determine the major virulence factors involved in UPEC induced PCD. Lipopolysaccharide (LPS) is one of the best characterized virulence factors of *E. coli* in multiple experimental systems. Previous investigations have described impaired spermatogenesis in acute inflammation animal models induced by intraperitoneal LPS injection [236,237]. In contrast, Nagaosa and colleagues found that neither dead *E. coli* nor LPS injected into

the seminiferous tubules could induce a detrimental effect on spermatogenesis [190]. These conflicting observations indicate distinct mechanisms may be involved in different infection models. Systemic and local inflammatory responses can be mounted by intraperitoneal LPS injection that subsequently affects testicular function [32,45]. However, the immune response evoked by dead bacteria or LPS within the seminiferous tubules appears to play little role in spermatogenic impairment when the germinal epithelium is directly exposed to *E. coli*. In agreement with the observations of Nagaosa and colleagues, my findings showed that the NPEC 470 strain expressing LPS did not decrease viability in SC and PTC (Figure 15). Therefore, other virulence factors produced by living UPEC such as secreted soluble toxins are assumed to contribute to the death of infected testicular cells. Another study on a pore-forming toxin described a series of cell death cascades which is similar to my observations in UPEC infected SC and PTC [176]. As an important virulence factor thoroughly characterized, an *E. coli* pore-forming toxin HlyA is able to induce Ca^{2+} influx and manipulate cell death in various target cells [238]. By employing various *E. coli* strains, it was revealed that only those strains with HlyA encoding sequence were able to induce SC and PTC death (Figure 15). Furthermore, HlyA (+) *E. coli* strains caused phosphatidylserine exposure and plasma membrane disintegration in infected SC and PTC (Figure 16). Therefore, HlyA appears to be a primary candidate contributing to the pathogenesis of UPEC infection causing damage within the testis and inducing programmed necrosis in SC and PTC. Future studies need to investigate if blocking the binding of HlyA to cell membrane can abolish the lethal effect of UPEC on target cells.

4.8 UPEC induce SC and PTC death with inflammatory consequence

Although it is increasingly acknowledged that necrosis and apoptosis demonstrate more morphological and biochemical similarities than initially thought, making a distinction between the different modes of cell death is still necessary, particularly considering that necrosis is usually associated with inflammatory responses. The rupture of the plasma membrane in necrotic cells allows intracellular contents to be

spilled into extracellular milieu to elicit an immune response. HMGB1 belongs to the damage-associated molecular pattern (DAMP) molecules released from necrotic cells [239]. Previous investigations reported an upregulation of HMGB1 in the testis in a LPS-induced acute inflammation model, indicating that the testis was under stress [237]. However, in this study the expression of HMGB1 remained unchanged whilst this protein was released from the nuclei in UPEC infected testis (Figures 25). Furthermore, HMGB1 redistribution to the cytoplasm was also observed in both SC and PTC following infection with HlyA (+) *E. coli* strains (Figure 26). It has been reported that active secretion of HMGB1 can be triggered by the activation of NFκB pathway in macrophages [165]. However, in infected testis, the release of HMGB1 was not associated with the NFκB pathway as UPEC infection did not trigger IkBα degradation and p65 nuclear translocation in testis (Figure 27). These results favor necrotic injury in testicular cells, as apoptotic cells firmly retain HMGB1 within nuclei even after undergoing secondary necrosis and autolysis [166]. Extracellularly, HMGB1 becomes a pro-inflammatory molecule with high affinity to several receptors such as RAGE and TLRs [240,241]. Therefore, released HMGB1 may serve as a signal from necrotic testicular cells to neighboring cells for inflammation induction.

During infection pathogens adopt various strategies to suppress host immune responses thus facilitating survival [242]. In light of this, programmed necrosis may serve as an alternative backup mechanism to eliminate invading pathogens as well as damaged testicular cells when caspase-dependent apoptosis is repressed during UPEC infection. My findings describe a series of biochemical events and morphological features surrounding UPEC induced programmed necrosis in SC and PTC. However, the advantage of adopting programmed instead of unregulated necrosis in testicular somatic cells upon UPEC infection has yet to be elucidated. Similar to my observations, externalization of phosphatidylserine was found in programmed necrosis induced by the DNA alkylating agent N-methyl-N-nitro-N-nitrosoguanidine (MNNG) [148]. Importantly, it has been further proved that exposure of phosphatidylserine acts as a signal for phagocytic clearance of such necrotic corpse and thus leading to a less severe inflammatory response [148,223]. These findings

may provide crucial information for answering why programmed necrosis is adopted under certain conditions. Given the testis is considered as an immune privileged site, attenuated inflammatory response elicited by programmed necrosis may be a strategy employed for the elimination of pathogens and whilst minimizing the disruption of testicular functions.

In conclusion, my PhD project characterizes the detrimental effects of UPEC infection on testis. Furthermore, the findings presented in this thesis delineate various necrotic cascades instead of caspase-dependent apoptotic pathways implicated in UPEC induced programmed cell death of SC and PTC (Figure 28). This thesis therefore provides a greater insight into the underlying molecular mechanisms by which testicular cells, specifically somatic cells in the seminiferous epithelium, respond to UPEC infection. Future studies are critical to elucidate upstream signaling pathways involved in the testicular cells demise following infection. Critically, the identification of the *E. coli* pore-forming toxin HlyA as a primary candidate for the induction of SC and PTC death may provide a better understanding of mechanisms employed by UPEC which exert deleterious effects on host cells. Further investigations are still required to evaluate if the damaging effects of UPEC can be attenuated by blocking the binding of HlyA to the membrane of target cells, which may lay the foundations for potential therapeutics in the future.

It is also important to remember that the disturbance of spermatogenesis in bacterial orchitis is usually irreversible, even after antibiotic treatment which can effectively eliminate invading pathogens. Given the impact of UPEC infection is not only limited to germ cells but also influences testicular somatic cells, it is necessary for future studies to dissect the role of somatic cells demise in spermatogenesis impairment. Critically, UPEC induced SC and PTC death is found to be highly orchestrated forms of PCD. Future studies will need to incorporate a comprehensive delineation of signaling pathways controlling programmed necrosis in UPEC induced orchitis, which may pave the way for amelioration of current therapeutic strategy.

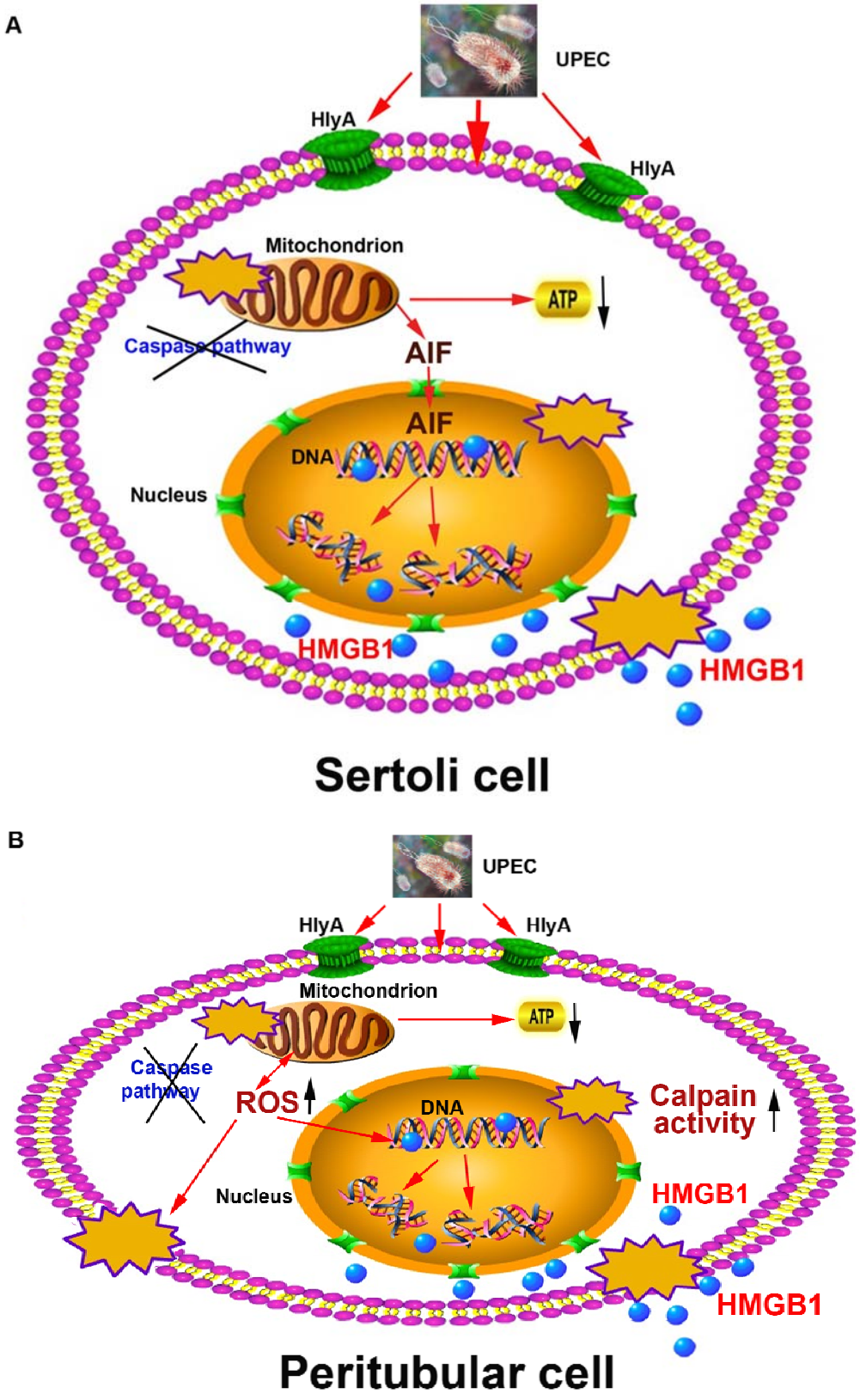

Figure 28 UPEC induced programmed necrosis in Sertoli (A) and peritubular cells (B).

5 SUMMARY

Infection and inflammation of the male reproductive tract are main aetiological factors of infertility. Inflammatory infertility is often based on loss of germ cell function and number. Uropathogenic *E. coli* (UPEC) is a relevant pathogen in urogenital infections. The aim of this study was to explore the pathomechanism that lead to germ cell loss during *E. coli* infection. Thus as a first step an *in vivo* model of epididymo-orchitis was established in rat by injecting a relevant strain of UPEC into the vas deferens in close proximity to the epididymis. Mimicking an infection ascending from the urinary tract, in the testis UPEC bacteria were found exclusively in the interstitial space 7 days post infection. Tracer experiments revealed that the integrity of the blood-testis and blood epididymis barrier was intact 7 days post-infection indicating that evasion of bacteria occurs probably intracellularly. In the testis, UPEC infection resulted in impairment of spermatogenesis by germ cell loss, damage of testicular somatic cells, a decrease in sperm numbers and a significant increase in TUNEL (+) cells. To investigate potential mechanism of germ cell death, hall mark steps of apoptosis were investigated. Activation of caspase-8 (extrinsic apoptotic pathway), caspase-3/-6 (intrinsic apoptotic pathway), caspase-1 (pyroptosis pathway) and the presence of 180 bp DNA fragments, all of which serve as indicators of the classical apoptotic pathway, were not observed in infected testis. Notably, electron microscopical examination revealed degenerative features of Sertoli cells (SC) in UPEC infected testis. Subsequent investigations focused on *in vitro* responses of SC and peritubular cells (PTC). Using UPEC wild type and mutant strains, it was shown that only α-hemolysin (+) *E. coli* strains were able to induce cell death of SC and PTC, but not strains that were lacking this pore forming virulence factor. Subsequent experiments revealed that the caspase-dependent apoptotic pathway was not involved in demise of these cells. Instead nuclear translocation of apoptosis inducing factor (AIF), rapid depletion of ATP, peripheral chromatin aggregation and condensation of nuclei was observed in UPEC treated SC. In contrast, activation of calpain, excessive production of reactive oxygen species (ROS), a gradual decline in

ATP levels and the homogenous condensation of nuclei were evident in UPEC induced PTC death. Furthermore, the passive release of high mobility group protein B1 (HMGB1), as an indication of the necrosis, was observed in SC, PTC and infected testis. In summary, the findings indicate that UPEC infection causes the induction of an organized self-destruction cascade termed programmed necrosis in the testis, which may ultimately be the major mechanism contributing to impairment of fertility.

6 ZUSAMMENFASSUNG

Infektion und Entzündung des männlichen Reproduktionstraktes gehören zu den wesentlichen Ursachen männlicher Infertilität. Die eingeschränkte Fertilität beruht oftmals auf einem Verlust an Keimzellen. Ziel der vorliegenden Arbeit war es die Pathomechanismen zu untersuchen, die zum Keimzellverlust führen. Deshalb wurde zunächst ein *in vivo* Modell in der Ratte etabliert, bei dem eine aus dem Harntrakt aufsteigende Epididymo-Orchitis durch Inokulation von uropathogenen *Escherichia coli* in den Ductus deferens nahe dem Nebenhoden modellhaft nachempfunden wurde. Sieben Tage nach Infektion wurden UPEC Bakterien ausschließlich im Interstitium des Hodens gefunden, obwohl sowohl die Blut-Hoden-Schranks als auch die Blut-Nebenhoden-Schranke intakt waren, wie begleitende Tracerstudien ergeben haben. Darüberhinaus führte die UPEC Infektion im Hoden zu einer Beeinträchtigung der Spermatogenese durch Keimzellverlust ausgedrückt durch eine reduzierte Anzahl an Spermatozoen, einer Schädigung der somatischen Zellen, und einer deutlich erhöhten Anzahl an TUNEL (+) Zellen im infizierten Hoden. Die für einen Zelltod durch den klassischen Apoptosesignalweg charakteristische Aktivierung von Caspase-8 (extrinsischer apoptotischer Signalweg), Caspase-3/-6 (intrinsischer apoptotischer Signalweg) und Caspase-1 (Pyroptosis), sowie die Bildung von ca. 180 bp langen DNA Fragmenten konnten in infizierten Hoden jedoch nicht beobachtet werden. Degenerative Veränderungen von Sertoli Zellen (SC) in infizierten Hoden wurden elektronenmikroskopisch nachgewiesen. *In vitro* konnte mit Hilfe von UPEC Wildtyp und Mutanten gezeigt werden, dass ein Zelltod in SC und Peritubulär-Zellen (PTC) abhängig von der Expression des Poren-bildenden Virulenzfaktors α-Hämolysin (+) ist. Weitere Experimente konnten zeigen, dass der Caspase-abhängige Apoptose-Signalweg nicht für den Zelltod der SC und PTC verantwortlich ist. Hingegen konnte in infizierten SC eine Translokation von AIF (apoptosis inducing factor) in den Zellkern, eine schnelle Depletion von ATP, periphere Chromatinaggregation und nukleäre Kondensation beobachtet werden. In Gegensatz dazu fanden sich in UPEC infizierten PTC eine Aktivierung von Calpain, eine

massive Produktion von ROS (reactive oxygen species), eine schrittweise Erniedrigung der ATP-Spiegel sowie eine homogene nukleare Kondensation als charakteristische Merkmale. In SC und PTC als auch im infizierten Hoden wurde eine passive Freisetzung des High-Mobility-Group-Protein B1 (HMGB1), einem Nekrosemarker, beobachtet. Zusammenfassend kann festgestellt werden, dass eine UPEC Infektion im Hoden zu einem Keimzellverlust durch einen organisierten Selbstzerstörungsprozess führt, der als programmierte Nekrose bezeichnet wird.

7 REFERENCES

1. Nieschlag E, Behre HM, Nieschlag S. Andrology : male reproductive health and dysfunction. (3rd ed). Springer: Heidelberg ; New York, 2010.
2. Cooper TG. Sperm maturation in the epididymis: a new look at an old problem. *Asian J Androl* 2007; 9: 533-539.
3. Siegel MJ, Coley BD. Pediatric imaging. In: The core curriculum. (ed)^(eds). Lippincott Williams & Wilkins: Philadelphia, 2006.
4. Lavin N. Manual of endocrinology and metabolism. (2nd ed). Little, Brown: Boston, 1994.
5. Ehmcke J, Schlatt S. A revised model for spermatogonial expansion in man: lessons from non-human primates. *Reproduction* 2006; 132: 673-680.
6. de Rooij DG. Stem cells in the testis. *Int J Exp Pathol* 1998; 79: 67-80.
7. Wang H, Xiong W, Chen Y, *et al.* Evaluation on the phagocytosis of apoptotic spermatogenic cells by Sertoli cells in vitro through detecting lipid droplet formation by Oil Red O staining. *Reproduction* 2006; 132: 485-492.
8. Dufour JM, Dass B, Halley KR, *et al.* Sertoli cell line lacks the immunoprotective properties associated with primary Sertoli cells. *Cell Transplant* 2008; 17: 525-534.
9. Mital P, Hinton BT, Dufour JM. The Blood-Testis and Blood-Epididymis Barriers Are More Than Just Their Tight Junctions. *Biology of Reproduction* 2011.
10. Griswold MD. Protein secretions of Sertoli cells. *Int Rev Cytol* 1988; 110: 133-156.
11. Fenichel P, Rey R, Poggioli S, *et al.* Anti-Mullerian hormone as a seminal marker for spermatogenesis in non-obstructive azoospermia. *Hum Reprod* 1999; 14: 2020-2024.
12. Toulis KA, Iliadou PK, Venetis CA, *et al.* Inhibin B and anti-Mullerian hormone as markers of persistent spermatogenesis in men with non-obstructive azoospermia: a meta-analysis of diagnostic accuracy studies. *Hum Reprod Update* 2010; 16: 713-724.
13. Dejucq N, Dugast I, Ruffault A, *et al.* Interferon-alpha and -gamma expression in the rat testis. *Endocrinology* 1995; 136: 4925-4931.
14. Kontogeorgos G, Messini I, Kyrodimou E, *et al.* Immunohistochemical localization of interleukin-6 in peripheral human endocrine glands. *Endocrine* 2002; 17: 135-140.
15. Bhushan S, Tchatalbachev S, Klug J, *et al.* Uropathogenic Escherichia coli block MyD88-dependent and activate MyD88-independent signaling pathways in rat testicular cells. *J Immunol* 2008; 180: 5537-5547.
16. Wartenberg H, Kinsky I, Viebahn C, *et al.* Fine structural characteristics of testicular cord formation in the developing rabbit gonad. *J Electron Microsc Tech* 1991; 19: 133-157.
17. Monsees TK, Franz M, Gebhardt S, *et al.* Sertoli cells as a target for reproductive hazards. *Andrologia* 2000; 32: 239-246.
18. Albrecht M. Insights into the nature of human testicular peritubular cells. *Annals of Anatomy - Anatomischer Anzeiger* 2009; 191: 532-540.
19. Schell C, Albrecht M, Mayer C, *et al.* Exploring human testicular peritubular cells: identification of secretory products and regulation by tumor necrosis factor-alpha. *Endocrinology* 2008; 149: 1678-1686.

20. Rossi F, Ferraresi A, Romagni P, *et al.* Angiotensin II stimulates contraction and growth of testicular peritubular myoid cells in vitro. *Endocrinology* 2002; 143: 3096-3104.
21. Fernandez D, Bertoldi MV, Gomez L, *et al.* Identification and characterization of Myosin from rat testicular peritubular myoid cells. *Biol Reprod* 2008; 79: 1210-1218.
22. Zhou Q, Nie R, Prins GS, *et al.* Localization of androgen and estrogen receptors in adult male mouse reproductive tract. *J Androl* 2002; 23: 870-881.
23. Mackay S, Smith RA. Effects of growth factors on testicular morphogenesis. *Int Rev Cytol* 2007; 260: 113-173.
24. El Ramy R, Verot A, Mazaud S, *et al.* Fibroblast growth factor (FGF) 2 and FGF9 mediate mesenchymal-epithelial interactions of peritubular and Sertoli cells in the rat testis. *J Endocrinol* 2005; 187: 135-147.
25. Mooradian AD, Morley JE, Korenman SG. Biological actions of androgens. *Endocr Rev* 1987; 8: 1-28.
26. Krause WKHN, Rajesh K. Immune Infertility: The Impact of Immune Reactions on Human Infertility. In. 1st ed. (ed)^(eds). Springer: Berlin, 2009.
27. Teuscher C, Wild GC, Tung KS. Immunochemical analysis of guinea pig sperm autoantigens. *Biol Reprod* 1982; 26: 218-229.
28. Kohno S, Munoz JA, Williams TM, *et al.* Immunopathology of murine experimental allergic orchitis. *J Immunol* 1983; 130: 2675-2682.
29. Fijak M, Meinhardt A. The testis in immune privilege. *Immunol Rev* 2006; 213: 66-81.
30. Schuppe HC, Meinhardt A. Immune privilege and inflammation of the testis. *Chem Immunol Allergy* 2005; 88: 1-14.
31. Fijak M, Bhushan S, Meinhardt A. Immunoprivileged sites: the testis. *Methods Mol Biol* 2011; 677: 459-470.
32. O'Bryan MK, Gerdprasert O, Nikolic-Paterson DJ, *et al.* Cytokine profiles in the testes of rats treated with lipopolysaccharide reveal localized suppression of inflammatory responses. *Am J Physiol Regul Integr Comp Physiol* 2005; 288: R1744-1755.
33. Kern S, Robertson SA, Mau VJ, *et al.* Cytokine secretion by macrophages in the rat testis. *Biol Reprod* 1995; 53: 1407-1416.
34. Mital P, Kaur G, Dufour JM. Immunoprotective Sertoli cells: making allogeneic and xenogeneic transplantation feasible. *Reproduction* 2009; 139: 495-504.
35. Li Y, Xue W, Tian X, *et al.* Improved survival and function of rat cryopreserved islets by coculture with sertoli cells. *Artif Organs* 2011; 35: 634-644.
36. De Cesaris P, Filippini A, Cervelli C, *et al.* Immunosuppressive molecules produced by Sertoli cells cultured in vitro: biological effects on lymphocytes. *Biochem Biophys Res Commun* 1992; 186: 1639-1646.
37. Selawry HP, Kotb M, Herrod HG, *et al.* Production of a factor, or factors, suppressing IL-2 production and T cell proliferation by Sertoli cell-enriched preparations. A potential role for islet transplantation in an immunologically privileged site. *Transplantation* 1991; 52: 846-850.
38. D'Agostino P, Milano S, Barbera C, *et al.* Sex hormones modulate inflammatory mediators produced by macrophages. *Ann N Y Acad Sci* 1999; 876: 426-429.

39. Liva SM, Voskuhl RR. Testosterone acts directly on CD4+ T lymphocytes to increase IL-10 production. *J Immunol* 2001; 167: 2060-2067.
40. Suarez-Pinzon W, Korbutt GS, Power R, *et al.* Testicular sertoli cells protect islet beta-cells from autoimmune destruction in NOD mice by a transforming growth factor-beta1-dependent mechanism. *Diabetes* 2000; 49: 1810-1818.
41. Schlatt S, de Kretser DM, Hedger MP. Mitosis of resident macrophages in the adult rat testis. *J Reprod Fertil* 1999; 116: 223-228.
42. Gerdprasert O, O'Bryan MK, Muir JA, *et al.* The response of testicular leukocytes to lipopolysaccharide-induced inflammation: further evidence for heterogeneity of the testicular macrophage population. *Cell Tissue Res* 2002; 308: 277-285.
43. Bergh A, Damber JE, van Rooijen N. The human chorionic gonadotrophin-induced inflammation-like response is enhanced in macrophage-depleted rat testes. *J Endocrinol* 1993; 136: 415-420.
44. Winnall WR, Muir JA, Hedger MP. Rat resident testicular macrophages have an alternatively activated phenotype and constitutively produce interleukin-10 in vitro. *J Leukoc Biol* 2011; 90: 133-143.
45. O'Bryan MK, Schlatt S, Phillips DJ, *et al.* Bacterial lipopolysaccharide-induced inflammation compromises testicular function at multiple levels in vivo. *Endocrinology* 2000; 141: 238-246.
46. Hayes R, Chalmers SA, Nikolic-Paterson DJ, *et al.* Secretion of bioactive interleukin 1 by rat testicular macrophages in vitro. *J Androl* 1996; 17: 41-49.
47. Gaytan F, Bellido C, Aguilar E, *et al.* Requirement for testicular macrophages in Leydig cell proliferation and differentiation during prepubertal development in rats. *J Reprod Fertil* 1994; 102: 393-399.
48. Bergh A, Damber JE, van Rooijen N. Liposome-mediated macrophage depletion: an experimental approach to study the role of testicular macrophages in the rat. *J Endocrinol* 1993; 136: 407-413.
49. Afane M, Dubost JJ, Sauvezie B, *et al.* Modulation of Leydig cell testosterone production by secretory products of macrophages. *Andrologia* 1998; 30: 71-78.
50. Hales DB. Testicular macrophage modulation of Leydig cell steroidogenesis. *J Reprod Immunol* 2002; 57: 3-18.
51. Rival C, Lustig L, Iosub R, *et al.* Identification of a dendritic cell population in normal testis and in chronically inflamed testis of rats with autoimmune orchitis. *Cell Tissue Res* 2006; 324: 311-318.
52. Rival C, Theas MS, Suescun MO, *et al.* Functional and phenotypic characteristics of testicular macrophages in experimental autoimmune orchitis. *J Pathol* 2008; 215: 108-117.
53. Rival C, Guazzone VA, von Wulffen W, *et al.* Expression of co-stimulatory molecules, chemokine receptors and proinflammatory cytokines in dendritic cells from normal and chronically inflamed rat testis. *Mol Hum Reprod* 2007; 13: 853-861.
54. el-Demiry M, James K. Lymphocyte subsets and macrophages in the male genital tract in health and disease. A monoclonal antibody-based study. *Eur Urol* 1988; 14: 226-235.
55. Hedger MP. Testicular leukocytes: what are they doing? *Rev Reprod* 1997; 2: 38-47.

56. Jacobo P, Guazzone VA, Jarazo-Dietrich S, *et al.* Differential changes in CD4+ and CD8+ effector and regulatory T lymphocyte subsets in the testis of rats undergoing autoimmune orchitis. *J Reprod Immunol* 2009; 81: 44-54.
57. Bergh A, Widmark A, Damber JE, *et al.* Are leukocytes involved in the human chorionic gonadotropin-induced increase in testicular vascular permeability? *Endocrinology* 1986; 119: 586-590.
58. Lysiak JJ. The role of tumor necrosis factor-alpha and interleukin-1 in the mammalian testis and their involvement in testicular torsion and autoimmune orchitis. *Reprod Biol Endocrinol* 2004; 2: 9.
59. Schuppe HC, Meinhardt A, Allam JP, *et al.* Chronic orchitis: a neglected cause of male infertility? *Andrologia* 2008; 40: 84-91.
60. Bhushan S, Schuppe H-C, Tchatalbachev S, *et al.* Testicular innate immune defense against bacteria. *Molecular and Cellular Endocrinology* 2009; 306: 37-44.
61. Guazzone VA, Jacobo P, Theas MS, *et al.* Cytokines and chemokines in testicular inflammation: A brief review. *Microsc Res Tech* 2009; 72: 620-628.
62. Girling JE, Hedger MP. Toll-like receptors in the gonads and reproductive tract: emerging roles in reproductive physiology and pathology. *Immunol Cell Biol* 2007; 85: 481-489.
63. Wu H, Wang H, Xiong W, *et al.* Expression patterns and functions of toll-like receptors in mouse sertoli cells. *Endocrinology* 2008; 149: 4402-4412.
64. Hedger MP, Meinhardt A. Cytokines and the immune-testicular axis. *J Reprod Immunol* 2003; 58: 1-26.
65. Amjad AI, Soder O, Sultana T. Role of testicular interleukin-1alpha tIL-1alpha in testicular physiology and disease. *J Coll Physicians Surg Pak* 2006; 16: 55-60.
66. Abu Elheija M, Dyomin V, Ganaiem M, *et al.* Distinct expression of interleukin-1alpha, interleukin-1beta, and interleukin-1 receptor antagonist in testicular tissues and cells from human biopsies with normal and abnormal histology. *J Interferon Cytokine Res* 2011; 31: 401-408.
67. Cudicini C, Lejeune H, Gomez E, *et al.* Human Leydig cells and Sertoli cells are producers of interleukins-1 and -6. *J Clin Endocrinol Metab* 1997; 82: 1426-1433.
68. De SK, Chen HL, Pace JL, *et al.* Expression of tumor necrosis factor-alpha in mouse spermatogenic cells. *Endocrinology* 1993; 133: 389-396.
69. Bornstein SR, Rutkowski H, Vrezas I. Cytokines and steroidogenesis. *Mol Cell Endocrinol* 2004; 215: 135-141.
70. Fiddes RJ, Brandon MR, Adams TE. Functional expression of an ovine growth hormone receptor in transfected Chinese hamster ovary cells. *Mol Cell Endocrinol* 1992; 86: 37-47.
71. Hales DB. Interleukin-1 inhibits Leydig cell steroidogenesis primarily by decreasing 17 alpha-hydroxylase/C17-20 lyase cytochrome P450 expression. *Endocrinology* 1992; 131: 2165-2172.
72. Lie PP, Cheng CY, Mruk DD. Interleukin-1{alpha} is a regulator of the blood-testis barrier. *FASEB J* 2011; 25: 1244-1253.
73. Li MW, Xia W, Mruk DD, *et al.* Tumor necrosis factor {alpha} reversibly disrupts the

blood-testis barrier and impairs Sertoli-germ cell adhesion in the seminiferous epithelium of adult rat testes. *J Endocrinol* 2006; 190: 313-329.

74. Xia W, Wong EW, Mruk DD, *et al.* TGF-beta3 and TNFalpha perturb blood-testis barrier (BTB) dynamics by accelerating the clathrin-mediated endocytosis of integral membrane proteins: a new concept of BTB regulation during spermatogenesis. *Dev Biol* 2009; 327: 48-61.
75. Mauduit C, Gasnier F, Rey C, *et al.* Tumor necrosis factor-alpha inhibits leydig cell steroidogenesis through a decrease in steroidogenic acute regulatory protein expression. *Endocrinology* 1998; 139: 2863-2868.
76. Hales DB, Diemer T, Hales KH. Role of cytokines in testicular function. *Endocrine* 1999; 10: 201-217.
77. Com E, Bourgeon F, Evrard B, *et al.* Expression of antimicrobial defensins in the male reproductive tract of rats, mice, and humans. *Biol Reprod* 2003; 68: 95-104.
78. World Health Organization. WHO Manual for the Standardized Investigation, Diagnosis and Management of the Infertile Male. ed). Cambridge University Press: Cambridge, 2004.
79. Dohle GR, Colpi GM, Hargreave TB, *et al.* EAU guidelines on male infertility. *Eur Urol* 2005; 48: 703-711.
80. Ellis PJ, Furlong RA, Conner SJ, *et al.* Coordinated transcriptional regulation patterns associated with infertility phenotypes in men. *J Med Genet* 2007; 44: 498-508.
81. Spiess AN, Feig C, Schulze W, *et al.* Cross-platform gene expression signature of human spermatogenic failure reveals inflammatory-like response. *Hum Reprod* 2007; 22: 2936-2946.
82. Diemer T, Huwe P, Ludwig M, *et al.* Urogenital infection and sperm motility. *Andrologia* 2003; 35: 283-287.
83. Diemer T, Huwe P, Michelmann HW, *et al.* Escherichia coli-induced alterations of human spermatozoa. An electron microscopy analysis. *Int J Androl* 2000; 23: 178-186.
84. Agarwal A, Saleh RA. Role of oxidants in male infertility: rationale, significance, and treatment. *Urol Clin North Am* 2002; 29: 817-827.
85. Comhaire FH, Mahmoud AM, Depuydt CE, *et al.* Mechanisms and effects of male genital tract infection on sperm quality and fertilizing potential: the andrologist's viewpoint. *Hum Reprod Update* 1999; 5: 393-398.
86. Ludwig M. Diagnosis and therapy of acute prostatitis, epididymitis and orchitis. *Andrologia* 2008; 40: 76-80.
87. Berger RE, Alexander ER, Harnisch JP, *et al.* Etiology, manifestations and therapy of acute epididymitis: prospective study of 50 cases. *J Urol* 1979; 121: 750-754.
88. Ochsendorf FR. Sexually transmitted infections: impact on male fertility. *Andrologia* 2008; 40: 72-75.
89. Wiles T, Kulesus R, Mulvey M. Origins and virulence mechanisms of uropathogenic Escherichia coli. *Experimental and Molecular Pathology* 2008; 85: 11-19.
90. Pellati D, Mylonakis I, Bertoloni G, *et al.* Genital tract infections and infertility. *Eur J Obstet Gynecol Reprod Biol* 2008; 140: 3-11.
91. Johnson JR, Scheutz F, Ulleryd P, *et al.* Host-pathogen relationships among Escherichia coli isolates recovered from men with febrile urinary tract infection. *Clin Infect Dis* 2005; 40:

813-822.

92. Lipsky BA. Prostatitis and urinary tract infection in men: what's new; what's true? *Am J Med* 1999; 106: 327-334.
93. Hviid A, Rubin S, Muhlemann K. Mumps. *Lancet* 2008; 371: 932-944.
94. Philip J, Selvan D, Desmond AD. Mumps orchitis in the non-immune postpubertal male: a resurgent threat to male fertility? *BJU Int* 2006; 97: 138-141.
95. Willems WR, Hornig C, Bauer H*, et al.* A case of Coxsackie A9 virus infection with orchitis. *J Med Virol* 1978; 3: 137-140.
96. Kisbenedek L, Nemeth A. Granulomatous orchitis and spermatic granuloma. *Int Urol Nephrol* 1975; 7: 141-148.
97. Merino G, Carranza-Lira S, Murrieta S*, et al.* Bacterial infection and semen characteristics in infertile men. *Arch Androl* 1995; 35: 43-47.
98. Marrs CF, Zhang L, Foxman B. Escherichia colimediated urinary tract infections: Are there distinct uropathogenicE. coli(UPEC) pathotypes? *FEMS Microbiology Letters* 2005; 252: 183-190.
99. Stamm WE, Norrby SR. Urinary tract infections: disease panorama and challenges. *J Infect Dis* 2001; 183 Suppl 1: S1-4.
100. Emdy L. Virulence factors of uropathogenic Escherichia coli. *International Journal of Antimicrobial Agents* 2003; 22: 29-33.
101. Schembri MA, Klemm P. Biofilm formation in a hydrodynamic environment by novel fimh variants and ramifications for virulence. *Infect Immun* 2001; 69: 1322-1328.
102. Oelschlaeger TA, Dobrindt U, Hacker J. Virulence factors of uropathogens. *Curr Opin Urol* 2002; 12: 33-38.
103. Rietschel ET, Brade H, Holst O*, et al.* Bacterial endotoxin: Chemical constitution, biological recognition, host response, and immunological detoxification. *Curr Top Microbiol Immunol* 1996; 216: 39-81.
104. Wiles TJ, Kulesus RR, Mulvey MA. Origins and virulence mechanisms of uropathogenic Escherichia coli. *Exp Mol Pathol* 2008; 85: 11-19.
105. Fiorentini C, Fabbri A, Matarrese P*, et al.* Hinderance of apoptosis and phagocytic behaviour induced by Escherichia coli cytotoxic necrotizing factor 1: two related activities in epithelial cells. *Biochem Biophys Res Commun* 1997; 241: 341-346.
106. Guerinot ML. Microbial iron transport. *Annu Rev Microbiol* 1994; 48: 743-772.
107. Gal-Mor O, Finlay BB. Pathogenicity islands: a molecular toolbox for bacterial virulence. *Cell Microbiol* 2006; 8: 1707-1719.
108. Lloyd AL, Rasko DA, Mobley HLT. Defining Genomic Islands and Uropathogen-Specific Genes in Uropathogenic Escherichia coli. *Journal of Bacteriology* 2007; 189: 3532-3546.
109. Oelschlaeger TA, Dobrindt U, Hacker J. Pathogenicity islands of uropathogenic E. coli and the evolution of virulence. *Int J Antimicrob Agents* 2002; 19: 517-521.
110. Brzuszkiewicz E. How to become a uropathogen: Comparative genomic analysis of extraintestinal pathogenic Escherichia coli strains. *Proceedings of the National Academy of Sciences* 2006; 103: 12879-12884.

111. Welch RA, Burland V, Plunkett G, 3rd, *et al.* Extensive mosaic structure revealed by the complete genome sequence of uropathogenic Escherichia coli. *Proc Natl Acad Sci U S A* 2002; 99: 17020-17024.

112. Luo C, Hu G-Q, Zhu H. Genome reannotation of Escherichia coli CFT073 with new insights into virulence. *BMC Genomics* 2009; 10: 552.

113. Kaper JB, Nataro JP, Mobley HLT. Pathogenic Escherichia coli. *Nature Reviews Microbiology* 2004; 2: 123-140.

114. Palladino MA, Johnson TA, Gupta R, *et al.* Members of the Toll-Like Receptor Family of Innate Immunity Pattern-Recognition Receptors Are Abundant in the Male Rat Reproductive Tract. *Biology of Reproduction* 2007; 76: 958-964.

115. Emody L, Batai I, Jr., Kerenyi M, *et al.* Anti-Escherichia coli alpha-hemolysin in control and patient sera. *Lancet* 1982; 2: 986.

116. Mulvey MA, Lopez-Boado YS, Wilson CL, *et al.* Induction and evasion of host defenses by type 1-piliated uropathogenic Escherichia coli. *Science* 1998; 282: 1494-1497.

117. Real J-M, Munro P, Buisson-Touati C, *et al.* Specificity of immunomodulator secretion in urinary samples in response to infection by alpha-hemolysin and CNF1 bearing uropathogenic Escherichia coli. *Cytokine* 2007; 37: 22-25.

118. Böhme L, Rudel T. Host cell death machinery as a target for bacterial pathogens. *Microbes and Infection* 2009; 11: 1063-1070.

119. Peter ME. Programmed cell death: Apoptosis meets necrosis. *Nature* 2011; 471: 310-312.

120. Lamkanfi M, Dixit VM. Manipulation of Host Cell Death Pathways during Microbial Infections. *Cell Host & Microbe* 2010; 8: 44-54.

121. Kerr JF, Wyllie AH, Currie AR. Apoptosis: a basic biological phenomenon with wide-ranging implications in tissue kinetics. *Br J Cancer* 1972; 26: 239-257.

122. Susin SA, Daugas E, Ravagnan L, *et al.* Two distinct pathways leading to nuclear apoptosis. *J Exp Med* 2000; 192: 571-580.

123. Nagata S. Apoptotic DNA fragmentation. *Exp Cell Res* 2000; 256: 12-18.

124. Lockshin R. Caspase-independent cell deaths. *Current Opinion in Cell Biology* 2002; 14: 727-733.

125. Rizzuto R, Pinton P, Ferrari D, *et al.* Calcium and apoptosis: facts and hypotheses. *Oncogene* 2003; 22: 8619-8627.

126. Jaattela M, Tschopp J. Caspase-independent cell death in T lymphocytes. *Nat Immunol* 2003; 4: 416-423.

127. Riedl SJ, Shi Y. Molecular mechanisms of caspase regulation during apoptosis. *Nature Reviews Molecular Cell Biology* 2004; 5: 897-907.

128. Shi Y. Mechanisms of caspase activation and inhibition during apoptosis. *Mol Cell* 2002; 9: 459-470.

129. Lamkanfi M, Kalai M, Vandenabeele P. Caspase-12: an overview. *Cell Death Differ* 2004; 11: 365-368.

130. Fischer H, Koenig U, Eckhart L, *et al.* Human caspase 12 has acquired deleterious mutations. *Biochem Biophys Res Commun* 2002; 293: 722-726.

131. Kroemer G, Reed JC. Mitochondrial control of cell death. *Nat Med* 2000; 6: 513-519.
132. Reed JC, Zha H, Aime-Sempe C, *et al.* Structure-function analysis of Bcl-2 family proteins. Regulators of programmed cell death. *Adv Exp Med Biol* 1996; 406: 99-112.
133. Dejean LM, Martinez-Caballero S, Manon S, *et al.* Regulation of the mitochondrial apoptosis-induced channel, MAC, by BCL-2 family proteins. *Biochim Biophys Acta* 2006; 1762: 191-201.
134. Cain K, Bratton SB, Cohen GM. The Apaf-1 apoptosome: a large caspase-activating complex. *Biochimie* 2002; 84: 203-214.
135. Acehan D, Jiang X, Morgan DG, *et al.* Three-dimensional structure of the apoptosome: implications for assembly, procaspase-9 binding, and activation. *Mol Cell* 2002; 9: 423-432.
136. Deveraux QL, Reed JC. IAP family proteins--suppressors of apoptosis. *Genes Dev* 1999; 13: 239-252.
137. Wilkinson JC, Cepero E, Boise LH, *et al.* Upstream regulatory role for XIAP in receptor-mediated apoptosis. *Mol Cell Biol* 2004; 24: 7003-7014.
138. Boise LH, Gonzalez-Garcia M, Postema CE, *et al.* bcl-x, a bcl-2-related gene that functions as a dominant regulator of apoptotic cell death. *Cell* 1993; 74: 597-608.
139. Chen G, Goeddel DV. TNF-R1 signaling: a beautiful pathway. *Science* 2002; 296: 1634-1635.
140. Wajant H. The Fas signaling pathway: more than a paradigm. *Science* 2002; 296: 1635-1636.
141. Micheau O, Tschopp J. Induction of TNF receptor I-mediated apoptosis via two sequential signaling complexes. *Cell* 2003; 114: 181-190.
142. Wang K, Yin XM, Chao DT, *et al.* BID: a novel BH3 domain-only death agonist. *Genes Dev* 1996; 10: 2859-2869.
143. Oliver FJ, de la Rubia G, Rolli V, *et al.* Importance of poly(ADP-ribose) polymerase and its cleavage in apoptosis. Lesson from an uncleavable mutant. *J Biol Chem* 1998; 273: 33533-33539.
144. Constantinou C, Papas KA, Constantinou AI. Caspase-independent pathways of programmed cell death: the unraveling of new targets of cancer therapy? *Curr Cancer Drug Targets* 2009; 9: 717-728.
145. Susin SA, Lorenzo HK, Zamzami N, *et al.* Molecular characterization of mitochondrial apoptosis-inducing factor. *Nature* 1999; 397: 441-446.
146. Miramar MD, Costantini P, Ravagnan L, *et al.* NADH oxidase activity of mitochondrial apoptosis-inducing factor. *J Biol Chem* 2001; 276: 16391-16398.
147. Loeffler M, Daugas E, Susin SA, *et al.* Dominant cell death induction by extramitochondrially targeted apoptosis-inducing factor. *FASEB J* 2001; 15: 758-767.
148. Boujrad H, Gubkina O, Robert N, *et al.* AIF-mediated programmed necrosis: a highly regulated way to die. *Cell Cycle* 2007; 6: 2612-2619.
149. Daugas E, Susin SA, Zamzami N, *et al.* Mitochondrio-nuclear translocation of AIF in apoptosis and necrosis. *FASEB J* 2000; 14: 729-739.
150. Hangen E, Blomgren K, Benit P, *et al.* Life with or without AIF. *Trends Biochem Sci* 2010; 35: 278-287.
151. Martin SJ, Reutelingsperger CP, McGahon AJ, *et al.* Early redistribution of plasma membrane

phosphatidylserine is a general feature of apoptosis regardless of the initiating stimulus: inhibition by overexpression of Bcl-2 and Abl. *J Exp Med* 1995; 182: 1545-1556.

152. McDonald PP, Fadok VA, Bratton D*, et al.* Transcriptional and translational regulation of inflammatory mediator production by endogenous TGF-beta in macrophages that have ingested apoptotic cells. *J Immunol* 1999; 163: 6164-6172.
153. Duffield JS, Ware CF, Ryffel B*, et al.* Suppression by apoptotic cells defines tumor necrosis factor-mediated induction of glomerular mesangial cell apoptosis by activated macrophages. *Am J Pathol* 2001; 159: 1397-1404.
154. Kurosaka K, Watanabe N, Kobayashi Y. Production of proinflammatory cytokines by phorbol myristate acetate-treated THP-1 cells and monocyte-derived macrophages after phagocytosis of apoptotic CTLL-2 cells. *J Immunol* 1998; 161: 6245-6249.
155. Horino K, Nishiura H, Ohsako T*, et al.* A monocyte chemotactic factor, S19 ribosomal protein dimer, in phagocytic clearance of apoptotic cells. *Lab Invest* 1998; 78: 603-617.
156. Rovere P, Vallinoto C, Bondanza A*, et al.* Bystander apoptosis triggers dendritic cell maturation and antigen-presenting function. *J Immunol* 1998; 161: 4467-4471.
157. Savill J, Dransfield I, Gregory C*, et al.* A blast from the past: clearance of apoptotic cells regulates immune responses. *Nat Rev Immunol* 2002; 2: 965-975.
158. Majno G, Joris I. Apoptosis, oncosis, and necrosis. An overview of cell death. *Am J Pathol* 1995; 146: 3-15.
159. Zong WX. Necrotic death as a cell fate. *Genes & Development* 2006; 20: 1-15.
160. Artal-Sanz M, Tavernarakis N. Proteolytic mechanisms in necrotic cell death and neurodegeneration. *FEBS Lett* 2005; 579: 3287-3296.
161. Zong WX, Ditsworth D, Bauer DE*, et al.* Alkylating DNA damage stimulates a regulated form of necrotic cell death. *Genes Dev* 2004; 18: 1272-1282.
162. Wang H, Bloom O, Zhang M*, et al.* HMG-1 as a late mediator of endotoxin lethality in mice. *Science* 1999; 285: 248-251.
163. Sims GP, Rowe DC, Rietdijk ST*, et al.* HMGB1 and RAGE in inflammation and cancer. *Annu Rev Immunol* 2010; 28: 367-388.
164. Bianchi ME, Beltrame M. Upwardly mobile proteins. Workshop: the role of HMG proteins in chromatin structure, gene expression and neoplasia. *EMBO Rep* 2000; 1: 109-114.
165. Wu C-X, Sun H, Liu Q*, et al.* LPS Induces HMGB1 Relocation and Release by Activating the NF-κB-CBP Signal Transduction Pathway in the Murine Macrophage-Like Cell Line RAW264.7. *Journal of Surgical Research* 2011.
166. Scaffidi P, Misteli T, Bianchi ME. Release of chromatin protein HMGB1 by necrotic cells triggers inflammation. *Nature* 2002; 418: 191-195.
167. Bianchi ME, Manfredi A. Chromatin and cell death. *Biochim Biophys Acta* 2004; 1677: 181-186.
168. Christofferson DE, Yuan J. Cyclophilin A release as a biomarker of necrotic cell death. *Cell Death and Differentiation* 2010; 17: 1942-1943.
169. Golstein P, Kroemer G. Cell death by necrosis: towards a molecular definition. *Trends in Biochemical Sciences* 2007; 32: 37-43.

170. Proskuryakov SY, Gabai VL, Konoplyannikov AG. Necrosis is an active and controlled form of programmed cell death. *Biochemistry (Mosc)* 2002; 67: 387-408.

171. Degterev A, Hitomi J, Germscheid M, *et al.* Identification of RIP1 kinase as a specific cellular target of necrostatins. *Nat Chem Biol* 2008; 4: 313-321.

172. Galluzzi L, Kepp O, Kroemer G. RIP kinases initiate programmed necrosis. *J Mol Cell Biol* 2009; 1: 8-10.

173. Cho Y, Challa S, Moquin D, *et al.* Phosphorylation-Driven Assembly of the RIP1-RIP3 Complex Regulates Programmed Necrosis and Virus-Induced Inflammation. *Cell* 2009; 137: 1112-1123.

174. He S, Wang L, Miao L, *et al.* Receptor interacting protein kinase-3 determines cellular necrotic response to TNF-alpha. *Cell* 2009; 137: 1100-1111.

175. Declercq W, Vanden Berghe T, Vandenabeele P. RIP kinases at the crossroads of cell death and survival. *Cell* 2009; 138: 229-232.

176. Kennedy CL, Smith DJ, Lyras D, *et al.* Programmed cellular necrosis mediated by the pore-forming alpha-toxin from Clostridium septicum. *PLoS Pathog* 2009; 5: e1000516.

177. Vanlangenakker N, Vanden Berghe T, Krysko DV, *et al.* Molecular mechanisms and pathophysiology of necrotic cell death. *Curr Mol Med* 2008; 8: 207-220.

178. Eguchi Y, Shimizu S, Tsujimoto Y. Intracellular ATP levels determine cell death fate by apoptosis or necrosis. *Cancer Res* 1997; 57: 1835-1840.

179. Orrenius S. Reactive Oxygen Species in Mitochondria-Mediated Cell Death. *Drug Metabolism Reviews* 2007; 39: 443-455.

180. Herreweghe F, Festjens N, Declercq W, *et al.* Tumor necrosis factor-mediated cell death: to break or to burst, that's the question. *Cellular and Molecular Life Sciences* 2010; 67: 1567-1579.

181. Bergsbaken T, Fink SL, Cookson BT. Pyroptosis: host cell death and inflammation. *Nature Reviews Microbiology* 2009; 7: 99-109.

182. Bergsbaken T, Cookson BT. Macrophage activation redirects yersinia-infected host cell death from apoptosis to caspase-1-dependent pyroptosis. *PLoS Pathog* 2007; 3: e161.

183. Fink SL, Cookson BT. Caspase-1-dependent pore formation during pyroptosis leads to osmotic lysis of infected host macrophages. *Cell Microbiol* 2006; 8: 1812-1825.

184. Chen Y, Smith MR, Thirumalai K, *et al.* A bacterial invasin induces macrophage apoptosis by binding directly to ICE. *EMBO J* 1996; 15: 3853-3860.

185. Lamkanfi M, Dixit VM. Inflammasomes: guardians of cytosolic sanctity. *Immunol Rev* 2009; 227: 95-105.

186. Monack DM, Detweiler CS, Falkow S. Salmonella pathogenicity island 2-dependent macrophage death is mediated in part by the host cysteine protease caspase-1. *Cell Microbiol* 2001; 3: 825-837.

187. Frantz S, Ducharme A, Sawyer D, *et al.* Targeted deletion of caspase-1 reduces early mortality and left ventricular dilatation following myocardial infarction. *J Mol Cell Cardiol* 2003; 35: 685-694.

188. Schielke GP, Yang GY, Shivers BD, *et al.* Reduced ischemic brain injury in interleukin-1 beta

converting enzyme-deficient mice. *J Cereb Blood Flow Metab* 1998; 18: 180-185.

189. Weidner W, Krause W, Ludwig M. Relevance of male accessory gland infection for subsequent fertility with special focus on prostatitis. *Hum Reprod Update* 1999; 5: 421-432.
190. Nagaosa K, Nakashima C, Kishimoto A, *et al.* Immune response to bacteria in seminiferous epithelium. *Reproduction* 2009; 137: 879-888.
191. Fraczek M, Szumala-Kakol A, Jedrzejczak P, *et al.* Bacteria trigger oxygen radical release and sperm lipid peroxidation in in vitro model of semen inflammation. *Fertil Steril* 2007; 88: 1076-1085.
192. Demir A, Türker P, Önol FF, *et al.* Effect of experimentally induced Escherichia coli epididymo-orchitis and ciprofloxacin treatment on rat spermatogenesis. *International Journal of Urology* 2007; 14: 268-272.
193. Abe CM, Salvador FA, Falsetti IN, *et al.* Uropathogenic Escherichia coli (UPEC) strains may carry virulence properties of diarrhoeagenic E. coli. *FEMS Immunol Med Microbiol* 2008; 52: 397-406.
194. Ludwig M, Johannes S, Bergmann M, *et al.* Experimental Escherichia coli epididymitis in rats: a model to assess the outcome of antibiotic treatment. *BJU Int* 2002; 90: 933-938.
195. Soto SM, Smithson A, Martinez JA, *et al.* Biofilm formation in uropathogenic Escherichia coli strains: relationship with prostatitis, urovirulence factors and antimicrobial resistance. *J Urol* 2007; 177: 365-368.
196. Didenko VV, Ngo H, Baskin DS. Early necrotic DNA degradation: presence of blunt-ended DNA breaks, 3' and 5' overhangs in apoptosis, but only 5' overhangs in early necrosis. *Am J Pathol* 2003; 162: 1571-1578.
197. Andrabi SA, Dawson TM, Dawson VL. Mitochondrial and Nuclear Cross Talk in Cell Death. *Annals of the New York Academy of Sciences* 2008; 1147: 233-241.
198. Cande C, Vahsen N, Kouranti I, *et al.* AIF and cyclophilin A cooperate in apoptosis-associated chromatinolysis. *Oncogene* 2004; 23: 1514-1521.
199. Leist M, Single B, Castoldi AF, *et al.* Intracellular adenosine triphosphate (ATP) concentration: a switch in the decision between apoptosis and necrosis. *J Exp Med* 1997; 185: 1481-1486.
200. Perrin BJ, Huttenlocher A. Calpain. *Int J Biochem Cell Biol* 2002; 34: 722-725.
201. Spooner R, Yilmaz Ö. The Role of Reactive-Oxygen-Species in Microbial Persistence and Inflammation. *International Journal of Molecular Sciences* 2011; 12: 334-352.
202. Tsujimoto Y. Apoptosis and necrosis: intracellular ATP level as a determinant for cell death modes. *Cell Death Differ* 1997; 4: 429-434.
203. Shimizu S, Eguchi Y, Kamiike W, *et al.* Bcl-2 blocks loss of mitochondrial membrane potential while ICE inhibitors act at a different step during inhibition of death induced by respiratory chain inhibitors. *Oncogene* 1996; 13: 21-29.
204. Zetterstrom CK, Strand ML, Soder O. The high mobility group box chromosomal protein 1 is expressed in the human and rat testis where it may function as an antibacterial factor. *Hum Reprod* 2006; 21: 2801-2809.
205. Haidl G, Schuppe HC, Kohn FM, *et al.* [Evidence-based drug therapy for male infertility]. *Urologe A* 2008; 47: 1555-1556, 1558-1560.

206. Foxman B. Epidemiology of urinary tract infections: incidence, morbidity, and economic costs. *Dis Mon* 2003; 49: 53-70.

207. Diemer T, Weidner W, Michelmann HW, *et al.* Influence of Escherichia coli on motility parameters of human spermatozoa in vitro. *Int J Androl* 1996; 19: 271-277.

208. Kumar V, Prabha V, Kaur S, *et al.* Receptor dependent immobilization of spermatozoa by sperm immobilization factor isolated from Escherichia coli: proof of evidence. *Int J Urol* 2011; 18: 597-603.

209. Chassin C, Vimont S, Cluzeaud F, *et al.* TLR4 facilitates translocation of bacteria across renal collecting duct cells. *J Am Soc Nephrol* 2008; 19: 2364-2374.

210. Bower JM, Eto DS, Mulvey MA. Covert operations of uropathogenic Escherichia coli within the urinary tract. *Traffic* 2005; 6: 18-31.

211. Itoh M, Takeuchi Y, De Rooij D. Histopathology of the seminiferous tubules in mice injected with syngeneic testicular germ cells alone. *Arch Androl* 1995; 35: 93-103.

212. Ruwanpura SM, McLachlan RI, Stanton PG, *et al.* Pathways involved in testicular germ cell apoptosis in immature rats after FSH suppression. *Journal of Endocrinology* 2008; 197: 35-43.

213. Klumpp DJ, Rycyk MT, Chen MC, *et al.* Uropathogenic Escherichia coli induces extrinsic and intrinsic cascades to initiate urothelial apoptosis. *Infect Immun* 2006; 74: 5106-5113.

214. Perry SW, Epstein LG, Gelbard HA. Simultaneous in situ detection of apoptosis and necrosis in monolayer cultures by TUNEL and trypan blue staining. *Biotechniques* 1997; 22: 1102-1106.

215. Hild SA, Reel JR, Dykstra MJ, *et al.* Acute adverse effects of the indenopyridine CDB-4022 on the ultrastructure of sertoli cells, spermatocytes, and spermatids in rat testes: comparison to the known sertoli cell toxicant Di-n-pentylphthalate (DPP). *J Androl* 2007; 28: 621-629.

216. Huyghe S, Schmalbruch H, De Gendt K, *et al.* Peroxisomal multifunctional protein 2 is essential for lipid homeostasis in Sertoli cells and male fertility in mice. *Endocrinology* 2006; 147: 2228-2236.

217. Chapin RE, Morgan KT, Bus JS. The morphogenesis of testicular degeneration induced in rats by orally administered 2,5-hexanedione. *Exp Mol Pathol* 1983; 38: 149-169.

218. Creasy DM, Beech LM, Gray TJ, *et al.* The ultrastructural effects of di-n-pentyl phthalate on the testis of the mature rat. *Exp Mol Pathol* 1987; 46: 357-371.

219. Conradt B, Xue D. Programmed cell death. *WormBook* 2005: 1-13.

220. Moubarak RS, Yuste VJ, Artus C, *et al.* Sequential Activation of Poly(ADP-Ribose) Polymerase 1, Calpains, and Bax Is Essential in Apoptosis-Inducing Factor-Mediated Programmed Necrosis. *Molecular and Cellular Biology* 2007; 27: 4844-4862.

221. Kroemer G, El-Deiry WS, Golstein P, *et al.* Classification of cell death: recommendations of the Nomenclature Committee on Cell Death. *Cell Death Differ* 2005; 12 Suppl 2: 1463-1467.

222. Chen M, Jahnukainen T, Bao W, *et al.* Uropathogenic Escherichia coli toxins induce caspase-independent apoptosis in renal proximal tubular cells via ERK signaling. *Am J Nephrol* 2003; 23: 140-151.

223. Hirt UA, Leist M. Rapid, noninflammatory and PS-dependent phagocytic clearance of necrotic cells. *Cell Death Differ* 2003; 10: 1156-1164.

224. Yuste VJ, Moubarak RS, Delettre C, *et al.* Cysteine protease inhibition prevents mitochondrial

apoptosis-inducing factor (AIF) release. *Cell Death Differ* 2005; 12: 1445-1448.

225. Festjens N, Vanden Berghe T, Vandenabeele P. Necrosis, a well-orchestrated form of cell demise: signalling cascades, important mediators and concomitant immune response. *Biochim Biophys Acta* 2006; 1757: 1371-1387.
226. Bano D, Young KW, Guerin CJ*, et al.* Cleavage of the plasma membrane Na+/Ca2+ exchanger in excitotoxicity. *Cell* 2005; 120: 275-285.
227. Polster BM, Basanez G, Etxebarria A*, et al.* Calpain I induces cleavage and release of apoptosis-inducing factor from isolated mitochondria. *J Biol Chem* 2005; 280: 6447-6454.
228. Wang A, Fanning L, Anderson DJ*, et al.* Generation of reactive oxygen species by leukocytes and sperm following exposure to urogenital tract infection. *Arch Androl* 1997; 39: 11-17.
229. Aitken J, Krausz C, Buckingham D. Relationships between biochemical markers for residual sperm cytoplasm, reactive oxygen species generation, and the presence of leukocytes and precursor germ cells in human sperm suspensions. *Mol Reprod Dev* 1994; 39: 268-279.
230. Kaya M, Boleken ME, Zeyrek F*, et al.* Oxidative and antioxidative status in the testes of rats with acute epididymitis. *Urol Int* 2006; 76: 353-358.
231. Zorov DB, Juhaszova M, Sollott SJ. Mitochondrial ROS-induced ROS release: an update and review. *Biochim Biophys Acta* 2006; 1757: 509-517.
232. Marnett LJ. Oxyradicals and DNA damage. *Carcinogenesis* 2000; 21: 361-370.
233. Noguchi N, Yamashita H, Hamahara J*, et al.* The specificity of lipoxygenase-catalyzed lipid peroxidation and the effects of radical-scavenging antioxidants. *Biol Chem* 2002; 383: 619-626.
234. Lieberthal W, Menza SA, Levine JS. Graded ATP depletion can cause necrosis or apoptosis of cultured mouse proximal tubular cells. *Am J Physiol* 1998; 274: F315-327.
235. Lelli JL, Jr., Becks LL, Dabrowska MI*, et al.* ATP converts necrosis to apoptosis in oxidant-injured endothelial cells. *Free Radic Biol Med* 1998; 25: 694-702.
236. Kajihara T, Okagaki R, Ishihara O. LPS-induced transient testicular dysfunction accompanied by apoptosis of testicular germ cells in mice. *Medical Molecular Morphology* 2006; 39: 203-208.
237. Metukuri MR, Reddy CMT, Reddy PRK*, et al.* Bacterial LPS Mediated Acute Inflammation-induced Spermatogenic Failure in Rats: Role of Stress Response Proteins and Mitochondrial Dysfunction. *Inflammation* 2010; 33: 235-243.
238. Jonas D, Schultheis B, Klas C*, et al.* Cytocidal effects of Escherichia coli hemolysin on human T lymphocytes. *Infect Immun* 1993; 61: 1715-1721.
239. Bianchi ME. HMGB1 loves company. *J Leukoc Biol* 2009; 86: 573-576.
240. Chen G, Ward MF, Sama AE*, et al.* Extracellular HMGB1 as a proinflammatory cytokine. *J Interferon Cytokine Res* 2004; 24: 329-333.
241. Park JS, Svetkauskaite D, He Q*, et al.* Involvement of toll-like receptors 2 and 4 in cellular activation by high mobility group box 1 protein. *J Biol Chem* 2004; 279: 7370-7377.
242. Diacovich L, Gorvel J-P. Bacterial manipulation of innate immunity to promote infection. *Nature Reviews Microbiology* 2010; 8: 117-128.

8 ACKNOWLEDGEMENT

The experimental work of this dissertation was performed at the Department of Anatomy and Cell Biology, Justus-Liebig University Giessen, Germany, under the supervision of Prof. Dr. Andreas Meinhardt.

First and foremost, I owe my utmost gratitude to my supervisor, Prof. Dr. Andreas Meinhardt for providing me the precious chance of working in this project with his outstanding team. I truly appreciate the confidence, patience and geniality my supervisor has always shown to me during these three years. His supervision, inspiration, steadfast encouragement and enormous support enabled my development from a graduate student to an independent researcher.

I owe my gratitude to my second supervisor Prof. Dr. Trinad Chakraborty for his knowledgeable comments and constructive suggestions during our discussions. Additionally, I would like to thank him for generously providing the *E. coli* strains for our experiments.

I would like to sincerely thank Dr. Sudhanshu Bhushan for his technical and scientific guidance. Without his altruistic help I would not have accomplished this project so smoothly.

I am extremely thankful to Dr. Svetlin Tchatalbachev and his colleague Juri Schklarenko, who not only prepared bacteria for us, but also were always generously providing experimental material to me.

I would like to acknowledge Prof. Martin Bergmann for his essential help in electron microscopy and Prof. Gerhard Schuler for his technical support in testosterone measurement. I would like to thank Prof. Mohamed Lamkanfi from Ghent University for allowing me to show his figures of apoptosis and necrosis signalling pathways which I happily cite in my thesis. I am pleased to acknowledge the contribution of Dr. Marcelo Marconi in the *in vivo* experiment.

I am grateful to Dr. Jörg Klug for his critical suggestions on my experiments and Dr. Monika Fijak for her introduction in flow cytometry and her help with thesis

proofreading. I very much appreciate the great help from Tali Lang, Magdalena Walecki and Ferial Aslani in proofreading my thesis. I would like to thank Suada Fröhlich and Eva Schneider for their technical supervision and I thoroughly appreciate the kind help from all my other colleagues: Julius Chapiro, Sebastian Hollwegs, Bettina Schmidt, Philipp Lacher, Stefan Binder, Sven Moos, Lara-Jil Sauber, Kurt Reichermeier, Sylvia Schirmer, and Maria Dechant.

I would like to thank Patricia Berger, Katarzyna Wanecka and Eva Wewel for their administrative help.

It is my pleasure to thank Prof. Eveline Baumgart-Vogt and her GGL management team with Dr. Lorna Lueck and Zucchi Anna, who have put a lot of effort to organize and constantly improve the doctoral training programme for us.

I also much appreciate the generous help from Vijith Vijayan, Guofeng Qian, Yu Xiao and Wei Fan.

This is a great opportunity to express my deepest gratitude to my wife Sijia Meng for her infinite love, which is the greatest support for my growth and progress. I would like to thank my parents, Hanyuan Lu and Qunqing Lin, for their love, indoctrination and support. I also much appreciate the trust and love from my parents in-law, Min-er Meng and Liping Pan.

In the end, I owe my thanks to my motherland and the China Scholarship Council, which has provided me whit the great opportunity and financial support to study in Germany.

9 EHRENWÖRTLICHE ERKLÄRUNG

Ich erkläre: Ich habe die vorgelegte Dissertation selbständig und ohne unerlaubte fremde Hilfe und nur mit den Hilfen angefertigt, die ich in der Dissertation angegeben habe. Alle Textstellen, die wörtlich oder sinngemäß aus veröffentlichten oder nicht veröffentlichten Schriften entnommen sind, und alle Angaben, die auf mündlichen Auskünften beruhen, sind als solche kenntlich gemacht. Bei den von mir durchgeführten und in der Dissertation erwähnten Untersuchungen habe ich die Grundsätze guter wissenschaftlicher Praxis, wie sie in der „Satzung der Justus-Liebig-Universität Giessen zur Sicherung guter wissenschaftlicher Praxis“ niedergelegt sind, eingehalten.

I declare that I have completed this dissertation single-handedly without the unauthorized help of a second party and only with the assistance acknowledged therein. I have appropriately acknowledged and referenced all text passages that are derived literally from or are based on the content of published or unpublished work of others, and all information that relates to verbal communications. I have abided by the principles of good scientific conduct laid down in the charter of the Justus Liebig University of Giessen in carrying out the investigations described in the dissertation.

Giessen, den

_____

Yongning Lu